

## Verification of Pavement Deformation Prediction Models

*Master's Thesis in the Master's Programme Geo and Water Engineering*

AYAZ MUHAMMET

SETH BRAIMAH

Department of Civil and Environmental Engineering

*Division of Geo Engineering*

*Road and Traffic Group*

CHALMERS UNIVERSITY OF TECHNOLOGY

Göteborg, Sweden 2010

Master's Thesis 2010:102



MASTER'S THESIS 2010:102

# Verification of Pavement Deformation Prediction Models

Master's Thesis in the Master's Programme Geo and Water Engineering

AYAZ MUHAMMET

SETH BRAIMAH

Department of Civil and Environmental Engineering

*Division of Geo Engineering*

*Road and Traffic Group*

CHALMERS UNIVERSITY OF TECHNOLOGY

Göteborg, Sweden 2010

Verification of Pavement Deformation Prediction Models

Master's Thesis in the *Master's Programme Geo and Water Engineering*

AYAZ MUHAMMET

SETH BRAIMAH

© AYAZ MUHAMMET AND SETH BRAIMAH, 2010

Examensarbete / Institutionen för bygg- och miljöteknik,  
Chalmers tekniska högskola 2010:102

Department of Civil and Environmental Engineering

Division of Geo Engineering

Road and Traffic Group

Chalmers University of Technology

SE-412 96 Göteborg

Sweden

Telephone: + 46 (0)31-772 1000

Cover:

The figure on the cover page shows predicted deformations by M-E PDG.

Department of Civil and Environmental Engineering

Göteborg, Sweden 2010

Verification of Pavement Deformation Prediction Models  
Master's Thesis in the *Master's Programme Geo and Water Engineering*  
AYAZ MUHAMMET  
SETH BRAIMAH  
Department of Civil and Environmental Engineering  
Division of Geo Engineering  
Road and Traffic Group  
Chalmers University of Technology

## ABSTRACT

The estimations of permanent deformation development for pavement structure by permanent deformation prediction models are believed to be accurate. In this thesis, two known permanent deformation prediction models; MMOPP and M-E PDG used abroad, are validated with the RST rut depth measurement on a number of constructed pavement sections in Sweden, between Ljungskile and Uddevalla.

The prediction of permanent deformation development by computer programs MMOPP and M-E PDG is based on their response and performance models. M-E PDG has JULEA as the response model and NCHRP1- 37A as the performance model. Whereas, MMOPP has WESDEF as the response model and two phase model as the performance model. The main prediction parameters are material properties, traffic volumes and environmental conditions subjected to the pavement.

The verification was achieved by comparing the measured deformation from RST with the predicted deformations. The results from the predicted models were observed to be of similar pattern as that of the measured deformation in the road sections, even though anomalies occurred in the pattern for some road sections.

Keywords: Permanent deformation, Rutting, Wearing, Pavement structure, RST, Traffic load, Material behavior, MMOPP, M-E PDG.

Validering av Spårbildningsmodeller  
Examensarbete inom Geo and Water Engineering  
AYAZ MUHAMMET AND SETH BRAIMAH  
Institutionen för bygg- och miljöteknik  
Avdelningen för Geologi och Geoteknik  
Väg- och trafikplanering  
Chalmers tekniska högskola

## SAMMANFATTNING

Detta examensarbete beskriver två modeller för prognostisering av spårbildning i vägkroppen. Modellerna inkluderar MMOPP som är utvecklad i Danmark och M-E PDG från USA. Båda modellerna förutspår permanenta deformationer baserad på elasticitetsmodulen hos ingående lagren i vägkroppen och undergrunden. Resultaten från modellerna har jämförts med verkligt uppmätta spårdjup erhållna från RST mätningar från europavägen E6 mellan Ljungskile och Uddevalla. Modellerna baseras på linjärelastiskt beteende i vägkonstruktionens vid belastning.

Jämförelsen mellan prognostiserade spårdjup med uppmätta spårdjup visar en god noggrannhet i modellerna.

Nyckelord: Spårdjup, permanenta deformationer, vägkropp, undergrund, överbyggnad, RST, M-E PDG, MMOPP, responsmodell, slitage.

# Contents

ABSTRACT	I
SAMMANFATTNING	II
CONTENTS	III
PREFACE	VI
NOTATIONS	VII
1 INTRODUCTION	1
1.1 Background	1
1.2 Problem Description	1
1.3 Purpose and Goal	2
1.4 Methodology	2
2 LITERATURE REVIEW	4
2.1 Flexible Pavements	4
2.2 Pavement Serviceability	4
2.2.1 PSI	6
2.2.2 Cracks	6
2.2.3 Rutting	6
2.2.4 Measurement Methods	8
2.3 Deterioration of Pavement Structure	9
2.3.1 Traffic Loads	9
2.3.2 Environmental Loads	11
2.3.3 Material Behavior	13
2.4 Material Modelling	16
2.5 Shakedown Theory	17
2.6 Wearing due to Studded Tires	19
2.7 Pavement Design Models	20
2.7.1 Response Models	20
2.7.2 Performance Models	21
2.7.3 M-E PDG	21
2.7.4 MMOPP	26
3 INVESTIGATED ROAD SECTIONS	29
3.1 E6 Ljungskile-Uddevalla	29
3.1.1 Measured Rut	30
3.1.2 Ljungskile-Stinneröd and Stinneröd-Lerbo	31
3.1.3 Section Lerbo-Sund	32
3.1.4 Section Sunningen-Undavägen	33
3.1.5 Section Undavägen-Herrestad	34
3.2 Traffic Volumes	35

3.2.1	Heavy Traffic	35
3.2.2	Vehicles With Studded Tires	36
3.3	Wearing due to Studded tires	38
3.4	Calculation of Structural Deformation	39
3.4.1	MMOPP	39
3.4.2	M-E PDG	39
4	RESULTS	40
4.1	Wearing	40
4.2	MMOPP	40
4.3	M-E PDG	42
4.4	Comparison of Measured and Predicted Rut Depth	44
4.4.1	Ljungkile-Stinneröd	45
4.4.2	Stinneröd-Lerbo	46
4.4.3	Lerbo-Sund	47
4.4.4	Sunningen-Undavägen	48
4.4.5	Undavägen-Herrestad	49
4.5	Sensitivity Analysis	51
5	DISCUSSION	52
6	CONCLUSION	55
7	RECOMMENDATIONS	56
8	REFERENCES	57
9	APPENDICES	59



## Preface

This master thesis was performed for the Department of Civil and Environmental Engineering, at division of Geo Engineering. The thesis was supported by NCC and the Swedish Road Administration (SRA) in Gothenburg. The research was undertaken during the spring period in 2010.

Our profound gratitude goes to our supervisor Dr. Bo Johansson at NCC for his encouragement and suggestion through the thesis. Special thanks to our co-supervisor Helene Kennedy at NCC for her directions and expertise. Not forgetting, associate professor Gunnar Lannér at Road and Traffic Group at Chalmers University of Technology, for his encouragement and dedication.

We would also like to thank Carl-Gösta Enocksson at the Swedish Road Administration for his technical support both on site and at the office. The support of Anders Huvstig, a researcher at SRA is greatly acknowledged.

Finally, we would like to express our sincere thanks to our families and all love ones for their encouragement and moral support for making this thesis a reality.

Gothenburg, May 2010

Ayaz Muhammet

Seth Braimah

## Notations

PSI	Present Serviceability Index.
SV	Mean slope variance for the longitudinal profile.
C	Cracking for surface deterioration.
P	Patching for surface deterioration.
RD	Mean rut depth for transverse profile in inches.
ESAL	Equivalent Single Axle Load
AADT	Average Annual Daily Traffic in design lane.
A	Portion of heavy traffic in %.
C	Number of axles/heavy vehicle.
D	Factor describing average number of ESAL per heavy vehicle axle.
E	Correction factor considering the width of the road.
n	Design period in years.
k	Annual heavy traffic change in %.
$\sigma$	In-situ stress
u	Pore water pressure
$M_R$	Resilient modulus
$\Delta\sigma$	Stress change in triaxial test
$\Delta\varepsilon$	Unloading cyclic resilient strain change in triaxial test
$\theta$	Bulk stress, which is sum of the principal stresses ( $\sigma_1 + \sigma_2 + \sigma_3$ )
$K_1, K_2$	Material constants
$P_o$	Reference pressure
PD	Permanent deformation.
$\varepsilon_r^k$	Plastic strain in the sub layer k.
$h^k$	Thickness of sub layer k
n sub layer	Number of sub layers
$\varepsilon_p$	Plastic strain cumulated for N load repetition
$\varepsilon_r$	Resilient strain of asphalt material
N	Number of repeated load
$a_1, a_2, a_3$	Non-linear regression coefficient
T	Temperature in F
$\beta_{r1}, \beta_{r2}, \beta_{r3}$	National calibration factors for asphalt layers in M-E PDG
$k_1$	Depth parameter in M-E PDG.
$h_{ac}$	The total thickness of asphalt layers.

$\beta_{GB}$	National calibration factors for granular base layers in M-E PDG
$\beta_{SG}$	National calibration factors for subgrade in M-E PDG
$\delta_a$	Permanent deformation for layer (inch)
$\epsilon_0, \beta, \rho$	Material properties
$\epsilon_v$	Average vertical resilient strain in layers
$PD_{Total}$	Total permanent deformation
$PD_{AC}$	Permanent deformation in asphalt concrete layers
$PD_{GB}$	Permanent deformation in granular base
$PD_{SG}$	Permanent deformation in subgrade
$\epsilon_h$	Permanent strain in the bottom of the asphalt layer in MMOPP.
$\epsilon_0$	Limit of plastic shakedown (phase 1).
$\epsilon_p$	Plastic Strain
$\sigma_1$	Major principal stress
$\sigma'$	Reference stress (Atmospheric pressure, 0.1 MPa)
A,B,C	Calibration constants.
$AADT_{tot}$	Average Annual Daily Traffic (Heavy and passenger traffic)
$AADT_{heavy}$	Average Annual Daily Traffic for heavy traffic
$T_{Initial, Winter}$	Initial passenger traffic during winter in north direction.
$AADT_{Initial}$	Initial annual average daily traffic in both directions.
$AADT_{Initial, Heavy}$	Initial annual average daily traffic of heavy vehicles in both directions.
$AADT_{Winter}$	Annual Average daily traffic during winter period.

## List of Figures

- Figure 1.1: The steps involved in the prediction of permanent deformation compared with reality.
- Figure 2.1: Fundamental sketch of road and pavement design (SRA, 2008).
- Figure 2.2: Illustration of structural deformation caused by heavy traffic (WSDOT, 2008).
- Figure 2.3: Stress distribution in pavement structure (NCHPR, 2004).
- Figure 2.4: RST car used in Sweden (VTI, 2001).
- Figure 2.5: Cross sectional profile obtained from the sensors (Öberg, 2001).
- Figure 2.6: a) Load associated stresses in pavement structure. b) Stresses with respect to time.
- Figure 2.7: Illustration of an Equivalent Standard Axle Load, ESAL (VVTK, 2008).
- Figure 2.8: Frost in pavement structure (White, 2007).
- Figure 2.9:  $M_R$  under cyclic loading.
- Figure 2.10: Definition of  $M_R$  for cyclic triaxial loading.
- Figure 2.11: Effect of aggregate distribution to permanent deformation.
- Figure 2.12: Typical deformation in pavement materials (Ullidtz, 1998).
- Figure 2.13: Burger's material model and deformation under constant load.
- Figure 2.14: Elastic and plastic behaviour of materials under repeated cyclic load (Werkmeister, 2003).
- Figure 2.15: Illustration of wearing caused by studded tires (WSDOT, 2008).
- Figure 2.16: Critical stresses and strains in pavement structure (Werkmeister, 2003).
- Figure 2.17: Levels of pavement deformation (M-E PDG, 2004).
- Figure 2.18: Calibration of predicted against measured asphalt rutting in MnRoad test.
- Figure 3.1: Illustration of different selected sections of E6.
- Figure 3.2: Pavement construction in section Ljungskile-Lerbo. From left to right: Soil Cut, rock cut, border between rock and soil section and rock fill.
- Figure 3.3: Pavement construction in section Lerbo-Sund. From left to right: Pavement on rock cut, pavement on soil cut and pavement with rock fill.
- Figure 3.4: Pavement construction in section Sunningen-Undavägen. From left to right: Pavement on soil cut, pavement on rock cut and pavement with rock fill.
- Figure 3.5: Pavement construction in section Undavägen-Herrestad. From left to right: Pavement on soil cut, pavement on rock cut, pavement with rock fill and pavement with EPS.
- Figure 3.6: Annual traffic distribution in section Ljungskile-Lerbo in both directions (SRA, 2006).

- Figure 3.7: Annual traffic distribution in section Lerbo-Herrestad in both directions (SRA, 2006).
- Figure 4.1: Illustration of measured and predicted structural deformation in section RC1.
- Figure 4.2: Illustration of measured and predicted structural deformation in section SC2.
- Figure 4.3: Illustration of measured and predicted structural deformation in section SL3.
- Figure 4.4: Illustration of measured and predicted structural deformation in section RC4.
- Figure 4.5: Illustration of measured and predicted structural deformation in section RC5.
- Figure 4.6: Illustration of measured and predicted structural deformation in section SC6.
- Figure 4.7: Illustration of measured and predicted structural deformation in section RC7.
- Figure 4.8: Illustration of measured and predicted structural deformation in section RF8.
- Figure 4.9: Illustration of measured and predicted structural deformation in section SL9.
- Figure 4.10: Illustration of measured and predicted structural deformation in section SC10.

## List of Tables

- Table 2.1: Distress in asphalt pavements (Huang, 2004).
- Table 2.2: Estimation of heavy traffic in [%] and number of axles/heavy vehicle.
- Table 2.3: E-modulus of different pavement materials in summer (SRA, 2000).
- Table 2.4: E-modulus of different subgrade materials in summer (SRA, 2000).
- Table 2.5: Response models and their features and limitations.
- Table 2.6: Average temperatures of Boston and Gothenburg.
- Table 2.7: Factors of E-modulus for different season (MMOPP, 2007).
- Table 3.1: Selected sections.
- Table 3.2: Explanation to pavement sub layers in figure 3.2.
- Table 3.3: Explanation to pavement sub layers in figure 3.3.
- Table 3.4: Explanation to pavement sub layers in figure 3.4.
- Table 3.5: Explanation to pavement sub layers in figure 3.5.
- Table 3.6: Traffic data from Ljungskile to Lerbo (SRA, 2010).
- Table 3.7: Traffic data from Lerbo to Herrestad (SRA, 2010)
- Table 3.8: Estimated initial passenger vehicles/day in winter for observed sections.
- Table 3.9: Definition of pavement layers and E-Modulus in MMOPP for Section RC1.
- Table 3.10: Definition of pavement layers and E-Modulus in M-E PDG for Section RC1.
- Table 4.1: Estimated structural deformation in section RC1 and SC2.
- Table 4.2: Estimated structural deformation in section SL3 and RC4.
- Table 4.3: Estimated structural deformation in section RC5 and SC6.
- Table 4.4: Estimated structural deformation in section RC7 and RF8.
- Table 4.5: Estimated structural deformation in section SL9 and SC10.
- Table 4.6: Estimated structural deformation in section RC1.
- Table 4.7: Estimated structural deformation in section SL3 and RC4.
- Table 4.8: Estimated structural deformation in section SC6.
- Table 4.9: Estimated structural deformation in section RC7 and RF8.
- Table 4.10: Estimated structural deformation in section SL9 and SC10.
- Table 4.11: Rate of increment of permanent deformation in reality ( $D_{\text{Structural}}$ ), MMOPP and M-E PDG.
- Table 4.12: Sensitivity results of 30 % change in E-modulus.
- Table 9.1: Measured rut depth in mm for section Ljungskile-Stinneröd.
- Table 9.2: Measured rut depth in mm for section Stinneröd –Lerbo.
- Table 9.3: Measured rut depth in mm for section Lerbo-Sund.

Table 9.4: Measured rut depth in mm for section Sunningen-Undavägen.

Table 9.5: Measured rut depth in mm for section Undavägen-Herrestad.

Table 9.6: Traffic volumes and ESALs for section Ljungskile-Lerbo.

Table 9.7: Traffic volumes and ESALs for section Lerbo-Herrestad.

Table 9.8: Definition of pavement layers and E-Modulus in MMOPP for Section RC1.

Table 9.9: Definition of pavement layers and E-Modulus in MMOPP for Section SC2.

Table 9.10: Definition of pavement layers and E-Modulus in MMOPP for Section SL3.

Table 9.11: Definition of pavement layers and E-Modulus in MMOPP for Section RC4.

Table 9.12: Definition of pavement layers and E-Modulus in MMOPP for Section RC5.

Table 9.13: Definition of pavement layers and E-Modulus in MMOPP for Section SC6.

Table 9.14: Definition of pavement layers and E-Modulus in MMOPP for Section RC7.

Table 9.15: Definition of pavement layers and E-Modulus in MMOPP for Section RF8.

Table 9.16: Definition of pavement layers and E-Modulus in MMOPP for Section SL9.

Table 9.17: Definition of pavement layers and E-Modulus in MMOPP for Section SC10.

Table 9.18: Definition of pavement layers and E-Modulus in M-E PDG for Section RC1 and RC4.

Table 9.19: Definition of pavement layers and E-Modulus in M-E PDG for Section SL3.

Table 9.20: Definition of pavement layers and E-Modulus in M-E PDG for Section SC6.

Table 9.21: Definition of pavement layers and E-Modulus in M-E PDG for Section RC7.

Table 9.22: Definition of pavement layers and E-Modulus in M-E PDG for Section RF8.

Table 9.23: Definition of pavement layers and E-Modulus in M-E PDG for Section SL9.

Table 9.24: Definition of pavement layers and E-Modulus in M-E PDG for Section SC10.

# 1 Introduction

## 1.1 Background

The purpose of the pavement structure is to provide a smooth surface for vehicles during the expected life span. In Sweden, the predominant pavement type is flexible pavement. There have been investigations of technical aspects of flexible pavement structure using mechanistic analysis and mechanistic-empirical pavement models to achieve a accurate prediction of pavement distresses, both structural and functional.

The Swedish Road Administration (SRA) has developed a mechanistic-empirical model, PMS-Objekt, which evaluates the life span of the pavement structure. The model determines fatigue deterioration based on traffic volumes and climatic conditions.

However, rutting is one of the main pavement distresses. Therefore, pavement structures are designed to achieve acceptable rut depth during the design life span. Based on traffic volumes and axle loads, pavement engineers have developed models to predict rutting before construction, and also to mitigate potential serviceability problems. Rutting in pavement structure can be attributed to wearing due to studded tires and structural deformation by heavy vehicles. The structural deformation is estimated by permanent deformation models based on available traffic volumes and climate loads exposed to the pavement structure. Wearing in asphalt layers is common in Scandinavia due to studded tires. Therefore the Swedish Road and Transport Institute (VTI), has developed a model for estimating wearing due to studded tires.

The life span and the performance of pavement structure are directly related to permanent deformation in pavement structure. The total rut development is associated with wearing and structural deformations. With the aid of pavement response models including linear, non-linear and visco-elastic models estimations of stress and strain distribution can be predicted. Based on the structural response of pavement, long term accumulation of rutting can be estimated.

## 1.2 Problem Description

The development of analytical procedures permits the estimation of stresses, strains and deflections resulting from traffic volumes and material properties, pavement engineers have developed various permanent deformation prediction models. These models are widely used abroad for prediction of rut development for pavement structure. The models are empirically verified abroad based on climatic and geological conditions. However, there is no advanced empirical verification of these models in Sweden.

In this project, two selected models, Mathematical Model of Pavement Performance (MMOPP) and Mechanistic-Empirical Pavement Design Model (M-E PDG) will be evaluated.

### 1.3 Purpose and Goal

The purpose of this Master Thesis is to validate the structural deformation predicted by MMOPP and M-E PDG with a number of constructed sections of the highway E6 between Ljungskile and Uddevalla. The results from the models are compared to rut measurement done by Road Surface Tester (RST) car. The comparison will show the accuracy and reliability of the models. Additional calculations and analysis are made to explain possible differences between calculated and measured results. The emphasis for the comparison is based on annual structural deformation rate, thus deformation rate after the initial pre-compaction period.

During the working process, the following questions are answered:

- What is the measured annual rate of permanent deformation?
- What is the predicted annual rate of permanent deformation?
- How accurate are the permanent deformation prediction models?
- What is the cause to differences between measured ruts and predicted ruts?
- What is the cause of differences in results between MMOPP and M-E PDG?

### 1.4 Methodology

This subchapter entails the procedures involved to achieve the purpose of the project. The project started with an extensive discussion of the problem with the supervisors. With a precise idea on how permanent deformation has occurred on the highway E6, a detailed literature review was made on permanent deformation of pavement structures. The literature review included material behaviour, traffic loads and the effect of environmental loads to pavement structure. Further research was made on rut prediction models, M-E PDG and MMOPP.

With thorough understanding of parameters required for the rut prediction models, data was collected from the archives of the Swedish Road Administration (SRA). Data was obtained from construction drawings (horizontal, vertical and normal sections) produced during the design period. The collected data included; road sections constructed by different companies, pavement materials (bound and granular materials), subgrade type, pavement design on cut, fill and surface level and material properties. Concurrently, RST data was obtained from the SRA database. The measured rut depth was used in excel to produce figures that show the structural deformation behaviour on the E6.

Subsequently, traffic data obtained from the SRA was used to estimate ESALs. Furthermore, PMS Objekt was used to determine general values of material properties for the design of the pavement structure. Result from the PMS Objekt software coupled with SRA reports, provided material properties values to run trials of the rut prediction models to be compared with the measured rut depth. Upon critical discussion with our supervisors, changes were made on certain parameters (e.g. modulus, layer thickness, etc) to fit the reality. Sections were selected along the highway E6 based on subgrade type with uneven behaviour shown in the figures produced by the measured rut data.

Due to the fact that the measured rut depth is the total of wearing and structural deformation of the pavement structure, an excel program developed by VTI was used to estimate the wearing caused by studded tires.

Finally, the results from the prediction models were compared with RST data. The steps involved in the prediction of permanent deformation compared with reality is shown in Figure 1.1.

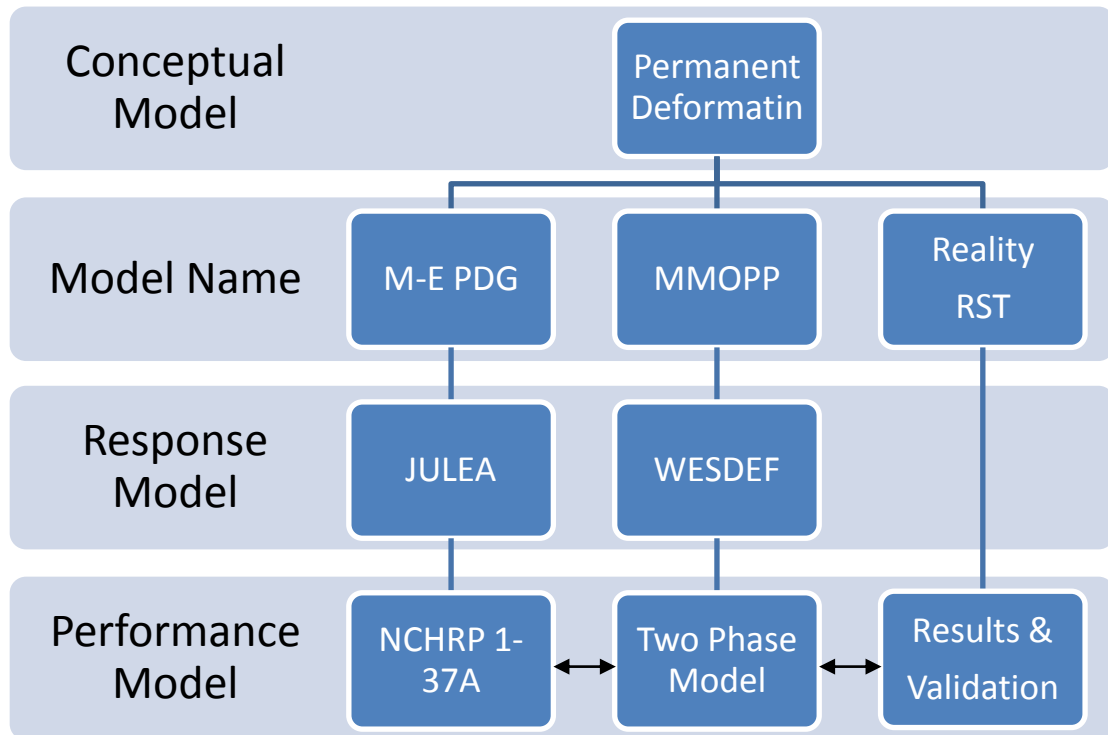


Figure 1.1: The steps involved in the prediction of permanent deformation compared with reality.

## 2 Literature Review

Review of literature aims at covering permanent deformation of pavement structure which includes; the wearing course, unbound granular materials and the sub grade. The literature investigation focused on pavement serviceability, Pavement distress (cracks, rutting mechanism, etc) and important parameters and theories of permanent deformation. Finally, description of MMOPP and M-E PDG are presented.

### 2.1 Flexible Pavements

In Sweden, the most prevailing pavement structure is flexible pavement which is suitable for the available traffic volumes and environmental condition. As shown in Figure 2.1, flexible pavement is composed of asphalt bound layers on top of unbound base and sub base granular material over a subgrade. Flexible pavements rely on sufficient strength and stiffness of the underlying unbound layers to support the load carrying capacity of the surface asphalt layers (VVTK, 2008).

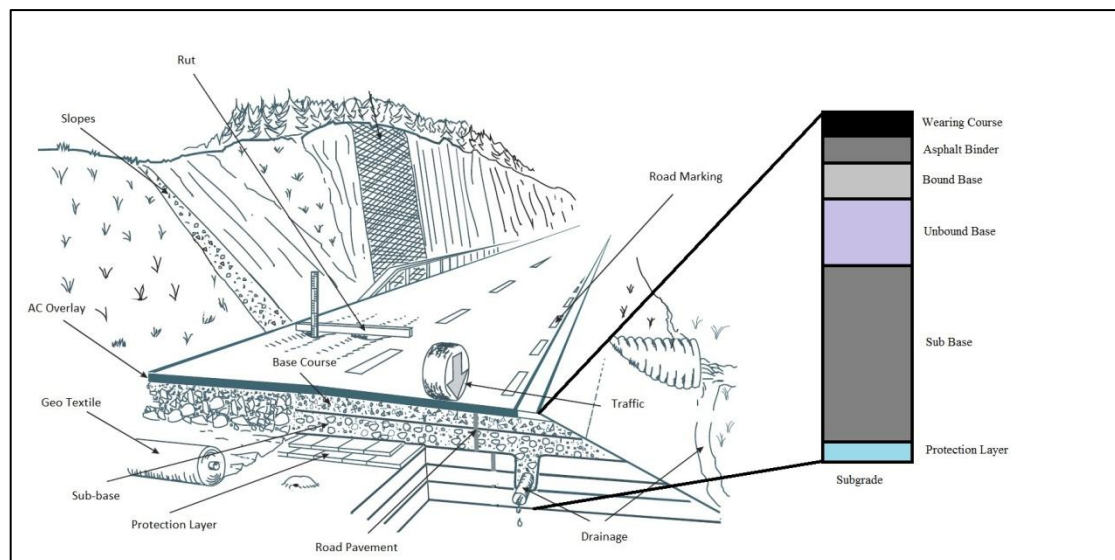


Figure 2.1: Fundamental sketch of road and pavement design (SRA, 2008).

In some cases, the base and/or the sub base are stabilized (with bituminous or cementitious admixtures) or absent depending on the strength and stiffness of the sub grade material. Hot mixed asphalt is the most common type of flexible pavement especially on moderate to heavily traffic highways. The most common aggregate type used in the mixture is 25 mm but there are varieties of gradation used in special situations. The surface course is further divided into wearing course and binder with each component contributing differently to a high pavement performance. The main design factors are traffic loads and temperature variations (U.S. Department of Transportation, 2006).

### 2.2 Pavement Serviceability

The state of pavement structure determines the costs involved in travel, including vehicle operation cost, delay and crash expenses. Together with the cost, the safety and comfort required by road users are emphasized. Pavement serviceability describes

the potential to serve a specific traffic volume at a present pavement condition. Uneven road surfaces result in wear and damage to vehicle suspension and tires (Huang, 2004; Öberg, 2001). The serviceability of road pavement is influenced by factors such as; climate, pavement thickness, traffic volumes and materials.

Evaluation of pavement serviceability depends on the data collection of pavement surface. Pavement distresses depict defects in construction caused by traffic load and environment. The effect of road surface distress can be structural and /or functional and the source of distress as load or non-load associated as shown in Table 2.1. The critical distresses involved in pavement serviceability state determination are ruts and cracks which are further discussed (Huang, 2004).

*Table 2.1: Distress in asphalt pavements (Huang, 2004).*

Type of distress	Structural	Functional	Load depended	Non-load
Fatigue cracking	Yes	No	Yes	No
Settlement	No	Yes	No	Yes
Rutting	No	Yes	Yes	No
Swelling	Yes	Yes	No	Yes
Wearing	No	Yes	No	Yes

The serviceability condition of pavement structure is often described by the following indices; present serviceability index (PSI), performance index (PI), present serviceability rating (PSR).

### 2.2.1 PSI

The most used index to determine the serviceability condition of a road is PSI and was developed at the AASHO Road Test. The concept is based on both pavement roughness and distress condition, such as cracks, rutting, potholes, patching etc (Ullidtz, 1998). The index is expressed as:

$$PSI = 5.03 * 1.91 * \log(1 + SV) - 0.01 * \sqrt{(C + P)} - 1.38 * (RD)^2 \quad (\text{Eq. 2.1})$$

Where;

PSI	Present Serviceability Index.
SV	Mean slope variance for the longitudinal profile (Over one foot).
C	Major cracking in feet per 1000 square feet area.
P	Patching in square feet per 1000 square feet area.
RD	Mean rut depth for transverse profile in inches.

### 2.2.2 Cracks

Accumulation of fatigue damage caused by increase in successive vehicle load result in series of interconnected polygonal pattern in form of alligator skin, block cracking, longitudinal and transverse cracking (Papagiannakis et al., 2007). Alligator cracking originate from the bottom of the asphalt layer or stabilized base where high tensile stress occur under the tires. Block cracks are rectangular pieces caused by shrinkage of hot mix asphalt due to daily temperature variations which result in cyclic stresses and strains (Huang, 2004). Cracking is considered as one of the major structural distress and is measured in square feet or square meter of the surface area.

### 2.2.3 Rutting

Permanent deformation (rutting) of asphalts manifests itself as a settlement in the pavement wheel path. Water is collected in these wheel path and cannot drain freely from the surface which is a potential safety hazard. The development of rut in asphalt layers has generally been described by two main stages. The primary stage is consolidation (densification) while the second stage consists of shear deformation (plastic flow not associated with volume change). In extreme cases, both may occur concurrently leading to distortion of layers (Werkmeister, 2003). Permanent deformation occurs longitudinally along the wheel path of vehicle and small bulging on the side wheel path with increase in wheel load applications as shown in Figure 2.2.

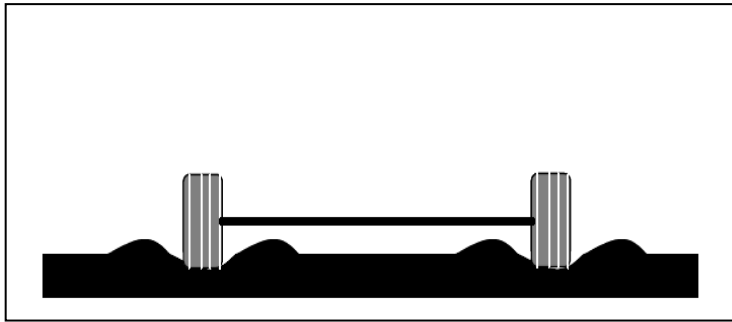


Figure 2.2: Illustration of structural deformation caused by heavy traffic (WSDOT, 2008).

Permanent deformation concentrated on the surface asphalt layers tend to give a narrow rut depth, while deep seated permanent deformation from the underlying unbound layers and subgrade typically gives much broader rut width on the surface (FHWA, 2006).

The two major phenomena, thus consolidation and shear deformation contributes in varying degrees to the permanent deformation in all pavement layers including the asphalt concrete course, asphalt base course, unbound base and the subgrade. Application of high wheel loads and tire pressure of heavy traffic on asphalt concrete layers, particularly near the surface, result in permanent deformation in the asphalt layer. Permanent deformation in the subgrade is considered to be maximum due to excessive vertical stress on the top of the sub grade by heavy wheel loads. However, limiting the subgrade deformation is achieved by good asphalt pavement design, thus by distribution of stresses as shown in Figure 2.3.

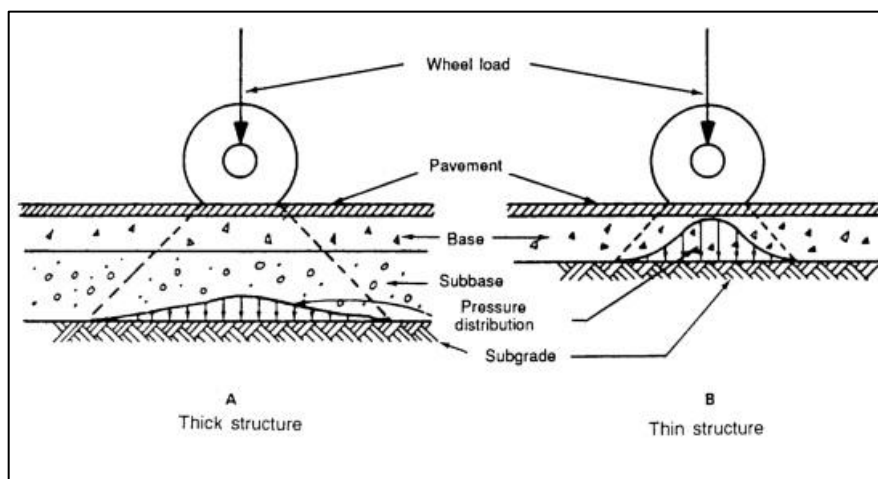


Figure 2.3: Stress distribution in pavement structure (NCHPR, 2004).

If high stresses are subjected to weak pavement structure, the pavement layers under the wheel loads initially undergoes densification and subsequently shear flow in the various pavement layers. Under such situation, all the components of the pavement structure contribute to the total deformation of the pavement. The rut depth under the wheel paths will then be the sum of the permanent deformation of all the pavement layers.

Further research work of Eisenmann and Hilmer (1982) also concluded if the pavement has been compacted to higher density during construction, it is unlikely for further densification during the application of wheel loads, and rutting is induced predominantly due to shear flow of asphalt mixture (Korkiala-Tanttu, 2009).

## 2.2.4 Measurement Methods

Measurement of pavement surface distresses are performed annually in Sweden. The data, rut depth and IRI, is compiled by the SRA in a data base for each 20 meters of road. The measurement is performed by a Road Surface Tester (RST) car see Figure 2.4 (Öberg, 2001).



Figure 2.4: RST car used in Sweden (VTI, 2001).

The rut data is obtained by 17 sensors distributed over 3.65 meters, by which a cross sectional profile is acquired as shown in Figure 2.5. The profile is used as foundation to calculate maximum rut depth for each wheel path. For each meter of road surface, 10 measurements are done and average for 20 meters is presented in the database (Öberg, 2001).

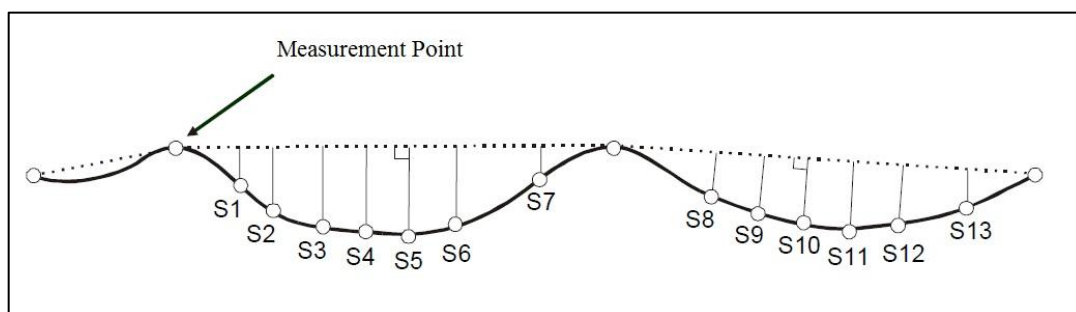


Figure 2.5: Cross sectional profile obtained from the sensors (Öberg, 2001).

## 2.3 Deterioration of Pavement Structure

There are couple of distresses which contribute to pavement deterioration. But the most prevalent distress affecting pavement structure is known as permanent deformation (i.e. rutting). Extreme pavement deformation result in higher rehabilitation cost. One of the main aspect of pavement design philosophy is limitation of rut development in the pavement structure. Although measuring rut depth is normally considered as simple task, the prediction of rut development is extremely complex (Lekarp et al 2000).

Pavement deformation can be categorized into elastic (resilient) deformation which are those that are recoverable and plastic (permanent) deformation which are non-recoverable. Permanent deformation can further be classified as primary densification, creep and structural failure. The cause of these deformations may be due to inadequate maintenance, excessive load, environmental and climatic conditions and disintegration of pavement component materials. Furthermore, the rate of accumulation depends on factors such as; material properties, stress level, and loading condition. These stages are further described in the Shakedown theory which tries to explains into details how stresses in granular material are distributed for elastic and permanent deformation.

Currently available mechanistic flexible pavement design and analysis procedure can be used to design a flexible pavement with adequate structural capacity to minimize the strains induced by the traffic loads, thus reduction of permanent deformation.

### 2.3.1 Traffic Loads

Wheel load on pavement result in distribution and reduction of stresses throughout the pavement structure, as shown in Figure 2.3. Especially for flexible pavement, stresses induced in a pavement structure by traffic loads are highest in the upper layers and diminishes with depth. Stresses acting on elemental cube of pavement system experience normal and shear stresses on the opposite sides of the cube, as pavement are subjected to traffic load as shown in Figure 2.6a. The resulting stresses are represented as principal stresses  $\sigma_1$ ,  $\sigma_2$  and  $\sigma_3$  (Lekarp, 1997). The principal stresses are independent of a chosen coordinate system. When a pavement structure is subjected to loads induced by traffic wheel, it is classified as a dynamic load. The resultant stress consists of horizontal, vertical and shear component. These stresses are rotationally and changes as the wheel load passes. According to Figure 2.6b, the principal stresses are horizontal and vertical whereas the shear stress component is nullified, that is, directly underneath the center of the wheel. This is a result of reversal shear stress as the wheel passes (Lekarp, 1999).

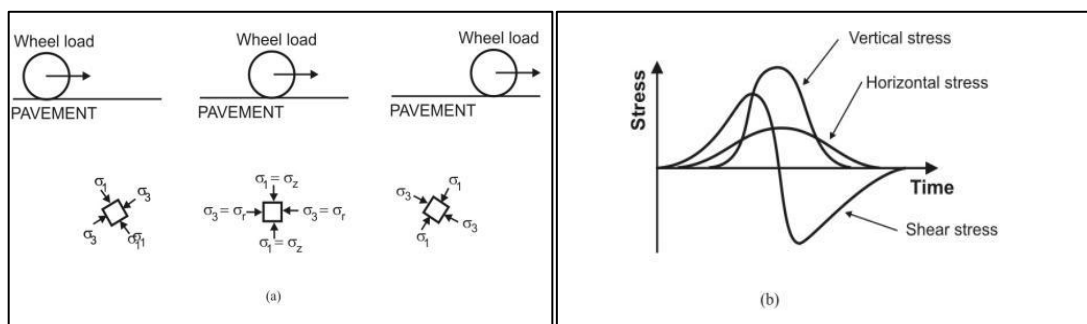


Figure 2.6: a) Load associated stresses in pavement structure. b) Stresses with respect to time.

Accumulation of permanent deformation is a gradual process by which each of the load application contributes to a small increment of deformation. The factor to consider when analyzing the behavior of material is number of load cycles.

According to researchers, the effect of load cycles on the resistance deformation of granular material increase as moisture content decrease. Further investigation indicates that, after relatively large number of load application, the rate of plastic deformation will experience sudden increase. This development of permanent deformation may not be expressible as a simple function, because, materials which appears to be approaching stable condition turns to be unstable once it is subjected to further loading.

### 2.3.1.1 Definition of ESAL

Although it is not complicated to determine the number of loads subjected to pavement structure, it turns out to be fairly difficult to determine the extent of damage the loads contributes to the pavement structure during the life span. This complication is overcome by introduction of Equivalent Single Axle Load (ESAL). The approach includes conversion of wheel from various repetitions and magnitudes, mixed vehicle traffic, to damage from equivalent loads i.e. ESAL. The used ESAL in Sweden is 100 kN axel as shown in Figure 2.7 .

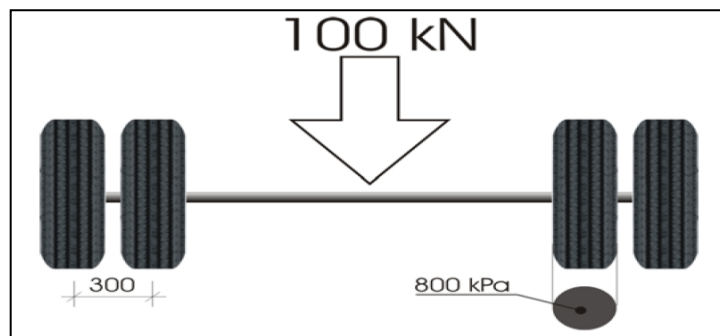


Figure 2.7: Illustration of an Equivalent Standard Axle Load, ESAL (VVTK, 2008).

The ESAL conversion, relates various axle combination to 100 kN single axle load by introducing equivalency factors. The traffic conversion formula is expressed as follows (VVTK, 2008):

$$ESAL = AADT * A * C * D * E * 3.65 * \left(1 + \frac{100}{k}\right) * \left(\left(1 + \frac{k}{100}\right)^n - 1\right) \quad (\text{Eq. 2.2})$$

ESAL	Equivalent Single Axle Load
AADT	Average Annual Daily Traffic in design lane.
A	Portion of heavy traffic in %.
C	Number of axles/heavy vehicle.
D = 0.3	Factor describing average number of ESAL per heavy vehicle axle.
E = 0.8	Correction factor considering the width of the road.
n	Design period in years.
k	Annual heavy traffic change in %.

Forecasting the traffic amount becomes therefore an essential element in pavement design. The process simply starts with traffic count or by studying historical traffic data followed by estimation of heavy traffic (White, 2007).

In Sweden, the portions of heavy traffic are available as average values for different types of roads including national road, regional road and local road (SRA, 2000). The values are presented in Table 2.2. Further information needed for estimation of number of ESALs subjected to pavement structures is number of axles per heavy vehicle, which can be acquired by traffic count or historical data. Values for Swedish roads are also presented in Table 2.2.

Table 2.2: Estimation of heavy traffic in [%] and number of axles/heavy vehicle.

Type of Road	Portion of heavy traffic	Number of axles/heavy vehicle
National road	14	5
Regional road	8	4.5
Local road	5	3.8

There are difficulties in estimation due to high variation in load size of heavy traffic-pool. Further complication arises considering direction of the traffic. An example of such problem is highlighted in petrol producing countries, where gas trucks are fully loaded in one direction and empty in the opposite direction of the road. Thus, the traffic have different ESAL factors in each direction of the road.

The relative damage to the pavement structure caused by the varying axle loads can be converted to equivalent number of standard loads. The damage of a particular load,  $W_x$ , relative to the standard axle load,  $W_{10}$ , is expressed by Generalized Fourth Power Law as (AASHTO, 2004):

$$Relative\ Damage = \left(\frac{W_x}{W_{10}}\right)^4 \quad (Eq. 2.3)$$

### 2.3.2 Environmental Loads

Environmental factors have been contributing immensely to the deterioration of pavement structure. According to Monismith and Finn (Korkiala-Tanttu, 2009), the presence of moisture in pavement structure can be related to the prevailing environmental conditions. Although the amount of water content presence has a positive influence on the strength and stiffness of unbound material, its impact is much noticeable on the resilient modulus when the material comes close to saturation. Moisture content is dependent on seasonal variation and capillary action. Werkmeister (2003) reported that, low moisture content increases the strength of the materials. The effect depends on the content of fines; that is, the resilient modulus decreases when the material reaches saturation. More importantly, the performance of pavement structure is dependent on the conductivity of the unbound granular materials (UGM). Thus, if there is an accumulation of moisture, the pavement may develop excess pore pressure reducing the effective stress ( $\sigma^1$ ) leading to less material strength as shown in equation 2.3. Haynes and Yoder (1963) found the total permanent strain rose by

more than 100% as the degree of saturation increase from 60% to 80%. Thom and Brown (1987) also suggested that, a large increase in permanent strain could occur even without the generation of excess pore water pressure, and stated further that the relatively small increase in water can trigger a remarkable increase in permanent strain.

$$\sigma^1 = \sigma - u \quad (\text{Eq. 2.4})$$

Where  $\sigma$  is the in-situ stress and  $u$  is the pore water pressure.

Temperature variation in a country also contributes to permanent deformation. The Swedish Road Administration (2008) published a document which categorizes the climate zone into five regions. These climate zones characterize the temperature throughout the year and the ground freezing potential.

Another environmental effect is frost penetration due to the cold weather condition. This result in stronger subgrade in the winter but weaker during the spring period. Although frost heave result in creep settlement and pavement roughness, most devastating effect happens in the spring season when the ice melts and saturates the subgrade. It is therefore necessary to protect the subgrade by using non-frost susceptible material within the frost penetration zone (Huang, 2009). Figure 2.8 illustrate the process (White, 2007).

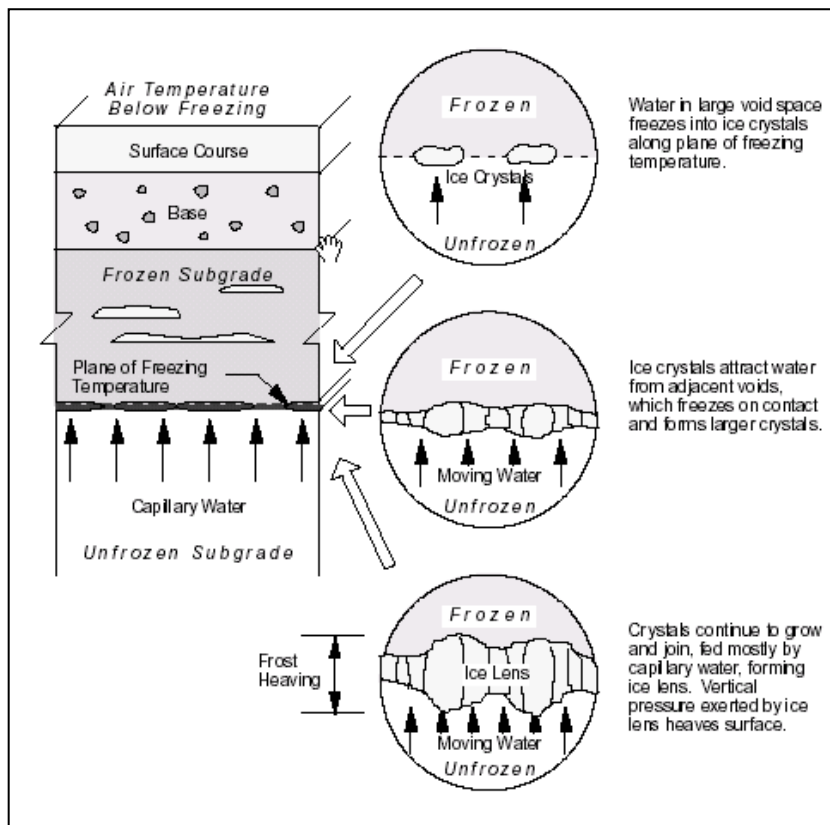


Figure 2.8: Frost in pavement structure (White, 2007).

### 2.3.3 Material Behavior

Characteristic property of material determines the layer thickness in pavement design. Although the resilient modulus alone cannot duly characterize the functionality of the UGM, it should be capable to safely handle the stresses without excessive deformation. However, important mechanical characteristic of pavement material is stiffness. The relative stiffness of various layers dictates the distribution of stresses and strain within the pavement system. It may rather seem unusual that stiffness is considered important in material property for pavements. However, Load carrying capacity is an essential parameter to pavement structural design, which provides sufficient pavement strength to avoid permanent deformation.

The AASHTO Design Guide beginning in 1986 have recommended the resilient modulus ( $M_R$ ) for characterizing support of flexible pavement. Also the NCHRP 1-37A Design Guide recommends the  $M_R$  as a primary material property input for unbound materials. Investigators in 1950 used repeated load triaxial to evaluate the stiffness and other behavior of unbound pavement materials.

$M_R$  is the ratio of the recoverable (elastic) strain after many cycles of loading (Figure 2.9), thus the measure of stiffness. In a cyclic triaxial test the  $\sigma_a$  and  $\epsilon_a$  are the stress and strain in the axial direction respectively. The axial stress is cycled at a constant magnitude ( $\Delta\sigma$ ), with an induced unloading cyclic resilient strain ( $\Delta\epsilon$ ) as shown in Figure 2.10 (U.S. Department of Transportation, 2006).

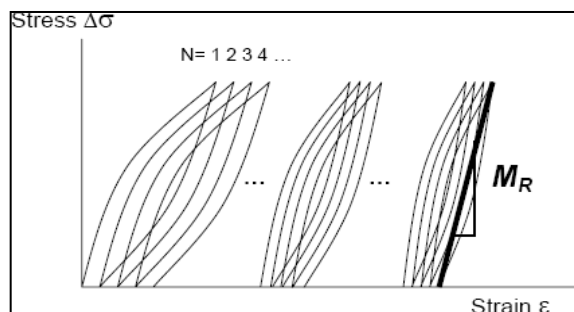


Figure 2.9:  $M_R$  under cyclic loading.

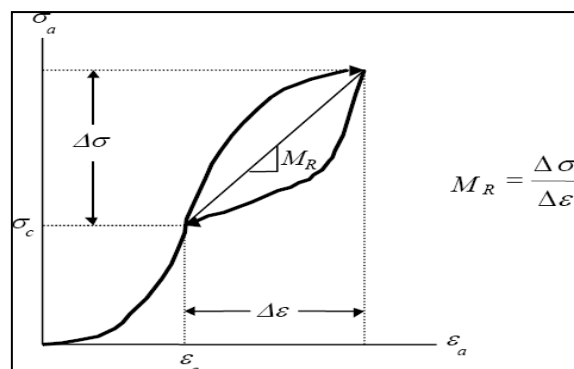


Figure 2.10: Definition of  $M_R$  for cyclic triaxial loading.

The resilient modulus ( $M_R$ ) is then be express as:

$$M_R = \frac{\Delta\sigma}{\Delta\epsilon} \quad (\text{Eq. 2.5})$$

Another relationship used in determining the resilient modulus with respect to stress is the K- $\theta$  model by Hicks and Monismith (1971).

$$M_R = K_1 * \left(\frac{\theta}{p_0}\right)^{K_2} \quad (\text{Eq. 2.6})$$

Where,

$\theta$  Bulk stress = sum of the principal stresses ( $\sigma_1 + \sigma_2 + \sigma_3$ )

$K_1$  and  $K_2$  Material constants

$P_0$  Reference pressure

The E-modulus of bound and unbound materials listed in Table 2.3 and Table 2.4 are based on falling weight deflectometer tests (FWD) on Swedish roads.

Table 2.3: E-modulus of different pavement materials in summer (SRA, 2000).

Material type	E-Modulus [MPa]
Bituminous Layer	4000
Unbound Base	200-700
Unbound Subbase	200-600

Table 2.4: E-modulus of different subgrade materials in summer (SRA, 2000).

Material type	E-Modulus [MPa]
Soft Clay	5-25
Clay	20-60
Dry crust	30-80
Silt	15-45
Sand	30-100
Rock	1000

### **Material Factors**

The factors that influence material behavior include density, water content, gradation, fine content and temperature.

The impact of density on pavement structure can be described by the degree of compaction. It has been regarded in previous studies as being significantly important for the long-term behavior of granular materials (Thom and Brown 1988). Resistance to permanent deformation under repeated cyclic loading increases as a result of

increased in density (Holubec 1969; Barksdale 1972, 1991; Allen 1973; Marek 1977; Thom and Brown, 1988). Observations made by Barksdale (1972) proved that, an average of 185% more axial strain when the material is compacted at 95% instead of 100% of the maximum compactive density obtained from the hammer drop test.

Suggestion made by Holubec (1969) indicated a reduction in plastic deformation due to increased in density especially for large angular aggregates. For rounded aggregate, it is virtually not the case because a decrease in deformation with an increase in density is not considered to be significant. These aggregates have relatively higher density than the angular aggregate for the same compaction effort.

Grading of UGM is also of importance to deformation resistance in the pavement structure. Previous studies indicate stiffness of a material to some extent dependent on the particle size and distribution. Literature has no clear distinction on the impact of fines contents on material stiffness. However, (Thom and Brown 1987; Kamel et al.1993) reported that, the resilient modulus generally decrease with an increase in fines. Hicks and Monismith (Austin, 2002) noticed some reduction in the resilient modulus with an increase in fine content for partially crushed aggregate, whereas the effect was reported to be opposite when the aggregate were fully crushed. Kolisoja (Korkiala-Tanttu, 2009) also discovered a high content of fines make material more sensitive to accumulation of water content.

The Swedish Road Administration has carried out several test on deformation properties for types of coarse crushed rock for base course material with test road and accelerated pavement tests. The maximum grain size varied between 90 mm up to 300 mm (Fredrickson and Lekarp, 2004). Figure 2.11 illustrates the rut depth test results of their research and number of load application. As shown in Figure 2.11, the coarse crushed rock base course material deform less than the fine grain.

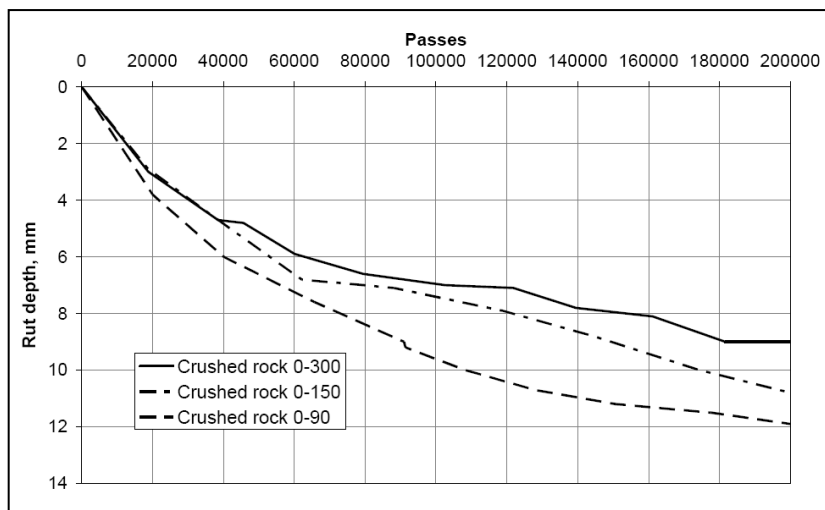


Figure 2.11: Effect of aggregate distribution to permanent deformation.

Austin (2002) investigated the impact of aggregate type and surface characteristics on aggregate permanent deformation. And it was concluded that, the flat shape aggregate are more susceptible to deformation than the crushed angular type. However, cubic aggregates, rounded river gravel with smooth surface is much susceptible to rutting than crushed aggregates.

With temperature as a significant parameter to the resilient modulus, the material strength also depends on temperature. Asphaltic materials are highly sensitive to temperature variations. At cold temperature and short loading time, the material will tend to behave in an elastic mode with high E-modulus. In contrast, at high temperature and long loading time, the material approaches viscoelastic-plastic mode.

Water content in UGM is another factor affecting the E-modulus in pavement structure. A decrease in moisture content leads to suction which increases the cohesion between the particles. Thus, low content of moisture result in increase of E-modulus. However, high moisture content can develop pore pressure, resulting in decrease of effective stresses and subsequently a decrease of E-modulus.

## 2.4 Material Modelling

Pavement materials generally do not deform under traffic volumes with purely elastic behaviour. They often show viscous, visco-elastic or plastic deformations. The theory of material behaviour describes the way material responses to load based on material properties. It consists of relationship between stress and strain (linear or non linear), time dependency of strain under constant load level (viscous or non viscous) and degree to which material recover after removal of stress (elastic or plastic). The theory of elasticity is used for calculating responses (i.e. stresses, strains and deflection) in pavement structure. Typical deformation behaviour in pavement materials are shown in Figure 2.12 (Ullidtz, 1998).

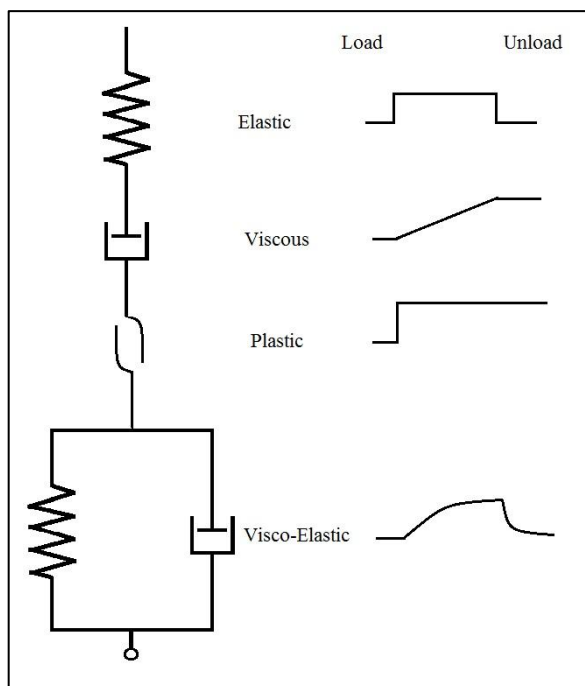


Figure 2.12: Typical deformation in pavement materials (Ullidtz, 1998).

Permanent deformations are independent of time as shown in Figure 2.12 but in reality is not instantaneous.

In reality, pavement materials are non linear (especially UGM), but linear model would be applied in case of small load.

Deformation properties of bituminous materials depend on temperature as well as the loading time. At low temperatures the materials behaviour is elastic and viscous at high temperatures. When the loading time is short, it is also elastic and viscous with long loading time. At intermediate temperature and loading time the material behaviour will be viscoelastic. Due to the these complexities in material behaviour, an elastic and viscous element may be combined in parallel (Kelvin's model) or in series (Maxwell's model) to represent the behaviour. In practice viscoelastic models require much time to completely recover the strain for deformation to be considered as plastic in nature. Unlike the Kelvin model, Maxwell model gives permanent deformation.

Further complications in material behaviour requires a combination of Maxwell and Kelvin models which is termed as Burger's model as shown in Figure 2.13.

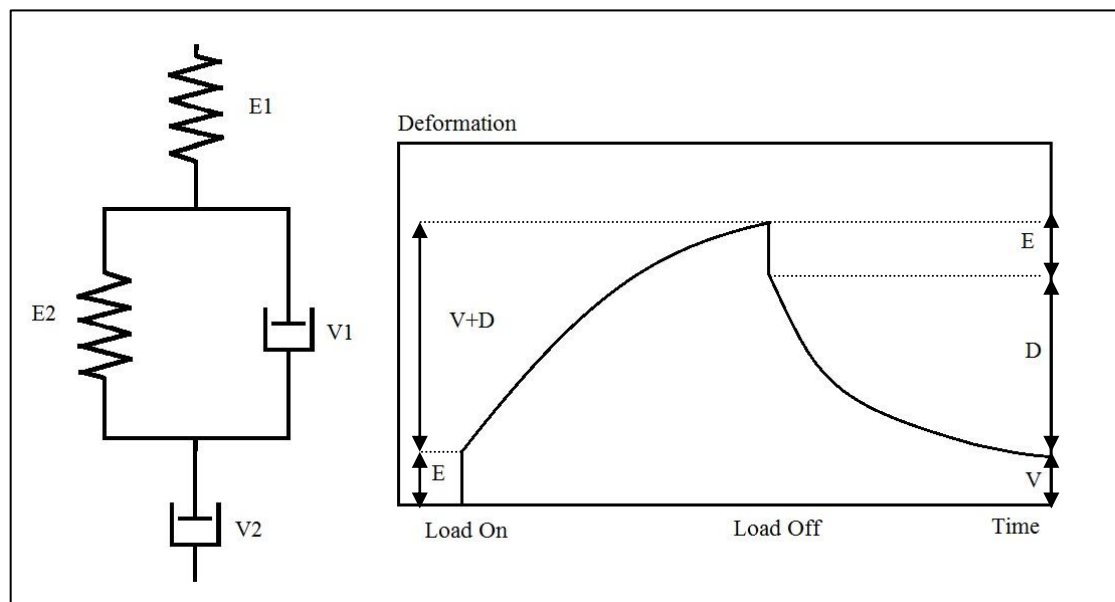


Figure 2.13: Burger's material model and deformation under constant load.

When the load is applied, the elastic component E1 reacts first and at the same time the elastic component E2 starts to react but slows down by viscous component V1. Element E2 and V1 makes together the viscoelastic component. The viscous component V2 is displaced relatively to the loading time (Blomberg, 2002).

## 2.5 Shakedown Theory

The theory of shakedown determines the long term behavior of unbound materials. The concept is based on materials been modelled to show elastic and plastic behaviour in response to the loading and unloading conditions imposed by traffic loads. Werkmeister (2004) and Arnold (2004) used permanent deformation based on Repeated Load Triaxial (RLT) tests to categorise the plastic response of different granular material into Range A,B and C.

At low stresses, the material is purely elastic, where no plastic deformation takes place upon unloading. As shown in Figure 2.14, the path of elastic response of loading and unloading is the same and there is no shift in horizontal direction. However, if there is an increase in load, the material begins to develop small level of permanent deformation over few cycles. Subsequently, as the cycle increases there will be no additional plastic deformation but yield the same deformation. The deformation at this level is small, because of particle slipping and density change as the material adjusts to the applied traffic loads. This is referred to as elastic shakedown (Range A).

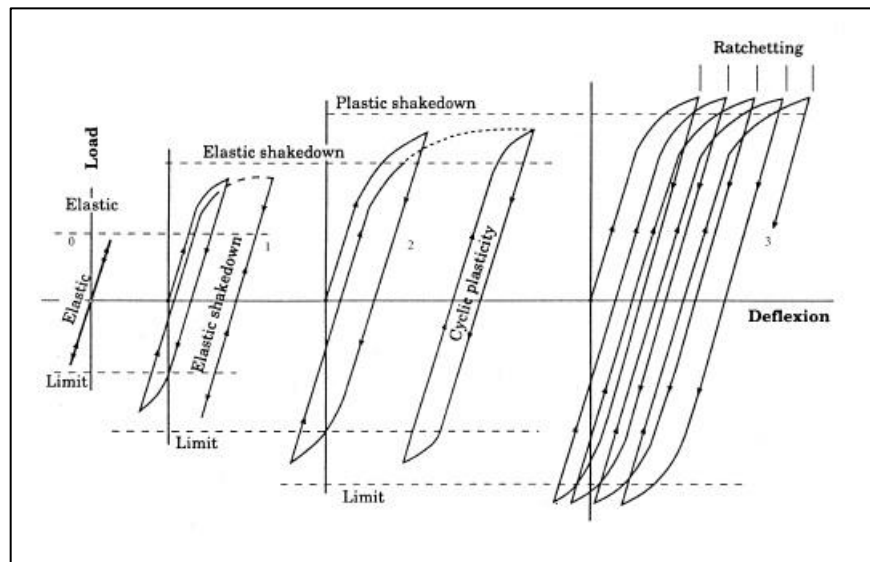


Figure 2.14: Elastic and plastic behaviour of materials under repeated cyclic load (Werkmeister, 2003).

Further increase in cycle loads result in plastic shakedown behaviour (Range B). Within this range, the material particles develop plastic deformation higher than that in elastic shakedown region. The plastic deformation development stops after a number of cycle loads. And this referred to as plastic shakedown limit. However, the plastic deformation does not stop completely, but continues to develop at constant rate. This range has been referred as plastic creep deformation. Materials in the plastic shakedown and plastic creep range experience a constant level of resilient deformation.

The last range, Range C, as shown in Figure 2.14, materials experience plastic deformation at an increase rate until complete failure. In this range, an aggregate experience significant crushing, abrasion and breakdown.

For better performance of pavement structure, Range A or B are required. Applied load defines a stress state within the boundary of Range A and B behaviour, and is called critical shakedown stress.

## 2.6 Wearing due to Studded Tires

Each winter, over 100 000 tons of particles are wear down from Swedish roads as a result of use of studded tire. This number was even higher in early 1980s, approximately 300 000 tons/winter due to poor pavement material. Rigorous research has enormously reduced the wearing as a result of several combined factors, for instance, improvements of the wearing properties of the HMA (Hot Mixed Asphalt) during 1990s. Even though the wearing due to studded is decreased substantially, it is important to consider its degradation on the pavement as a problem (Öberg 2001).

Studded tire can cause rut when studs chip into pavement surface, especially when the vehicle moves at high speed on the road. The extent of rut depth caused by studded tire can be attributed to the type of pavement surface (i.e. flexible or rigid pavement), stud length, vehicle speed, number of studs per tire, volume of traffic etc. The type of rut caused by studded tires is termed as “Ravelling.” Although the structural deformation and wearing produce the same result, the effect and appearance are quite different. Figure 2.15, illustrate wearing caused by studded tires. The Road Surface Tester (RST) used in measuring rut depth cannot distinguish between the two types of damage on the surface of the hot mix asphalt pavement.

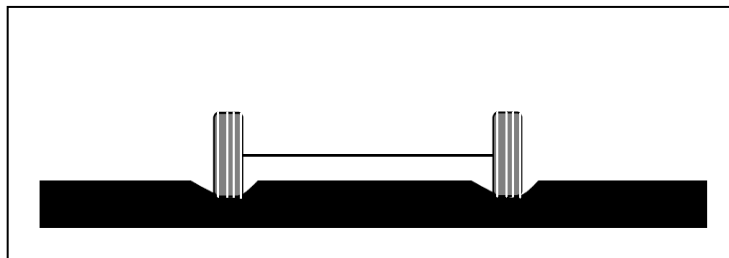


Figure 2.15 Illustration of wearing caused by studded tires (WSDOT, 2008).

The Swedish Road and Transport research Institute, VTI, has developed a model for prediction of asphalt wearing due to studded tires. The model is based on Microsoft Excel and consists of three parts, the wearing due to studded tires, the rut distribution over the road section and a part that predicts the costs. The model is developed based on wearing data from research and development work from the past twenty years (VTI, 2006).

## 2.7 Pavement Design Models

Modern models aim to predict the functional and structural deterioration of pavement layers during the design life. Pavement performance models are based on a long term studies. However, limited knowledge of material behavior and uncertainties in pavement structure, environmental condition and traffic loads contributes to the deficiencies in these models. Pavement response models can be categorized into multi-layer elastic and finite element models which evaluate pavement response.

### 2.7.1 Response Models

Multi-layer elastic model is an analytical model which determines stresses, strains and deflection at any point of multi-layer pavement structure as shown in Figure 2.16. The theory assumes the pavement structure to be homogeneous, isotropic and linearly elastic.

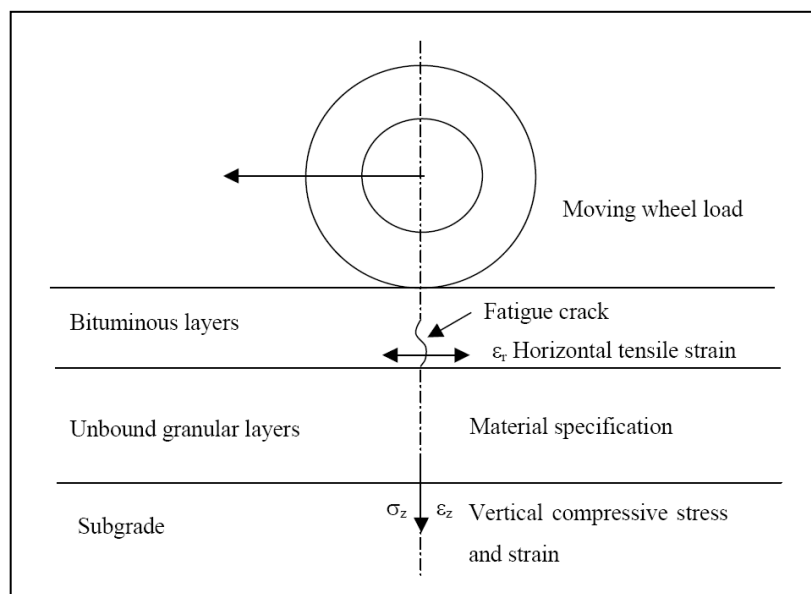


Figure 2.16: Critical stresses and strains in pavement structure (Werkmeister, 2003).

According to researchers (Boussinesq, 1985 and Burmister, 1945), the theory presumes the layers to be infinitely horizontal with no discontinuities and the bottom layer (subgrade) infinitely extends downwards. The most used input parameters for the model are material properties (modulus of elasticity and Poisson ratio), layer thicknesses and a static load condition.

In recent years several response models have been developed to determine the critical stresses and strains. These include VägFEM, VEROAD, NOAH, CIRCLY, JULEA, WESLEA, WESDEF, VESYS etc., see Table 2.5.

Table 2.5: Response models and theirs features and limitations.

Response model	Features	Limitations
VägFEM	FEM with linear or non-linear material behavior.	3D model that takes into account geometry of the road.
WESDEF	<ul style="list-style-type: none"> <li>- Seasonal changes.</li> <li>- Probabilistic analysis.</li> </ul>	Stress calculations is base on elastic multilayer theory.
JULEA	<ul style="list-style-type: none"> <li>- Lateral wander.</li> <li>- Seasonal changes.</li> </ul>	FEM with linear or non-linear material behavior.
VEROAD	Linear elastic and visco-elastic multilayer model.	Stress calculations based on elastic multilayer theory.
NOAH	<ul style="list-style-type: none"> <li>- Linear elastic and visco-elastic multilayer model.</li> <li>- Anisotropy.</li> </ul>	Stress calculations based on elastic multilayer theory.

## 2.7.2 Performance Models

The performance models are based on empirical relations of pavement response. Permanent deformation is determined from maximum compressive strains in the unbound materials. Deformation is directly calculated if the stress-permanent strain of the material is known. The accumulation of permanent deformations are then estimated with respect to number of load passes (traffic volumes), and environmental conditions. There are several models available for estimating the accumulation of permanent deformations. These include Gidel model (only for unbound materials), Dresden model (For entire pavement structure), NCHRP 1-37A (For entire pavement structure), and MMOPP (For entire pavement structure). NCHRP 1-37A, which is included in M-E PDG and MMOPP is further described in chapter 2.7.3 and 2.7.4.

## 2.7.3 M-E PDG

Mechanistic –Empirical Pavement Design Guide (M-E PDG) completed in 2004 was developed by the National Cooperative Highway Research Program (NCHRP) Project 1-37A to replace the AASHTO Design Guide developed in 1993. M-E PDG utilizes the existing mechanistic-based models and the databases from Long Term Pavement Performance (LTPP) program. The software incorporate elastic layer analysis to predict pavement deterioration in terms of cracking and rutting. The predictions are based on heavy traffic loads, sub grade type and layer thicknesses. Cumulative effect of environment and traffic contribute to the pavement performance (NCHRP, 2004).

Flexible pavement design rely on input parameters including traffic data (load categories for single, tandem, tridem and quad axles), material and sub grade characterization, performance criteria, climate factors and others (NCHRP, 2004). M-E PDG operates under hierarchical approach, that is different levels of input data:

- Level 1 requires the most comprehensive engineering design inputs. Level 1 data include material properties obtained from field tests or laboratory testing, e.g. triaxial tests. Further input data include traffic and environmental data.
- Level 2 uses testing results which are mostly correlated data. For example sub grade modulus can be estimated by empirical method with other tests, such as California Bearing Ratio (CBR) test, Cone Penetration Test (CPT), etc.
- Level 3 use national or regional default values to define input parameters.

Multi-layer elastic theory, is applied in the analysis procedure, with the exception of level 1 where the non linearity of unbound material is considered. Current research is based on this particular procedure for pavement design. JULEA is the response model in M-E PDG. The model estimates the response of the pavement structure by finite element linear elastic procedure.

M-E PDG considers rutting in three stages, primary, secondary and tertiary as shown in Figure 2.17. Permanent deformation in primary stage is associated with change in volume of material, thus compaction (Zhou et al, 2002). The secondary stage of rutting shows constant slow rate of increase in rutting with an increase in shear deformation at the same rate as shown in Figure 2.17. The tertiary stage shows high level of rutting related to plastic deformation under no volume change.

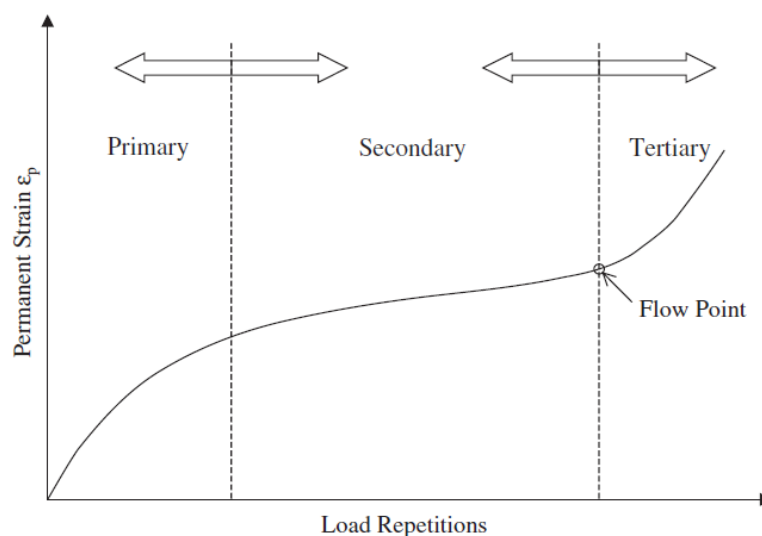


Figure 2.17: Levels of pavement deformation (M-E PDG, 2004).

### 2.7.3.1 Climate Conformity to Swedish Conditions

The existing climate data used in M-E PDG is from various American states. Therefore, comparison of climate data to Swedish conditions in Zone 2 was necessary since it has a significant influence on the pavement performance.

The zone 2 has a similar climate as Boston in Massachusetts state. The average temperatures of Gothenburg and Boston are shown in Table 2.6.

Table 2.6: Average temperatures of Boston and Gothenburg.

City	Jan	Feb	Mar	Apr	May	Jun	Jul	Aug	Sep	Oct	Nov	Dec
GBG	-1.0	-1.8	2.5	6.7	11.3	16.2	18.8	17.7	14.1	6.1	5.7	3.6
Boston	-1.5	-0.3	3.8	9.1	14.7	20	23.3	22.4	18.2	12.3	7.2	1.6

### 2.7.3.2 Estimation of Permanent Deformation

Permanent deformation is obtained by estimating the plastic deformation of each pavement layer (asphalt bound and unbound layers) over the pavement design life by the M-E PDG model. Deformation is estimated in each sub layer of a defined sub season using the incremental damage over the years. The cumulated permanent deformation, PD, at the mid-depth is an estimated deformation for each individual sub layer, as given in the expression below:

$$PD = \sum_{k=1}^n \epsilon_r^k * h^k \quad (\text{Eq. 2.7})$$

Where,

$\epsilon_r^k$  Plastic strain in the sub layer k.

$h^k$  Thickness of sub layer k

n sublayer Number of sub layers

The process is repeated for each axle load, lateral position of load (to account for wander effect) and sub increment of analysis period.

#### **Asphalt Layers**

Permanent deformation in asphalt bound layer is based upon laboratory procedure of load repetition of strain tests. The expression for permanent deformation in the asphalt bound layer is expressed as follows:

$$\frac{\epsilon_p}{\epsilon_r} = a_1 * T^{a_2} * N^{a_3} \quad (\text{Eq. 2.8})$$

Where,

$\epsilon_p$  Plastic strain cumulated for N load repetition

$\epsilon_r$  Resilient strain of asphalt material as a function of mix properties, temperature and loading time.

N Number of repeated load

$a_1, a_2, a_3$  Non-linear regression coefficient

T Temperature in F

In order for the laboratory repeated load test to fit the reality, a field calibrated factor  $\beta_{ri}$  is introduced to achieve the final field distress model. Thus, the equation 2.8 is updated as follow:

$$\frac{\varepsilon_p}{\varepsilon_r} = \beta_{r1} * a_1 * T^{\beta_{r2}a_2} * N^{\beta_{r3}a_3} \quad (\text{Eq. 2.9})$$

The equation 2.9 was further developed by researchers (Leahy, 1989; Ayres et al, 1998 & Kaloush et al, 2000) into subsequent expression:

$$\frac{\varepsilon_p}{\varepsilon_r} = k_1 * 10^{-3.4488} * T^{1.5606} * N^{0.479244} \quad (\text{Eq. 2.10})$$

It is achieved with the help of the national field calibrated model used in M-E PDG by numerical optimization and other modes of comparison. Where the national calibration factors,  $\beta_{r1}$ ,  $\beta_{r2}$  and  $\beta_{r3}$  are determined. In equation 2.10 it can be observed that a depth parameter  $k_1$  is introduced. This parameter has been obtained from MnRoad tests, for prediction of accurate rut depth of the model. The parameter,  $k_1$ , is defined as:

$$k_1 = (C_1 + C_2 * depth) * 0.328196^{depth} \quad (\text{Eq. 2.11})$$

$$C_1 = -0.1039 * h_{ac}^2 + 2.4868 * h_{ac} - 17.342 \quad (\text{Eq. 2.12})$$

$$C_2 = 0.0172 * h_{ac}^2 - 1.7331 * h_{ac} + 27.428 \quad (\text{Eq. 2.13})$$

Where,

$h_{ac}$  The total thickness of asphalt layers in inches.

Depth Computational point in inches.

$k_1$  is used to consider the variable confining pressure that occur at different depth. The parameter  $k_1$  is obtained by calibration of LTPP section to predicted deformations in asphalt layers as shown in Figure 2.18.

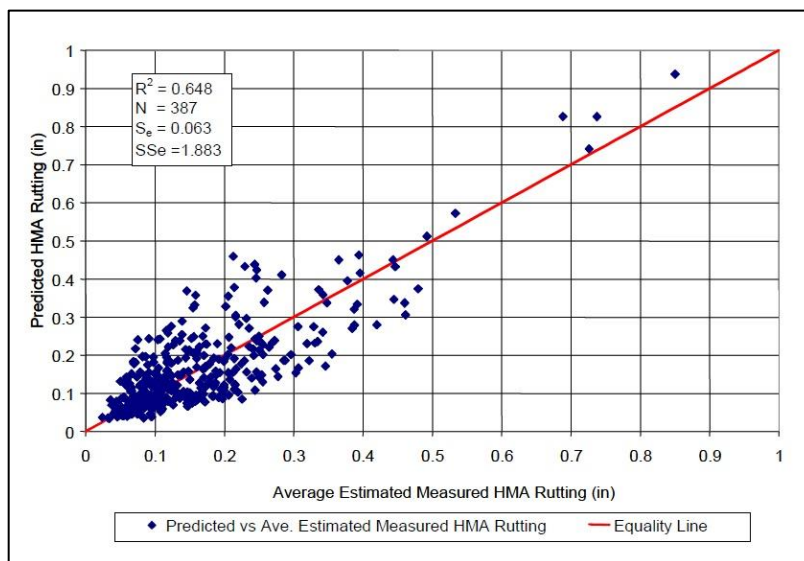


Figure 2.18: Calibration of predicted against measured asphalt rutting in MnRoad test.

### ***Unbound Layers***

Tseng and Lytton in 1989, postulated that the prediction for permanent deformation in unbound layers (granular base and subgrade) can be expressed as:

$$\delta_a(N) = \beta_i * \frac{\varepsilon_0}{\varepsilon_r} e^{-\left(\frac{\rho}{N}\right)^\beta} * \varepsilon_v * h \quad (\text{Eq. 2.14})$$

Subsequently, equation 2.14 is used in the M-E PDG model for prediction of permanent deformation in unbound layers.

Where,

$$\beta_i = \beta_{GB} = 1.673 \quad \text{For granular base}$$

And

$$\beta_i = \beta_{SG} = 1.35 \quad \text{For subgrade}$$

$\delta_a$  Permanent deformation for layer (inch)

N Number of traffic passes

$\varepsilon_0, \beta, \rho$  Material properties

$\varepsilon_r$  The resilient strain imposed in laboratory tests to obtain the material properties ( $\varepsilon_0, \beta, \rho$ ), (inches/inches)

$\varepsilon_v$  Average vertical resilient strain in layers

h Thickness of layer (inches)

M-EPDG rutting model allows user to access the effect of many pavement parameters. These parameters include; , monthly variation in surface and pavement temperature, change in asphalt and unbound modulus, pavement layer thickness, moisture variation in sub grade and unbound layers, traffic speed, penetration of asphalt binder, load configuration and lateral traffic effect.

The total permanent deformation in pavement structure is the summation of the individual layer permanent deformation for each season. The total permanent deformation is expressed as:

$$PD_{Total} = PD_{AC} + PD_{GB} + PD_{SG} \quad (\text{Eq. 2.15})$$

Where,

$PD_{AC}$  Permanent deformation in asphalt layers.

$PD_{GB}$  Permanent deformation in granular base.

$PD_{SG}$  Permanent deformation in subgrade.

## **2.7.4 MMOPP**

Mathematical Model Of Pavement Performance (MMOPP) is a pavement design model developed by the Danish road authorities. The MMOPP model can design flexible, semi-flexible and rigid pavements and simulate degradation of pavement structure due to traffic load, climate impact and selection of materials. The MMOPP is divided into two main functions, conventional analytical pavement design and performance model for prediction of pavement structure, which is used in this project.

The predicted degradation/permanent deformation is achieved by mathematically examining the pavement structure subjected to traffic load with the speed as variable. Furthermore, the method considers the fact that seasonal variations affects the permanent deformations.

In this section, the used models in MMOPP are described. The model describe pavement structure, load, climate, pavement response, structural degradation and permanent deformation.

### **2.7.4.1 Pavement Structure and Material Model**

The foundation of all pavement performance models is material characteristics and behaviour. In MMOPP, the description of the pavement structure is managed in two steps, the geometry which consist of the thickness of layers and the material properties, simply resilient modulus of each layer. The response of the bound layers is viscoelastic.

### 2.7.4.2 Climate Model

The model functions with the E-modulus as the main parameter for seasonal variations. A reference E-modulus is set for summer value. The factors for E-modulus at different seasons are shown in the Table 2.7, which corresponds to Swedish climate zone 2.

Furthermore, the climate model depends on the frost penetration. The magnitude of frost penetration can be estimated by equation 2.16 .

$$Frost\ Penetration = 45mm * \sqrt{Frost\ days} + \frac{Pavement\ Thickness\ (mm)}{2} \quad (Eq. 2.16)$$

The number of frost days are statistically calculated from historical data. The E-modulus of the subgrade depends on the magnitude of frost penetration, thus the deeper the frost penetration the higher E-modulus during frost period. On the other hand, as the frost thaw, the E-modulus reduces due to saturation of the subgrade.

Table 2.7: Factors of E-modulus for different season (MMOPP, 2007).

Season	Days	Temperature	E <sub>1</sub>	E <sub>2</sub>	E <sub>3</sub>	E <sub>m</sub>
-	-	(°C)	Wearing course	Bound base	Granular material	Subgrade
Winter	49	-2	4	4.2	10	20
Winter Thaw	10	1	3.7	0.33	10	20
Frost Thawing	15	1	3.7	0.67	0.7	0.6
Spring	46	4	3.1	1	0.85	0.8
Summer	143	20	1	1	1	1
Extreme summer	10	35	0.3	1	1	1
Autumn	92	7	2.6	1	1	1

### 2.7.4.3 Material Deformation Model

The permanent deformation prediction in MMOPP is divided in two parts, asphalt deformation and unbound granular material deformation.

The permanent deformation in asphalt materials with normal content of bitumen is described with Kirk's formula, expressed as follows:

$$\varepsilon_h = -0.000200 * \left(\frac{N}{10^6}\right)^{-0.178} \quad (Eq. 2.17)$$

Where,

$\varepsilon_h$  Permanent strain in the bottom of the asphalt layer.

N Number of load repetitions.

There is, however, a transition between laboratory and measured permanent strain, therefore the equation 2.18 is adjusted to be:

$$\varepsilon_h = -0.000230 * \left(\frac{N}{10^6}\right)^{-0.191} \quad (\text{Eq. 2.18})$$

Permanent deformation in UGM can be categorized into three phases, as shown in Figure 2.17. The estimation of permanent deformation in each phase is dependent on the equivalent layer thicknesses calculated from Odemark principles. The equivalent thicknesses are then used to calculate the plastic E-modulus. The three phases are defined as follows:

Phase 1: Decline rate of plastic strain.

Phase 2: Constant rate of plastic strain.

Phase 3: Increase rate of plastic strain (not considered in MMOPP).

Deformation caused by wheel load is not proportional to the vertical stress. Therefore, the estimation of plastic strain is given by following expressions:

Phase 1:

$$\varepsilon_p = A * N^B * \left(\frac{\sigma_1}{\sigma'}\right)^C \quad \text{For } \varepsilon_p < \varepsilon_0 \quad (\text{Eq. 2.19})$$

Phase 2:

$$\varepsilon_p = \varepsilon_0 + (N - N_0) * A^{\frac{1}{B}} * B * \varepsilon_0^{1-\frac{1}{B}} \left(\frac{\sigma_1}{\sigma'}\right)^{\frac{-C}{B}} \quad \text{For } \varepsilon_p > \varepsilon_0 \quad (\text{Eq. 2.20})$$

Where,

$$N_0 = \varepsilon_0^{\frac{1}{B}} * A^{\frac{-1}{B}} * \left(\frac{\sigma_1}{\sigma'}\right)^{\frac{-C}{B}} \quad (\text{Eq.2.21})$$

$\varepsilon_0$  Limit of plastic shakedown (phase 1).

$\varepsilon_p$  Plastic Strain

N Number of load repetitions

$\sigma_1$  Major principal stress

$\sigma'$  Reference stress (Atmospheric pressure, 0.1 MPa)

A,B,C Calibration constants.

The major stresses from the load are calculated as average from the top and bottom stress for each layer. The stresses are estimated based on the seasonal variations of the pavement materials as described in section 2.7.4.2.

### 3 Investigated Road Sections

#### 3.1 E6 Ljungskile-Uddevalla

The analyzed parts of the highway E6 are constructed in different stages, by different construction companies. The section between Ljungskile-Stinneröd-Lerbo, approximately 5.5 km, was built in two stages by NCC construction company in 1995. The pavement was constructed according to “BYA 84” guideline. In 2000, Peab continued the construction of E6, 3.6 km, from Lerbo to Sund. This part of the E6 was constructed according to “Väg 94” Guidelines. The two remaining parts, between Sunningen and Herrestad, approximately 2.3 km, are constructed by Svevia and were opened for traffic in 2000. The entire section is illustrated in Figure 3.1. The pavement is constructed according to “Väg 94” Guidelines.

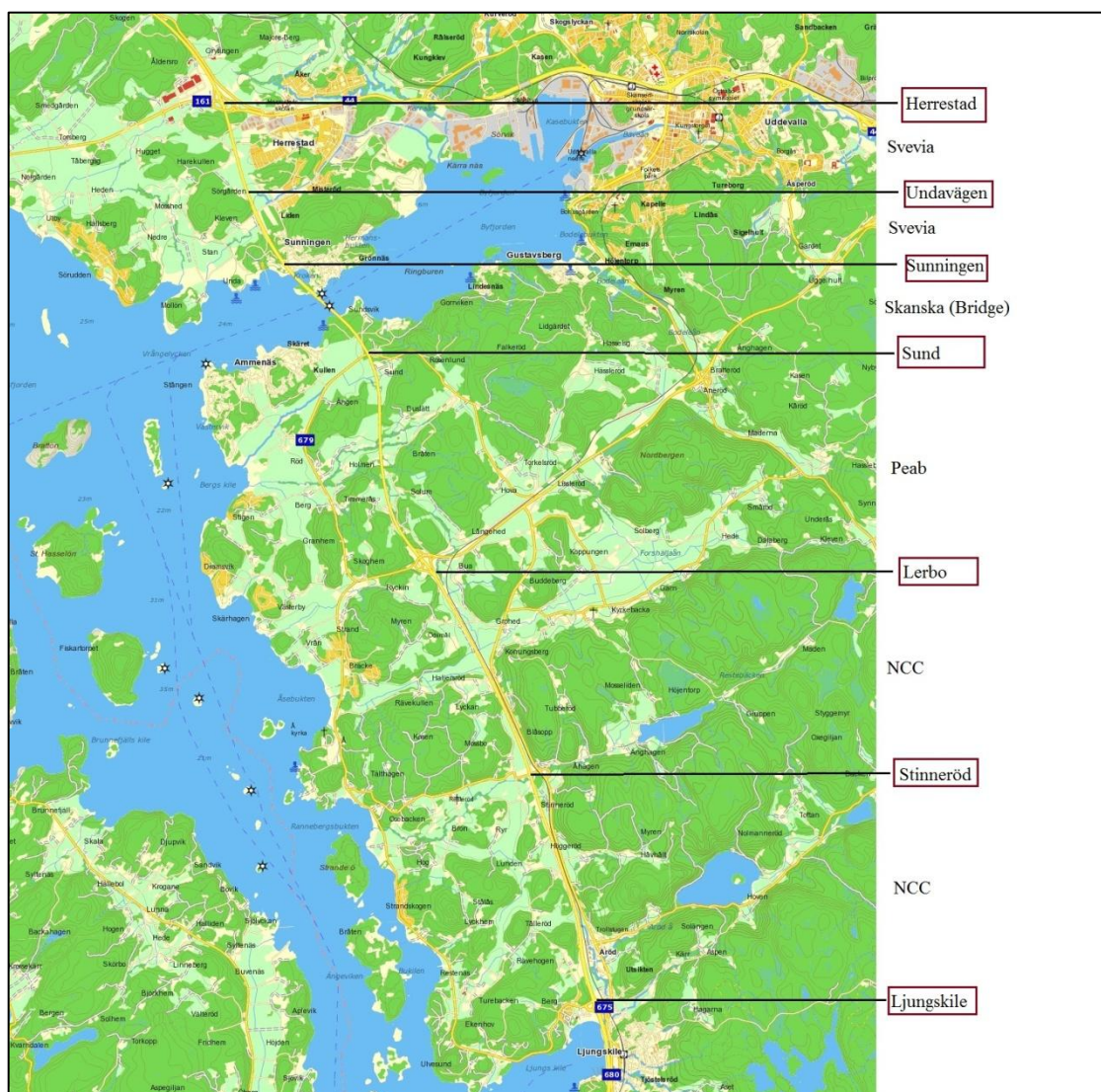


Figure 3.1: Illustration of different selected sections of E6.

The distance co-ordinates for each section according to consultant drawings are given below in meters.

Ljungskile-Stinneröd                      55/765-57/875

Stinneröd-Lerbo	0-4/760
Lerbo-Sund	4/130-7/700
Sunningen-Undavägen	9/561-10/780
Undavägen-Herrestad	10/780-11/800

### 3.1.1 Measured Rut

The data produced by RST which were obtained from the SRA database are presented in Appendix 2 as average values for each selected section to be analyzed. The road sections are renamed in Table 3.1.

Table 3.1: Selected sections.

Section	Section	Formation level	Section	Renamed subsection	Subgrade material
Ljungskile - Stinneröd	55/765 - 57/875	Rock cut	56/815- 56/915	RC1	Rock
		Soil cut	57/155- 57/275	SC2	Quick clay
Stinneröd - Lerbo	0/000 - 4/760	Surface level	01/494- 01/753	SL3	Dry crust
		Rock cut	01/950- 02/040	RC4	Rock
Lerbo - Sund	4/130- 7/700	Rock cut	04/772- 04/872	RC5	Rock
		Soil cut	04/892- 05/300	SC6	Sand, clay
Sunningen - Undavägen	9/561- 10/780	Rock cut	09/600- 09/900	RC7	Rock
		Rock Fill	10/360- 10/500	RF8	Dry crust
Undavägen - Herrestad	10/780- 11/800	Surface level	11/100- 11/200	SL9	Dry crust
		Soil cut	11/220- 11/460	SC10	Clay

The measured rut data is taken from the year where the road was opened to the first overlay maintenance. The subsections were selected where anomaly in rut depth could be seen as shown in Appendix 1A to Appendix 1E.

### 3.1.2 Ljungskile-Stinneröd and Stinneröd-Lerbo

Throughout the sections, the subgrade consists of rock and soft clay. The pavement structure was constructed as shown in Figure 3.2.

The subsections that have been identified of interest between Ljungskile and Stinneröd are a rock cut and a soil cut. The rock cut lies within 56/800 and 56/900 and was constructed according to Figure 3.2. The soil cut, lies between 57/155 and 57/275 and it is constructed according to Figure 3.2.

Further division of the road has been made from Stinneröd to Lerbo. Between 1/494 and 1/753, the pavement is constructed on surface level, thus no major excavation performed. The pavement is constructed according to Figure 3.2. The second subsection, a rock cut, is located between 1/950 and 1/040.

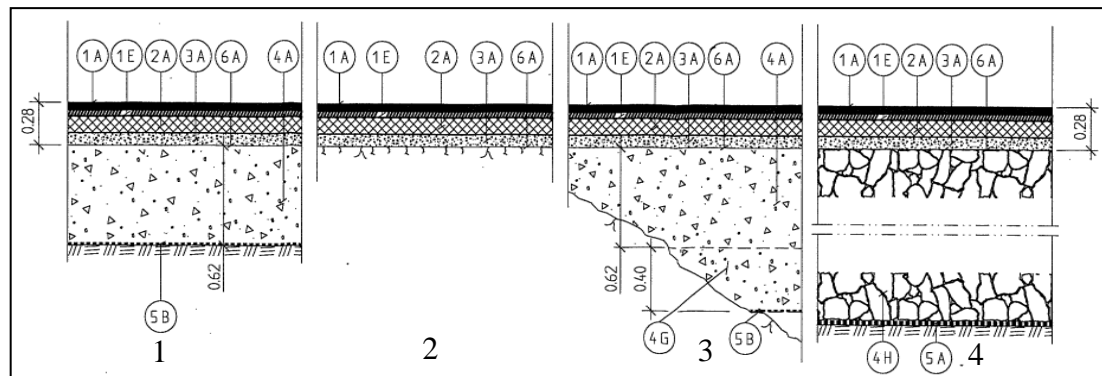


Figure 3.2: Pavement construction in section Ljungskile-Lerbo. From left to right: Soil Cut, rock cut, border between rock and soil section and rock fill.

The legend for pavement layer is shown in Table 3.2.

Table 3.2: Explanation to pavement sub layers in figure 3.2.

Label	Layer	Material	Thickness [mm]	BYA 84 Chapter
1A	Wearing Course	HABS 16	40	7:02
1E	Wearing Course	HAB 16 T	40	7:02
2A	Asphalt Base	AG 25	120	7:02
3A	Unbound Base	Crushed Rock	80	6:06
4A	Subbase	Crushed Rock	620	6:03
4G	Subbase	Crushed Rock	0-400	4:11
4H	Rock Embankment	Crushed Rock	Varying	5:05
5A	Material Separator	Geo-textile		6:01
5B	Material Separator	Geo-textile		6:01
6A	Sealing	Crushed Rock		5:05:04

### 3.1.3 Section Lerbo-Sund

Between Lerbo and Sund, the subgrade is composed of rock, clay with dry crust and silty clay. Because of the historical agriculture activities in the area, the soil surface is partly covered with a thin layer of organic soil. The section was opened for traffic in 2000, however, the wearing course was constructed in 2001.

Two sections have been identified, which are rock cut and soil cut. The rock cut is located between 4/4772-4/872 and the pavement was constructed according to Figure 3.3. The soil cut construction is located between 4/892-5/300 and was constructed according to Figure 3.3.

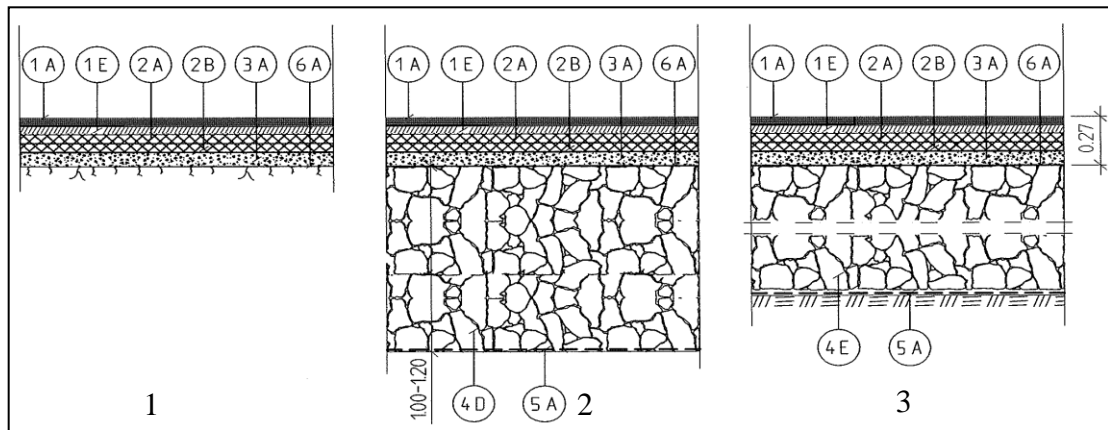


Figure 3.3: Pavement construction in section Lerbo-Sund. From left to right: Pavement on rock cut, pavement on soil cut and pavement with rock fill.

The legend for pavement layers is shown in Table 3.3.

Table 3.3: Explanation to pavement sub layers in figure 3.3.

Label	Layer	Material	Thickness [mm]	Väg 94 Chapter
1A	Wearing Course	ABS 16/B85	40	6
1E	Asphalt Binder	ABT 16/B85	60	6
2A	Asphalt Base	AGF 22/B180	45	6
2B	Asphalt Base	AGF 22/B180	45	6
3A	Unbound Base	Crushed Rock	80	5.5
4D	Subbase (Light Weight)	Blasted Stone	1000-1200	4.5.3
4E	Subbase	Blasted Stone	Varying	4.5.3
5A	Protection	Geo-textile		4.8.2
6A	Sealing	Crushed Rock		4.5.3.3

### 3.1.4 Section Sunningen-Undavägen

Two subsections of interest, a rock cut and a rock fill, are chosen to be analyzed. The rock cut is located between 9/600-9/900 and was constructed according to Figure 3.4. The rock fill is located between 10/360-10/500. The thickness of the fill is approximately 6 m in this particular subsection and the pavement was constructed as shown in Figure 3.4. The subgrade consists of silty clay with 3-4 m of dry crust.

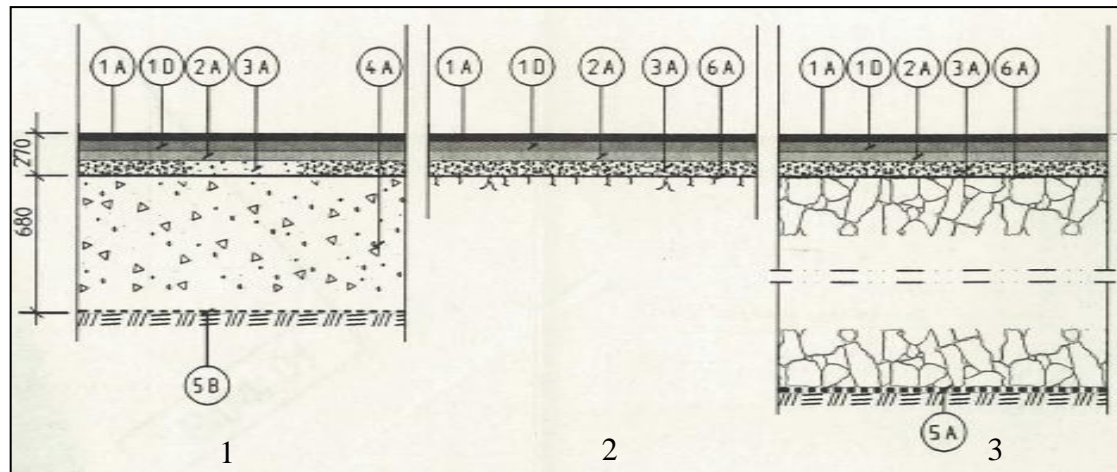


Figure 3.4: Pavement construction in section Sunningen-Undavägen. From left to right: Pavement on soil cut, pavement on rock cut and pavement with rock fill.

The legend to pavement layers in Figure 3.4 is shown in Table 3.4.

Table 3.4: Explanation to pavement sub layers in figure 3.4.

Label	Layer	Material	Thickness [mm]	Väg 94 Chapter
1A	Wearing Course	ABS 16/B85	40	6
1D	Asphalt Binder	ABT 22/B85	60	6
2A	Asphalt Base	AG 32/B180	90	6
3A	Unbound Base	Crushed Rock	80	5.5
4A	Sub-base	Crushed Rock	680	5.6
5A	Protection	Geo-textile		4.8.2
5B	Protection	Geo-textile		4.8.2
6A	Sealing	Crushed Rock		4.5.3.3

### 3.1.5 Section Undavägen-Herrestad

The subgrade is composed of silty clay with 3-4 m of dry crust in almost the entire section. The analyzed subsections are pavement construction on soil surface level and through soil cut. In both cases the pavement is constructed according to Figure 3.5.

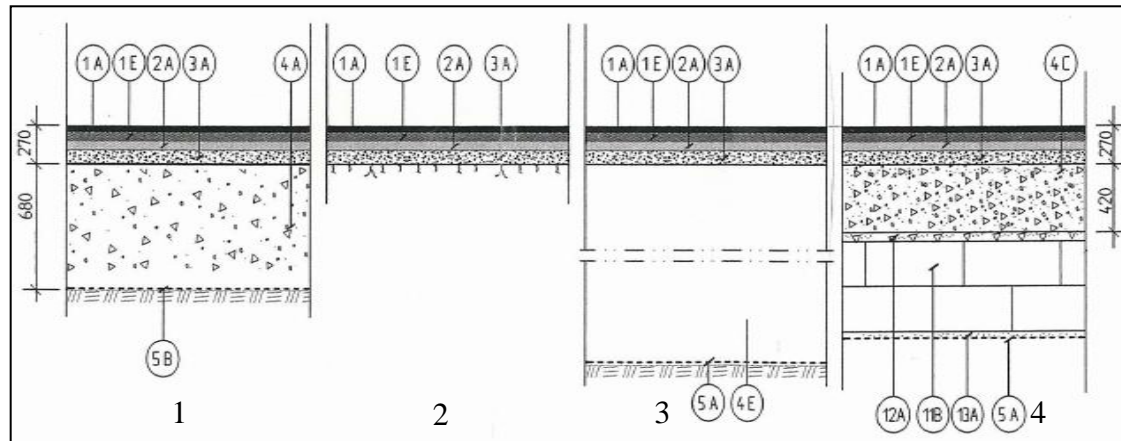


Figure 3.5: Pavement construction in section Undavägen-Herrestad. From left to right: Pavement on soil cut, pavement on rock cut, pavement with rock fill and pavement with EPS.

The legend for pavement construction is shown in Table 3.5.

Table 3.5: Explanation to pavement sub layers in figure 3.5.

Label	Layer	Material	Thickness [mm]	Väg 94 Chapter
1A	Wearing Course	ABS 16/B85	40	6
1E	Asphalt Binder	ABT 22/B85	60	6
2A	Asphalt Base	AG 32/B180	90	6
3A	Unbound Base	Crushed Rock	80	5.5
4A	Sub-base	Crushed Rock	680	5.6
4C	Subbase	Crushed Rock	420	5.6
4E	Subbase	Blasted Stone	1000	4.5.3
5A	Protection	Geo-textile		4.8.2
5B	Protection	Geo-textile		4.8.2
11B	Light Fill	EPS	Varying	
12A	Concrete layer	STD1,K40T	100	
13A	Sole Plate	Crushed Rock	100	

## 3.2 Traffic Volumes

Calculation of number of ESAL and vehicles with studded tires are based on the Average Annual Daily Traffic (AADT). In Table 3.6 and Table 3.7 the total vehicle passes (AADT<sub>tot</sub>) and the passes of heavy vehicles (AADT<sub>heavy</sub>) are shown.

Table 3.6: Traffic data from Ljungskile to Lerbo (SRA, 2010).

Count year	Direction	AADT <sub>tot</sub>	AADT <sub>heavy</sub>
1996	North	4700	660
1996	South	4700	660
2006	North	8970	1450
2006	South	9040	1410

Table 3.7: Traffic data from Lerbo to Herrestad (SRA, 2010)

Count year	Direction	AADT <sub>tot</sub>	AADT <sub>heavy</sub>
2000	North	4200	680
2000	South	4090	580
2006	North	6470	1150
2006	South	6240	1020

### 3.2.1 Heavy Traffic

The number of ESALs which the pavement have been subjected to, are calculated according to equation 3.1.

Assumptions are made regarding the calculations of ESALs. According to (Huvstig and Enocksson, 2010), 90 % of heavy vehicles use the design lane (right lane) of the highway.

$$N_{eq} = AADT * A * C * D * E * 3.65 * \left(1 + \frac{100}{k}\right) * \left(\left(1 + \frac{k}{100}\right)^n - 1\right) \quad (\text{Eq. 3.1})$$

The following assumptions are made:

A = 14 %      Percentage of heavy traffic.

C = 4.3      Axles/heavy vehicle.

D = 0.3      Conversion factor of ESAL.

E = 0.8      Cross sectional distribution factor.

k = 8.2 %      For Ljungskile to Lerbo and 9.2 % for Lerbo to Herrestad.

Detailed calculation of ESALs is shown in Appendix 3.

### 3.2.2 Vehicles With Studded Tires

The estimation of the number of vehicles contributing to wearing is based on annual traffic. Due to irregular traffic flow during a year, the estimation is relatively complicated. However, it is possible to approximate amount of traffic with studded tires rather accurately if annual traffic distributions are provided, see Figure 3.6 and Figure 3.7.

The winter period with studded tires is assumed to be five month, from November to April. The  $AADT_{Winter}$  is estimated to be 15000 vehicle/day in both directions for section Ljungskile-Lerbo in 2006 and is illustrated with green line in Figure 3.6. By back calculation and the ratio between AADT, marked with red line in Figure 3.6, and  $AADT_{Winter}$  the initial traffic with studded tires is expressed in equation 3.2:

$$T_{Initial, Winter} = \frac{(AADT_{Initial} - AADT_{Initial, Heavy})}{2} * \frac{AADT_{Winter}}{AADT} * \frac{70}{100} \quad (\text{Eq. 3.2})$$

Where,

$T_{Initial, Winter}$	Initial passenger traffic during winter in north direction.
$AADT_{Initial}$	Initial annual average daily traffic in both directions.
$AADT_{Initial, Heavy}$	Initial annual average daily traffic of heavy vehicles in both directions.
$AADT_{Winter}$	Average daily traffic during winter period.
$\frac{70}{100}$	70 % of passenger traffic uses right lane.

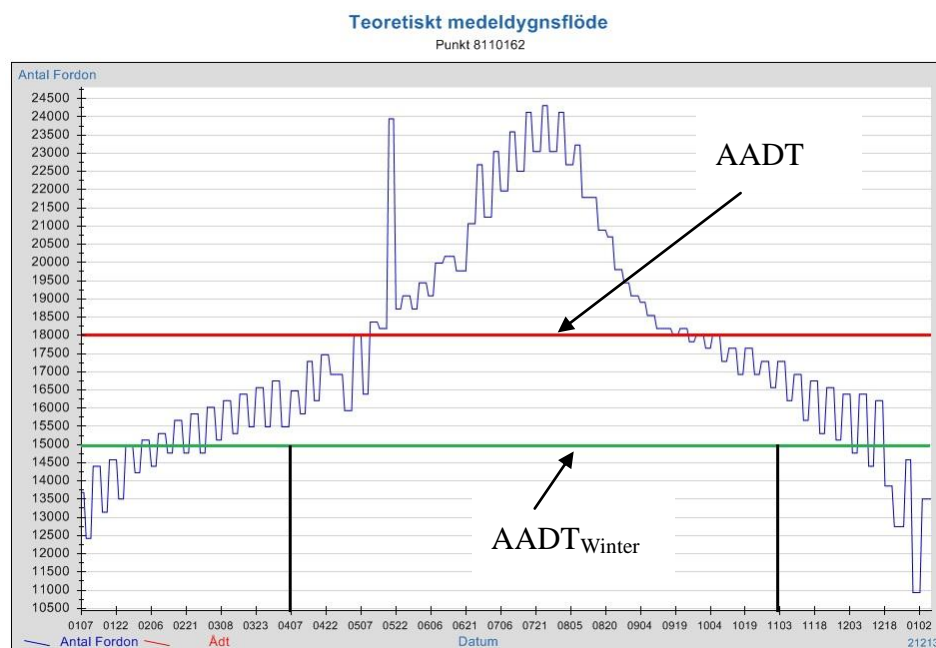


Figure 3.6: Annual traffic distribution in section Ljungskile-Lerbo in both directions (SRA, 2006).

The same procedure is applied for section Lerbo-Herresta, with annual traffic distribution according to Figure 3.7.

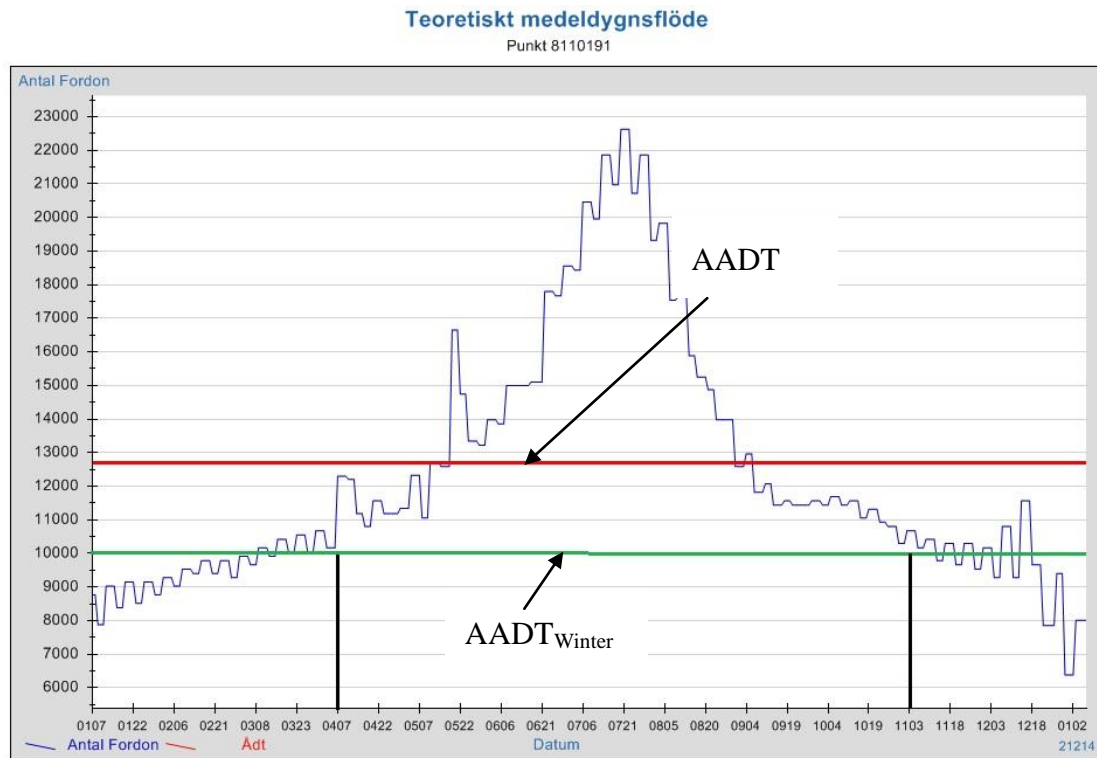


Figure 3.7: Annual traffic distribution in section Lerbo-Herrestad in both directions (SRA, 2006).

With insertion of traffic data in equation 4.2, following results in Table 3.8 are achieved .

Table 3.8: Estimated initial passenger vehicles/day in winter for observed sections.

Section	$AADT_{Initial}$	$AADT_{Initial, Heavy}$	$AADT_{Winter}$	AADT	$T_{Initial, Winter}$
Ljungskile - Lerbo	9400	1320	15000	18000	2350
Lerbo - Herrestad	8290	1260	10000	12700	1937

$AADT_{Initial}$  and  $AADT_{Initial, Heavy}$  for section Ljungskile-Lerbo was obtained from traffic counts in 1996.  $AADT_{Initial}$  and  $AADT_{Initial, Heavy}$  for section Lerbo-Herrestad was obtained from traffic counts in 2000.  $AADT_{Winter}$  and AADT was obtained from traffic counts in 2006 for both sections as shown in Figure 3.6 and Figure 3.7.

### 3.3 Wearing due to Studded tires

Wearing due to studded tires contributes to the total rut development of pavement structure. The Road Transport institute (Väg- och transportforsknings institutet, VTI) has developed a model for predicting wearing of pavement surface. It is programmed in Microsoft Excel.

The main parameters required for estimation includes “kulkvarn value” (similar to Los Angeles method) and percentage of passenger vehicles with studded tires. The used parameters are defined as follows:

Road type	Highway
Speed	110 km/h
$T_{\text{Initial, Winter}}$	Initial passenger traffic during winter in north direction.
Winter period	150 days (November to March)
Percentage of $AADT_{\text{Winter}}$	70% of the passenger traffic with studded tires.
Kulkvarn value	6

Calculations are shown in Appendix 4A and Appendix 4B.

### 3.4 Calculation of Structural Deformation

In this section, the specific input parameters for the models are defined. The calculations are implemented in accordance with the traffic situation and the defined parameters.

#### 3.4.1 MMOPP

The ground work of the model is based on categorization of pavement layers. The categories included are bound layers, Unbound layers and subgrade, as shown in Table 3.9 and Appendix 5.

Table 3.9: Definition of pavement layers and E-Modulus in MMOPP for Section RC1.

Layer	Pavement material	Thickness [mm]	E-Modulus [MPa]
Bound layer	Bituminous material	200	3650
Unbound layer	Crushed rock	80	300
Subgrade	Bedrock	***	1000

#### 3.4.2 M-E PDG

As mentioned in section 2.5.2, the rut prediction in M-E PDG is based on three levels, depending on the input parameters available. Due to the lack of tests along the section Ljungskile-Uddevalla, level three is implemented, thus general material properties are used. These are defined in Table 3.10.

Table 3.10: Definition of pavement layers and E-Modulus in M-E PDG for Section RC1.

Sub layers	Thickness [mm]	Bitumen penetration	E-modulus [MPa]
Asphalt concrete	40	85-100	***
Asphalt concrete	40	85-100	***
Asphalt base	120	120-150	***
Crushed stone	80	***	300
Bedrock	***	***	1000

The complete list of input parameters are given in Appendix 6.

## 4 Results

In this chapter the results of the predicted deformations for MMOPP and M-E PDG are presented. It also includes the estimated wearing along the highway E6.

### 4.1 Wearing

The estimated average wearing in section Ljungskile-Lerbo is 0.32 mm in 1996 and that of Lerbo-Herrestad is 0.26 mm in 2001. The average annual increase of wearing is 7%. The results is shown in Appendix 4A and Appendix 4B.

### 4.2 MMOPP

The predicted permanent structural deformation in MMOPP are presented in Table 4.1 to Table 4.5 for each section.

Table 4.1: Estimated structural deformation in section RC1 and SC2.

	RC1	SC2
Year	D <sub>Structural</sub> [mm]	D <sub>Structural</sub> [mm]
1996	0,3	3,23
1997	0,44	4,42
1998	0,57	5,48
1999	0,69	6,44

Table 4.2: Estimated structural deformation in section SL3 and RC4.

	SL3	RC4
Year	D <sub>Structural</sub> [mm]	D <sub>Structural</sub> [mm]
1999	1,22	0,31
2000	1,72	0,46
2001	2,22	0,6
2002	2,72	0,72
2003	3,22	0,85
2004	3,72	0,98
2005	4,22	1,12
2006	4,72	1,27
2007	5,22	1,42
2008	5,72	1,56
2009	6,22	1,69

Table 4.3: Estimated structural deformation in section RC5 and SC6.

	RC5	SC6
Year	D <sub>Structural</sub> [mm]	D <sub>Structural</sub> [mm]
2002	0,33	0.67
2003	0,5	1.01
2004	0,65	1.35
2005	0,79	1.69
2006	0,93	2.04
2007	1,08	2.38
2008	1,24	2.72
2009	1,41	3,06

Table 4.4: Estimated structural deformation in section RC7 and RF8.

	RC7	RF8
Year	D <sub>Structural</sub> [mm]	D <sub>Structural</sub> [mm]
2001	0,29	0,49
2002	0,45	0,82
2003	0,59	1,11
2004	0,72	1,4
2005	0,85	1,7
2006	0,98	2,01
2007	1,14	2,35
2008	1,3	2,69
2009	1,47	3,08

Table 4.5: Estimated structural deformation in section SL9 and SC10.

	SL9	SC10
Year	D <sub>Structural</sub> [mm]	D <sub>Structural</sub> [mm]
2001	0,61	0,96
2002	0,96	1,4
2003	1,27	1,8
2004	1,56	2,15
2005	1,87	2,5
2006	2,2	2,93
2007	2,54	3,35
2008	2,89	3,78
2009	3,28	4,23

### 4.3 M-E PDG

The predicted permanent structural deformation of M-E PDG are presented in Table 4.6 to Table 4.10 for each section. The original results are also shown in Appendix 7.

Table 4.6: Estimated structural deformation in section RC1.

	RC1	SC2
Year	D <sub>Structural</sub> [mm]	D <sub>Structural</sub> [mm]
1996	0,95	15,57
1997	1,29	18,04
1998	1,46	19,54
1999	1,65	20,74

Table 4.7: Estimated structural deformation in section SL3 and RC4.

	SL3	RC4
Year	D <sub>Structural</sub> [mm]	D <sub>Structural</sub> [mm]
1999	9,2	0,95
2000	10,73	1,29
2001	11,63	1,46
2002	12,38	1,65
2003	13,07	1,85
2004	13,67	2,04
2005	14,15	2,17
2006	14,62	2,32
2007	15,04	2,44
2008	15,49	2,6
2009	15,86	2,71

Table 4.8: Estimated structural deformation in section SC6.

	RC5	SC6
Year	Not considered	D <sub>Structural</sub> [mm]
2002		4,72
2003		5,5
2004		6,12
2005		6,52
2006		6,92
2007		7,3
2008		7,69
2009		7,96

Table 4.9: Estimated structural deformation in section RC7 and RF8.

	RC7	RF8
Year	D <sub>Structural</sub> [mm]	D <sub>Structural</sub> [mm]
2001	0,94	3.46
2002	1,26	4.07
2003	1,44	4.40
2004	1,62	4.71
2005	1,81	5.00
2006	1,99	5.28
2007	2,12	5.48
2008	2,26	5.7
2009	2,38	5.88

Table 4.10: Estimated structural deformation in section SL9 and SC10.

	SL9	SC10
Year	D <sub>Structural</sub> [mm]	D <sub>Structural</sub> [mm]
2001	4,51	5,93
2002	5,33	7
2003	5,79	7,61
2004	6,19	8,15
2005	6,58	8,65
2006	6,94	9,1
2007	7,2	9,44
2008	7,48	9,8
2009	7,7	10,1

## 4.4 Comparison of Measured and Predicted Rut Depth

Graphical presentation of the measured and predicted structural deformation are illustrated in Figure 4.1 to Figure 4.10. The measured rut depth consist of structural deformation ( $D_{\text{Structural}}$ ) and the wearing by studded tires ( $W$ ). Therefore, an expression for measured structural deformation is given as:

$$D_{\text{Structural}} = RST - W \quad (\text{Eq. 4.1})$$

Where, RST is the rut measurement obtained by the RST car.

These illustrations will enable a clear comparison of the selected sections to be analyzed. In some instances, as indicated in sub chapter 4.4.3 and 4.4.4, the measured rut depth could not be compared to the predicted due to anomaly in the direction of increment of rut depth. These sections include RC5 and RC7 as shown in Figure 4.5, and Figure 4.7. Furthermore, it is believed that the initial rut before the commencement of the traffic is approximately 3 mm. This initial rut is not considered by the prediction models (Johansson, 2010).

#### 4.4.1 Ljungskile-Stinneröd

As shown in Figure 4.1 and Figure 4.2, the predicted structural deformation for MMOPP in section RC1 is accumulating by 0.13 mm/year, whereas that of M-E PDG is 0.23 mm/year. Section SC2 has a predicted structural deformation of 1.07 mm/year for MMOPP and 1.7 mm/year for M-E PDG.

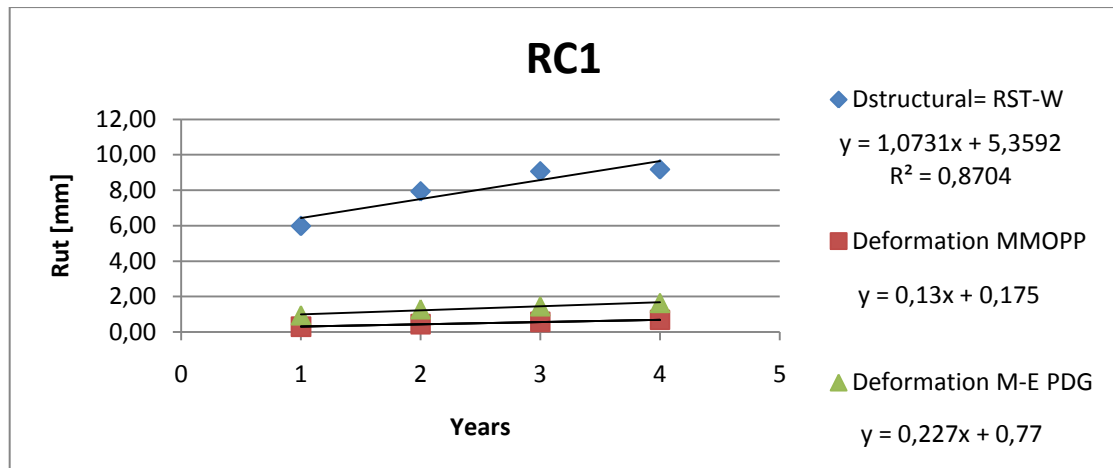


Figure 4.1: Illustration of measured and predicted structural deformation in section RC1.

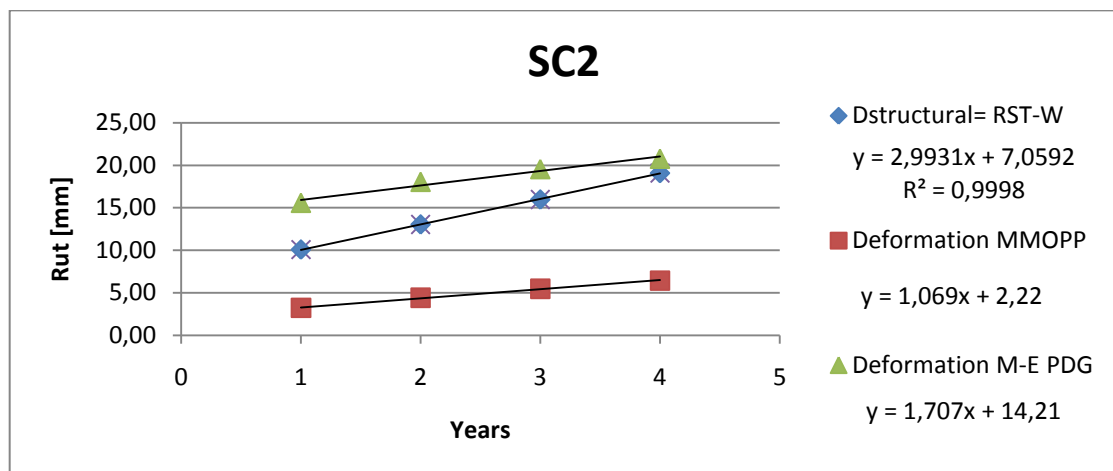


Figure 4.2: Illustration of measured and predicted structural deformation in section SC2.

#### Analysis

The measured annual rut development do not follow same pattern as predicted deformations in RC1 nor SC2. But the prediction models have similar pattern in annual rut development. It is also observed that the initial rut in Phase 1 is underestimated by the models in RC1. In the case of SC2, the initial rut in Phase 1 is overestimated in M-E PDG and underestimated in MMOPP.

#### 4.4.2 Stinneröd-Lerbo

The results for section SL3, as shown in Figure 4.3, show that the measured and the predicted structural deformation follow the same pattern of increment. The MMOPP estimates an accumulation of 0.5 mm/year whereas M-E PDG is 0.62 mm/year.

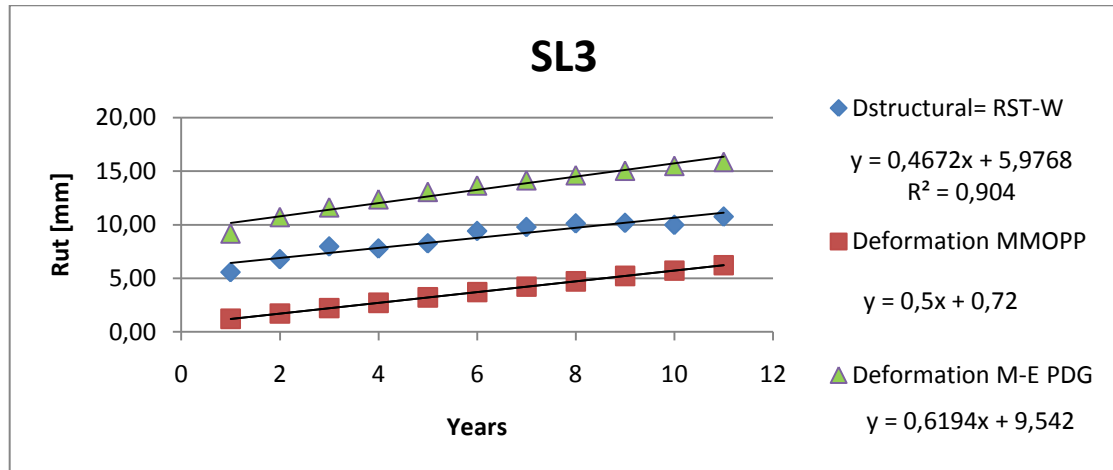


Figure 4.3: Illustration of measured and predicted structural deformation in section SL3.

Co-currently, in Figure 4.4 the behaviour of the measured and the predicted structural deformation is similar to the pattern in section SL3. The predicted structural deformation by MMOPP is 0.14 mm/year and M-E PDG is 0.17 mm/year, while the measured deformation is 0.1 mm/year with R-squared value of 0.53.

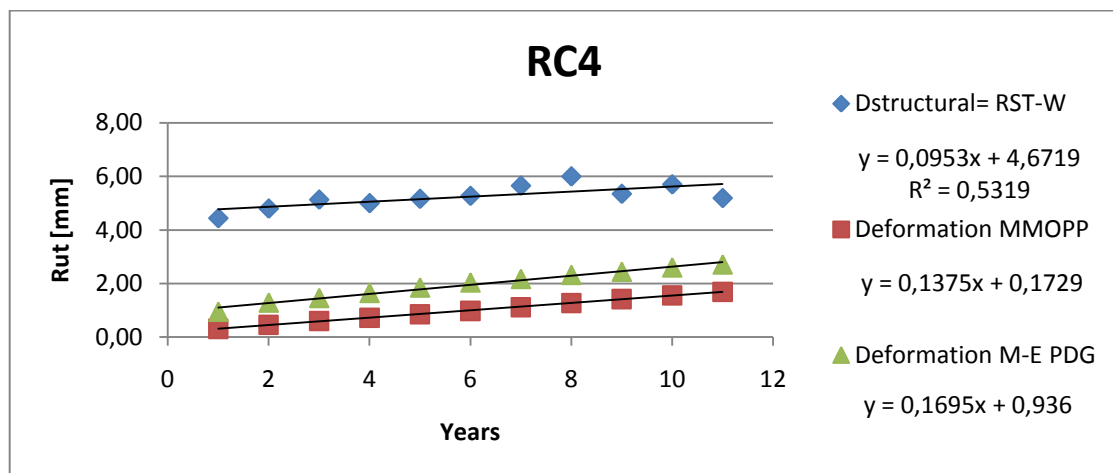


Figure 4.4: Illustration of measured and predicted structural deformation in section RC4.

#### Analysis

The measured annual rut development follows the same pattern as the predicted annual rut development in both SL3 and RC4. Regarding the deformations in Phase 1, the M-E PDG overestimates the deformation, whereas MMOPP predicts approximate deformation in SL3. The predicted deformations made by MMOPP in Phase 1 combined with the initial rut (3 mm), gives a similar rut development as the measured ruts in section SL3. For RC4, the models predicts a fairly accurate deformation in Phase 1 if the 3 mm of initial rut is considered.

### 4.4.3 Lerbo-Sund

In Figure 4.5, there is an anomaly in the behaviour of the measured structural deformation, thus a decreasing deformation in reality. This is due to small rut which the RST is unable to measure.

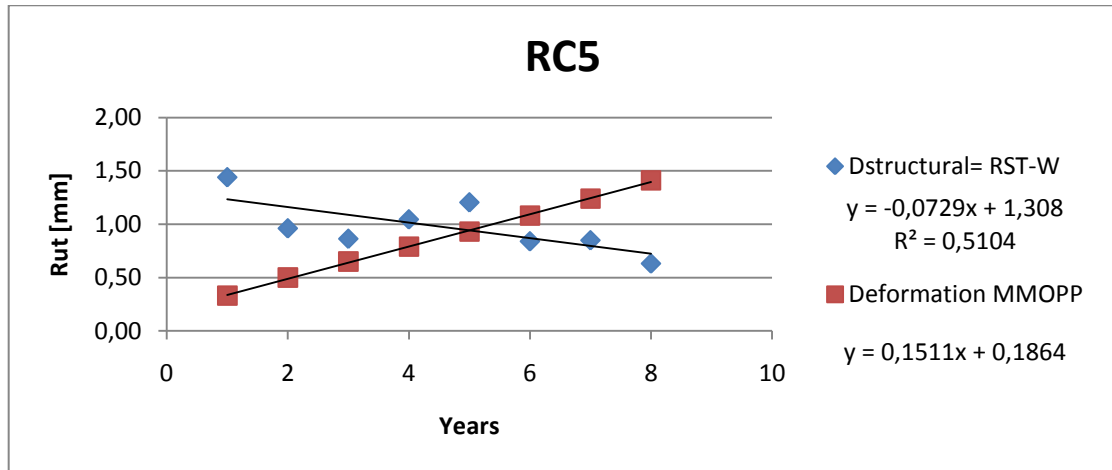


Figure 4.5: Illustration of measured and predicted structural deformation in section RC5.

In section SC6, both the predicted and the measured structural deformation follow a pattern which can be verified. As shown in Figure 4.6, the deformation is estimated to be 0.34 mm/year and 0.45 mm/year by MMOPP and M-E PDG respectively.

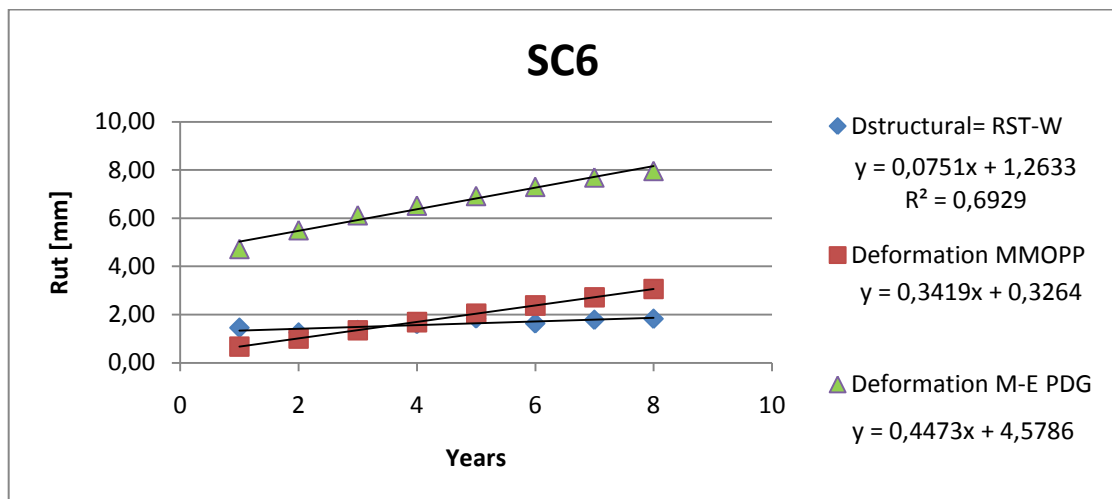


Figure 4.6: Illustration of measured and predicted structural deformation in section SC6.

#### Analysis

The negative inclination in measured ruts in RC5 is a result of an overestimation in wearing and small rut development which the RST could not measure accurately. The small deformation is shown by the prediction made in MMOPP. Regarding the ruts development in SC6, M-E PDG overestimates the deformations in Phase 1, although the overlay was constructed one year after the commencement of the traffic.

#### 4.4.4 Sunningen-Undavägen

The reduction of the measured deformation with time in section RC7 makes it impossible to be compared to the predicted deformation.

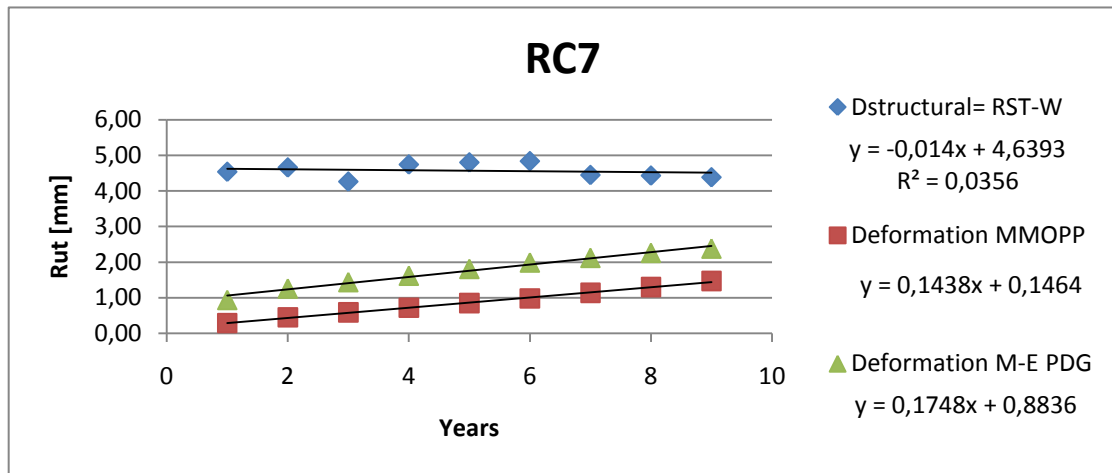


Figure 4.7: Illustration of measured and predicted structural deformation in section RC7.

According to the graphical presentation in Figure 4.8, the annual rut development for MMOPP and M-E PDG is estimated as 0.32 mm and 0.29 mm respectively and they follow the same pattern in annual rut development as in reality.

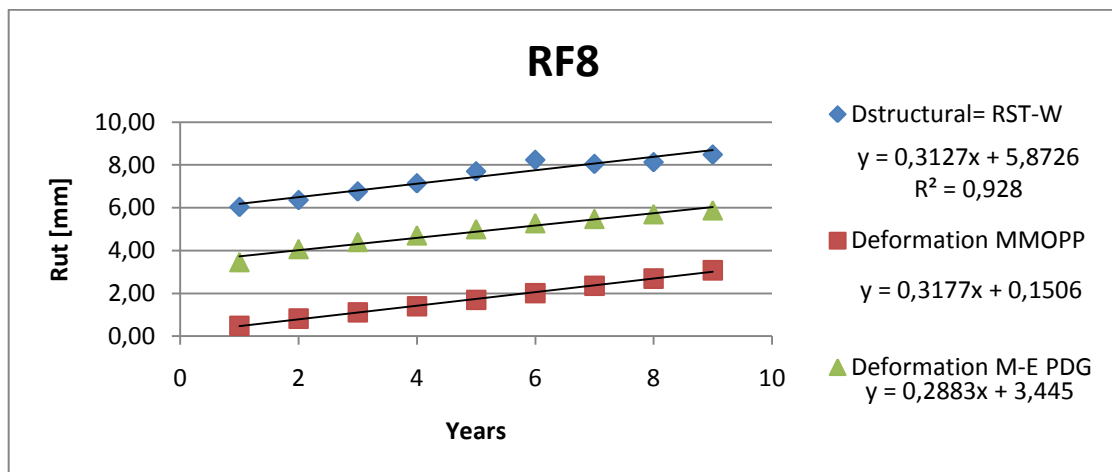


Figure 4.8: Illustration of measured and predicted structural deformation in section RF8.

#### Analysis

The negative inclination in measured ruts in RC7 is a result of an overestimation in wearing and small rut development which the RST could not measure accurately. The small deformation is shown by the prediction made in MMOPP and M-E PDG. Regarding the deformations in Phase 1 for both RC7 and RF8, if the initial rut of 3 mm is added to the predicted in M-E PDG, the pattern of deformation will fit the measured deformation development. Whereas MMOPP underestimates the deformations in Phase 1 even if 3 mm of initial rut is added.

#### 4.4.5 Undavägen-Herrestad

In section SL9, the annual deformation development is estimated to be 0.33 mm and 0.38 mm for MMOPP and M-E PDG respectively. Similarly, Figure 4.10 illustrates the deformation development with time in section SC10 as 0.40 mm/year and 0.5 mm/year for MMOPP and M-E PDG respectively.

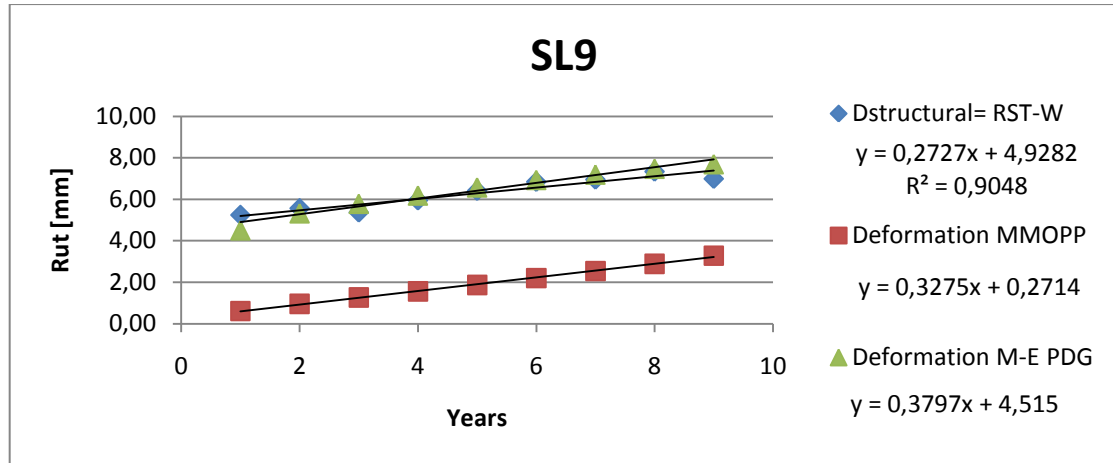


Figure 4.9: Illustration of measured and predicted structural deformation in section SL9.

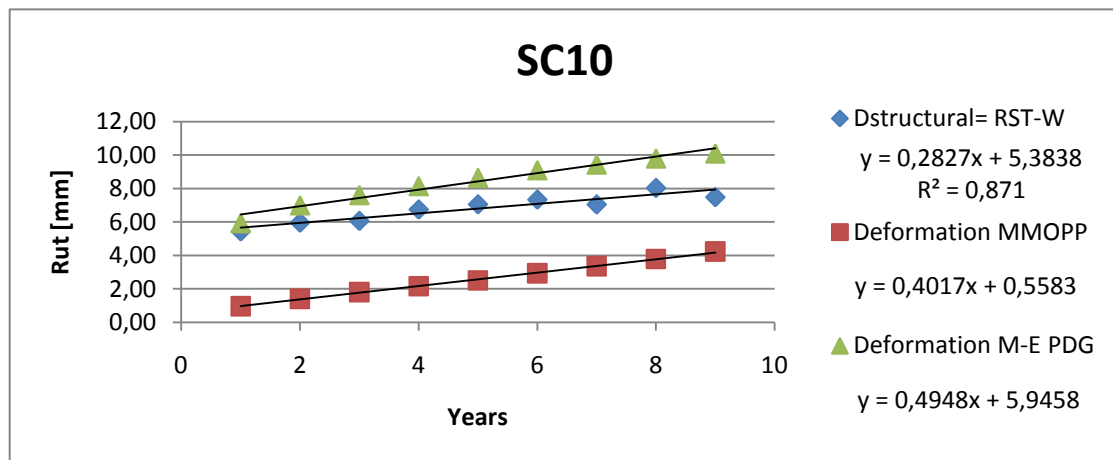


Figure 4.10: Illustration of measured and predicted structural deformation in section SC10.

#### Analysis

The measured annual rut development follows the same pattern as in prediction models in both sections. It is observed that the deformations in Phase 1 are overestimated if 3 mm of initial rut is considered. Whereas in MMOPP, the deformations in phase 1 are fairly accurate if 3 mm of initial ruts is considered in both sections.

Table 4.11 illustrates the annual deformation development in reality compared to predicted annual deformation development.

Table 4.11: Rate of increment of permanent deformation in reality ( $D_{Structural}$ ), MMOPP and M-E PDG.

Section	Annual deformation increase ( $D_{Structural}$ ) [mm/year]	MMOPP		M-E PDG	
		Annual increase [mm/year]	Ratio $=D_{Structural}/MMOPP$	Annual increase [mm/year]	Ratio $=D_{Structural}/M-E\ PDG$
RC1	1.07	0.13	8.23	0.23	4.65
SC2	2.99	1.07	2.80	1.71	1.75
SL3	0.47	0.50	0.94	0.62	0.76
RC4	0.10	0.14	0.71	0.17	0.59
RC5	-0.07	0.15	***	***	***
SC6	0.08	0.34	0.24	0.45	0.18
RC7	-0.01	0.14	***	0.17	***
RF8	0.31	0.32	0.97	0.29	1.07
SL9	0.27	0.33	0.82	0.38	0.71
SC10	0.28	0.40	0.7	0.49	0.57

As shown in the Table 4.11, there is a good correlation between reality and the permanent deformation prediction models in sections SL3, RC4, RF8, SL9 and SC10. However, RC5, and RC7 does not show a better correlation due to a reduction in rate of increment.

## 4.5 Sensitivity Analysis

A sensitivity analysis has been performed to assess the impact of input parameters on the results in M-E PDG. The sensitivity analysis examines how the output of the model, in this case the annual deformation development, responds to small changes in the parameters in the model. It shows which parameter is having the largest impact on the model.

The sensitivity analysis includes calculating how much the output  $V$  changes ( $\Delta V$ ) for a small change ( $\Delta P$ ) in the parameter  $P$  according to the expression:

$$S_P \approx \frac{\Delta V/V}{\Delta P/P} \quad (\text{Eq. 4.2})$$

When the absolute value of the sensitivity,  $S_P$ , is greater than one, the model output  $V$  is sensitive to the parameter  $P$ . This means that the parameter has a very large influence on the model. If  $S_P$  is close to zero, the parameter has a small influence on the model. The parameter to be considered is the E-modulus of the unbound layers due to its uncertainty. The coefficient of variation of E-modulus is believed to be at least 30 %. The sensitivity analysis is performed for sections SC2, SL9 and SC 10. For these section, a small change (30 %) of the E-modulus is considered for the sub base and subgrade separately. Therefore, the value of  $\Delta P/P$  will be 0.3 in equation 4.2. By calculations, as shown in Appendix 8, the results in Table 4.12 are achieved.

Table 4.12: Sensitivity results of 30 % change in E-modulus.

Section	Original annual deformation rate	Layer	$\Delta P/P$	Annual deformation rate with 30% increase in E-modulus	Sensitivity
SC2	1.7074	Subgrade	0.3	1.5171	0.372
		Sub base	0.3	1.5773	0.254
SL9	0.4172	Subgrade	0.3	0.3723	0.359
		Sub base	0.3	0.3662	0.407
SC10	0.4952	Subgrade	0.3	0.4638	0.211
		Subbase	0.3	0.4493	0.309

From Table 4.12, it is observed that the E-modulus is less sensitive on the annual deformation development in sections SC2, SL9 and SC10.

## 5 Discussion

The results from M-E PDG for RC1 has lower rate of annual deformation compared to reality. The difference between the annual deformation rate in the model and reality can partially be linked to the fact that M-E PDG does not consider deformations in rock. Furthermore, the reliability of the RST measurement is questionable due to the difference in the annual increment. However, MMOPP has the least annual increment, although it does consider deformations in rock. This is because M-E PDG has a higher rate of increment in asphalt layer than MMOPP. This can be attributed to the warmer climate condition in Boston compared to Gothenburg. In addition, the higher annual deformation in reality can be the cause of fractured or weak rock subgrade, which the prediction models do not consider. More so, anomalies in RC1 can also be linked to the variation in the subgrade, thus partly rock and soil.

For section SC2, the annual deformation increment in reality is high in comparison to the predicted annual increase for both MMOPP and M-E PDG. Due to the subgrade type (quick clay) in this section, the models predict the highest rate of deformation in the subgrade. But the reliability of the predicted deformation is questionable, because of the choice of subgrade class in the models. For instance, the softest clay in M-E PDG is classified as A-7-6 which was chosen to correspond to quick clay, may differ in material properties. In the case of MMOPP there is no option to select subgrade type, but the subgrade material is only described with the E-modulus.

For the result in section SL3, there is a good correlation between reality and the predicted annual deformation. Although there might be uncertainties in the results, the models tend to give a good representation of reality for pavement construction on surface level. It can further be noticed that the R-square value ( $\approx$  unit) confirm the annual linear increase of the measured deformation.

According to the results in section RC4, the annual deformation development in reality is same as the prediction made in MMOPP. The better correlation can be attributed to the relatively long term measurement obtained from RST. In the case of M-E PDG the annual deformation is slightly higher than reality and MMOPP. This difference can be explained by the in-situ stresses considered by M-E PDG. Although section RC1 and RC4 are both considered to have same subgrade, annual deformation of RC1 is higher than RC4 in reality. Beside the uncertainties involved in the RST measurement, the differences can mainly be attributed to the overlay period of section RC4. The overlay was done three years after commencement of the section.

In section RC5, there is a decreasing annual deformation in the RST measurements, which is impossible in reality. This can be explained by the uncertainties in the RST measurements. The decrease in annual deformation makes it difficult to compare reality to results from prediction models. The annual deformation in Section RC7 shows similar behaviour as in section RC5.

Results from section SC6, indicates a small annual deformation compared to the prediction models. This can be attributed to the assumed E-modulus of the subgrade in models. Therefore, the models predict higher deformation in the subgrade.

Section RF8 has an annual deformation in reality similar to result from prediction models. This similarity can be attributed to the reflected linear behaviour of the relatively large number of measured deformations in reality. From previous sections, the M-E PDG predict higher annual deformation compared to MMOPP. But in this section, RF8, it is otherwise. This is a result of the assumption made in M-E PDG for

the embankment. Thus, in M-E PDG the embankment is considered as subgrade due to limitations in the model. But in MMOPP provision is made for various layers as well as the subgrade.

In section SL9, the annual deformation in reality varies marginally from the predicted deformation. The annual deformation in reality for section SL9 is relatively small. It is a result of the subgrade type, which consist of 3-4 m of dry crust on top of clay. This is also reflected in the predicted deformations.

For section SC10, the annual deformation in reality is similar to section SL9, even though it is a soil cut on clay. This can be explained by the relatively thick sub base, which reduces the stresses on top of the subgrade.

In summary, the measured annual deformation for rock cut sections is low, with exception of RC1. The unexpected increase in annual deformation of section RC1 can be attributed to the deformation properties of the rock. Another factor that can affect the properties of the rock is linked to the blasting of the rock. The prediction models do not consider this deficiencies in the rock. Thus, the geometry in reality may differ from the defined geometry in the model.

From the results of the prediction models, it can be observed that M-E PDG predicts higher annual deformation compared to MMOPP. It is observed that the M-E PDG does not consider deformation in rock subgrade. But it gives higher deformation compared to MMOPP. It can be explained by differences in climate condition between Gothenburg and Boston.

Furthermore, the prediction of deformations by M-E PDG is based on heavy traffic volumes, material properties and climate conditions. However, the estimation of deformation was done in level 3, thus limitations in available material parameters. Therefore, there are uncertainties with these parameters which affect the results of deformation models. These uncertainties become greater in the properties of the subgrade due to the geological variations, such as groundwater level, suction and stratification of different soils. Further material uncertainties are linked to differences in geological conditions between USA and Sweden. The differences was noticeable when the material properties of the quick clay in section SC2 was defined in the model. According to M-E PDG, the clay material has a minimum E-modulus of around 30 MPa but in the case of section SC2 the quick clay is assumed to have an E-modulus of 5 MPa. This particular difference raise questions about existence of quick clay in USA and consequently calibration of the prediction model to such geological conditions.

Further uncertainties can be linked to the chosen climate conditions to represent Gothenburg. Due to slightly warmer climate in Boston it is reasonable to believe that the predicted deformations especially in the asphalt layers are lower in Gothenburg compared to Boston. Thus, the total deformation development in asphalt layer is believed to be less in Gothenburg.

In case of MMOPP, the subgrade type is not considered. Thus, there is no consideration of the geological properties of the material such as water content, groundwater level etc.. These factors highly affect the deformation properties of the subgrade. In MMOPP it is possible to define the climate condition of the concerned region, Zone 2 in Sweden. This makes it possible to predict deformations based on seasonal variations of the material properties. Furthermore, MMOPP does not

consider the in situ stresses of the pavement structure. This results in lower annual deformation in MMOPP compared to M-E PDG.

Regarding the wearing due to studded tires, there are uncertainties in the estimated wearing. These uncertainties are mainly linked to the assumptions made in the calculations, thus percentage of the passenger traffic that use the outer lane and the percentage of the passenger traffic with studded tires.

There are uncertainties in the data collected by the RST due to automated method of measurement. These uncertainties are mainly linked to the fact that the RST car can not differentiate between rut and other unevenness on the road surface. It is believed that the RST often underestimates the rut depth.

## 6 Conclusion

Several advantages were discovered in the use of the models during the work process. One of the early discoveries of M-E PDG was its ability to select the level accuracy for prediction based on available data. It was much easier to use the model because of its default parameters such as heavy traffic distribution, soil classification etc. However, there is an option to make changes in the parameters. Furthermore, there is an optional ability to deal with non-linear response of the unbound materials which makes it possible to describe the behaviour of the unbound material in a realistic way.

However, there are limitations in the model. These include the inability of the model to assess seasonal variations in E-modulus of the unbound materials. Furthermore, the possibility to estimate deformation based on exact climate conditions is limited for use outside USA.

Although there were lack of data to perform simulations in Level 1 and Level 2 in M-E PDG, the model was able to predict annual permanent deformation that followed the pattern as in reality in sections SL3, RC4, RF8, SL9 and SC10 in Level 3. However, deformations in sections RC1, SC2 and SC6 could not be estimated to fit the reality.

The annual rut development predicted by MMOPP follows the same pattern as prediction made by M-E PDG. The differences in the predicted annual rut development are mainly found to be a result of warmer climate assumed in M-E PDG and consideration of in situ stresses in M-E PDG. One of the obvious advantages of MMOPP compared to M-E PDG is the option of changing climate factors to fit the specific regional conditions. Further advantage of MMOPP is its ability to consider seasonal variations of material properties, although there are no option to select the type of subgrade. Consequently, the model does not distinguish seasonal variations in rock and soil material.

Based on the obtained results, both models are found to predict annual rut development in a fairly accurate way. Consequently, with simple test procedures of obtaining material properties by FWD, it was possible to predict annual deformation development as in reality. However, the models were not able to predict deformations as in reality in sections RC1, SC2 and SC6.

## 7 Recommendations

In order to make a precise validation of the models further studies has to be done. An accurate validation of the rut prediction models should be based on manual rut measurements instead of RST measurements. Due the uncertainties in the RST data especially in initial rut measurements, it turns out to be difficult to evaluate the models since the RST measurements are believed to underestimate the maximum rut depth. Manual rut measurements will lead to higher reliability in the measurement data and subsequently higher accuracy in the validation of the models.

To make a more accurate and reliable validation of the models, further investigations should be performed on material properties of the specific test roads. These investigations should include FWD measurements, which are believed to be enough for prediction of annual rut development.

For non-linear behaviour of the unbound materials, triaxial tests are required. More studies has to be done on the behaviour of the unbound material in the densification stage, which consequently will enable an accurate estimation of initial deformation (Primary stage in Figure 2.17). Further complications are linked to the overlay period of the wearing course, which often occurs one year after the commencement of the traffic. In such cases, the deformations in Phase 1 has already occurred, and consequently not visible in RST measurement after the final overlay. Therefore, it is recommended to evaluate the models based on roads where the commencement of the traffic is done after the final overlay.

In order to minimize the uncertainties regarding the traffic distribution over different lanes it is preferred to make future validations based on single lane roads. This will result in a more reliable estimation of traffic load subjected to the pavement structure.

For more precise validation of the models, wearing due to studded tires should be accurately estimated. For a precise estimation of the wearing, tests should be done on abrasion properties of the aggregate material in hot mixed asphalt.

## 8 References

HUANG, Y. H. (2004): *Pavement analysis and design*. Pearson Education, Upper Saddle River, N.J, {USA}.

PAPAGIANNAKIS, A. T., MASAD, E. (2008): *Pavement design and materials*. John Wiley, Hoboken, N.J, {USA}.

Ullidtz, P. (1998): *Modelling flexible pavement response and performance*. Polyteknisk Forlag, Lyngby, {Denmark}.

Kim, Y.R. (2009): *Modeling of asphalt concrete*. American society of engineers, Reston, {USA}.

Lekarp, F. (1999): Resilient and Permanent Deformation Behavior of Unbound Aggregate Under Repeated Loading. Ph.D. Thesis. Department of Infrastructure and Planning, Royal Institute of Technology, KTH, Stockholm, Sweden, 1999.

U.S. Department of Transportation (2006): *Geotechnical aspects of pavements*, National Highway Institute, Washington D.C., {USA}.

Werkmeister, S. (2003): Permanent Deformation Behaviour of Unbound Granular Materials in Pavement Constructions. Ph.D. Thesis. Technical University of Dresden, Dresden, Germany, 2003.

Blomberg, T (2002): *Bituminous Binders*. NESTE.

Huvstig, A. (2008): NordFoU – *Pavement performance models*. Vägverket, Göteborg, {Sweden}.

Öberg, G (2001): *Statliga belagda vägar: Tillståndet på vägytan och i väggroppen, effekter och kostnader*, (National paved roads: condition on the pavement surface and pavement structure, effects and costs. In Swedish), VTI, Linköping, {Sweden}.

Jacobson, T., Wågberg, L.G. (2006): *Utveckling och uppgradering av prognosmodell för beläggningsslitage, slitageprofil och årskostnad*, (Development and upgrade of prediction model for asphalt wearing, wearing profile and annual cost, In Swedish), VTI, Linköping, {Sweden}.

Vejdirektoratet (2007): *Dimensionering af befæstelser og forstærkningsbelægninger*, (Design of pavement surface and base layer, In Danish), Vejdirektoratet, Århus, {Denmark}.

Vejdirektoratet, (2007): *MMOPP Dimensioneringsprogram for vejbefæstelser*, (MMOPP design model for pavement structure, In Danish), Vejdirektoratet, Vejreglerådet, {Denmark}.

Vejdirektoratet, (2006): *Varmblandet asfalt*, (Hot mixed asphalt, In Danish), Vejdirektoratet, Vejreglerådet, {Denmark}.

NCHRP (2004): *Mechanistic-Empirical design of new & rehabilitated pavement structures*. AASHTO, Washington DC, {USA}.

U.S. Department of Transportation, (2001): *Adequacy of rut bar data collection*. Federal Highway administration, Georgetown, {USA}.

U.S. Department of Transportation, (2003): *Long-Term Pavement Performance; Information Management System, Pavement Performance Database Reference Guide*. Federal Highway Administration, Georgetown Pike, {USA}.

Long, F.M. (2001): *Permanent deformation of asphaltconcrete pavements: A nonlinear viscoelastic approach to mix analyses and design*. Ph.D. Thesis. Department of Civil and Environmental Engineering, University of California, Berkeley, USA, 2001.

NCHRP (2007): *Specification Criteria for Simple Performance Tests for Rutting*, Report 580, Transportation Research Board, Washington D.C., USA, 2007.

Schwartz, C.W. (2007): *Implementation of the NCHRP 1-37A Design Guide*. Department of Civil and Environmental Engineering, The University of Maryland, Maryland, USA, 2007.

Ullidtz, P. (1997): *Analytical tools for design of flexible pavements*. Technical University of Denmark, Lyngby, Denmark, 1997.

Arnold, G.K (2004): *Rutting of Granular Pavements*. Ph.D. Thesis. University of Nottingham and Queens University Belfast, Belfast, Northern Ireland.

Austin, A (2002): *Fundamental characterization of unbound base course materials under cyclic loading*. Master of Science Thesis. Department of Civil and Environmental Engineering, Louisiana State University, Louisiana, USA.

Korkiala-Tanttu, L. (2009): *Calculation method for deformation of unbound pavement materials*. Ph.D. Thesis. Department of Civil and Environmental Engineering, Helsinki University of Technology, Espoo, Finland, 2009.

Uthus, L. (2007). *Deformation Properties of Unbound Granular Aggregates*. Ph. D. Thesis. Department of Civil and Transport Engineering, Norwegian University of Science and Technology, Trondheim, Norway.

VTI (1996): *Dimensionering vid nybyggnad: Utformning av ett användarvänligt mekanistiskt/empiriskt dimensioneringssystem för svenska förhållanden*, (Designing new Construction: Development of a User friendly mechanistic/empirical design system for Swedish conditions, In Swedish), VTI, Linköping, Sweden.

VTI (2006): *Prognosmodell för beläggningsslitage*, (Prediction model for wearing, In Swedish), VTI, Linköping, Sweden.

Vägverket (2008): *Vägverkets tekniska krav vid dimensionering och utformning av överbyggnad och avvattning VVTK Väg*, (SRAs Technical demands for design of pavement. In Swedish), Vägverket, Borlänge, {Sweden}.

Vägverket (1994): *Mätning av spår och ojämnheter med mätbil*, (Measurement of ruts and roughness with measurement car. In Swedish), Vägverket, Borlänge, {Sweden}.

Vägverket (2000): *Bearbetning av deflektionsmätdata, erhållna vid provbelastning av väg med FWD-apparat*, (Processing deflection data, obtained from FWD measurement), Vägverket, Borlänge, {Sweden}.

Vägverket (1994): *Väg 94*, Vägverket, Borlänge, {Sweden}.

#### **Internet:**

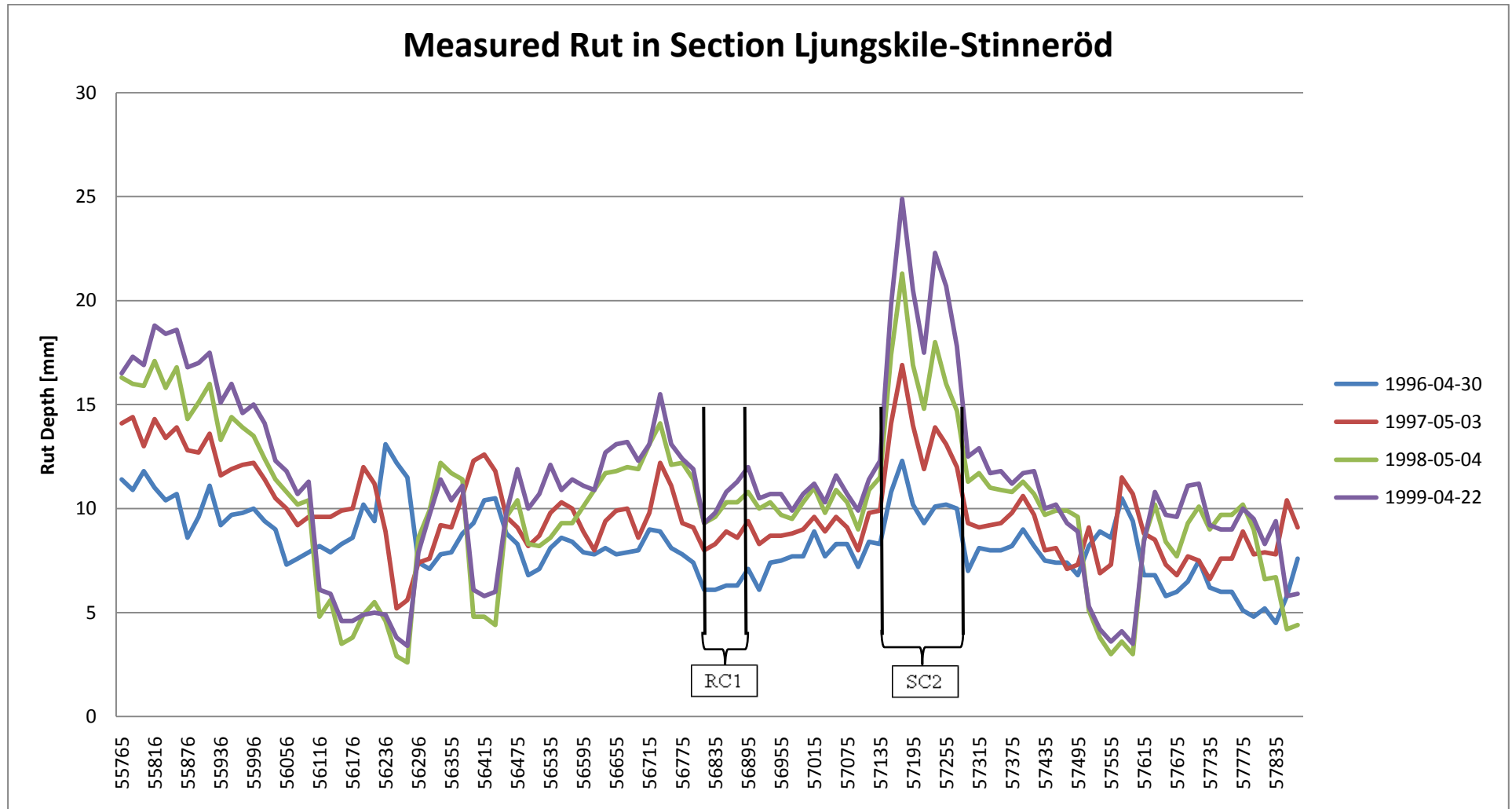
White, G. (2007): *Pavement Interactive*.

<http://pavementinteractive.org/index.php?title=ESAL>, March, 2010.

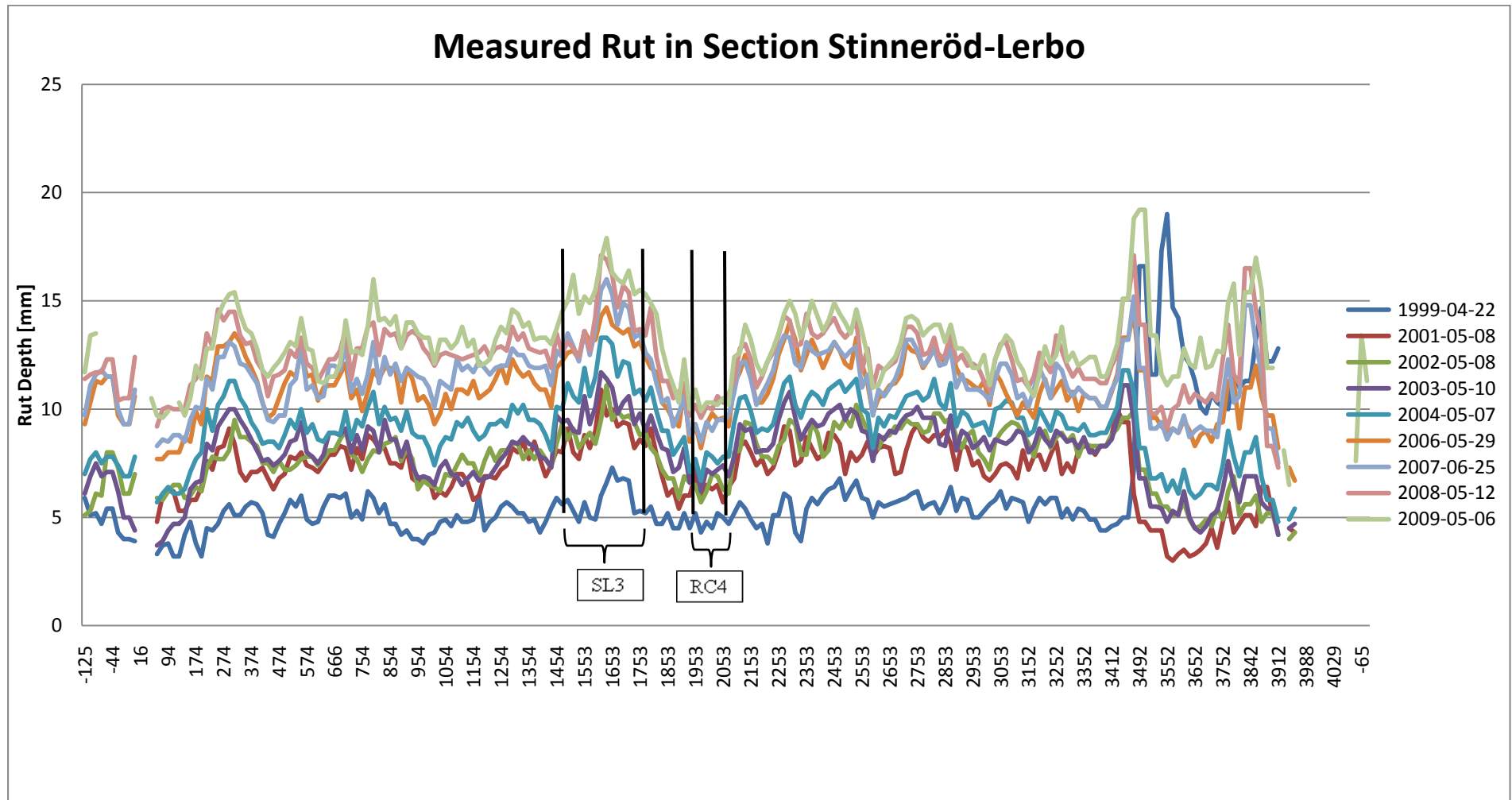
## 9 Appendices

APPENDIX 1A	60
APPENDIX 1B	61
APPENDIX 1C	62
APPENDIX 1D	63
APPENDIX 1E	64
APPENDIX 2	65
APPENDIX 3	67
APPENDIX 4A	68
APPENDIX 4B	69
APPENDIX 5	70
APPENDIX 6	72
APPENDIX 7	74
APPENDIX 8	79

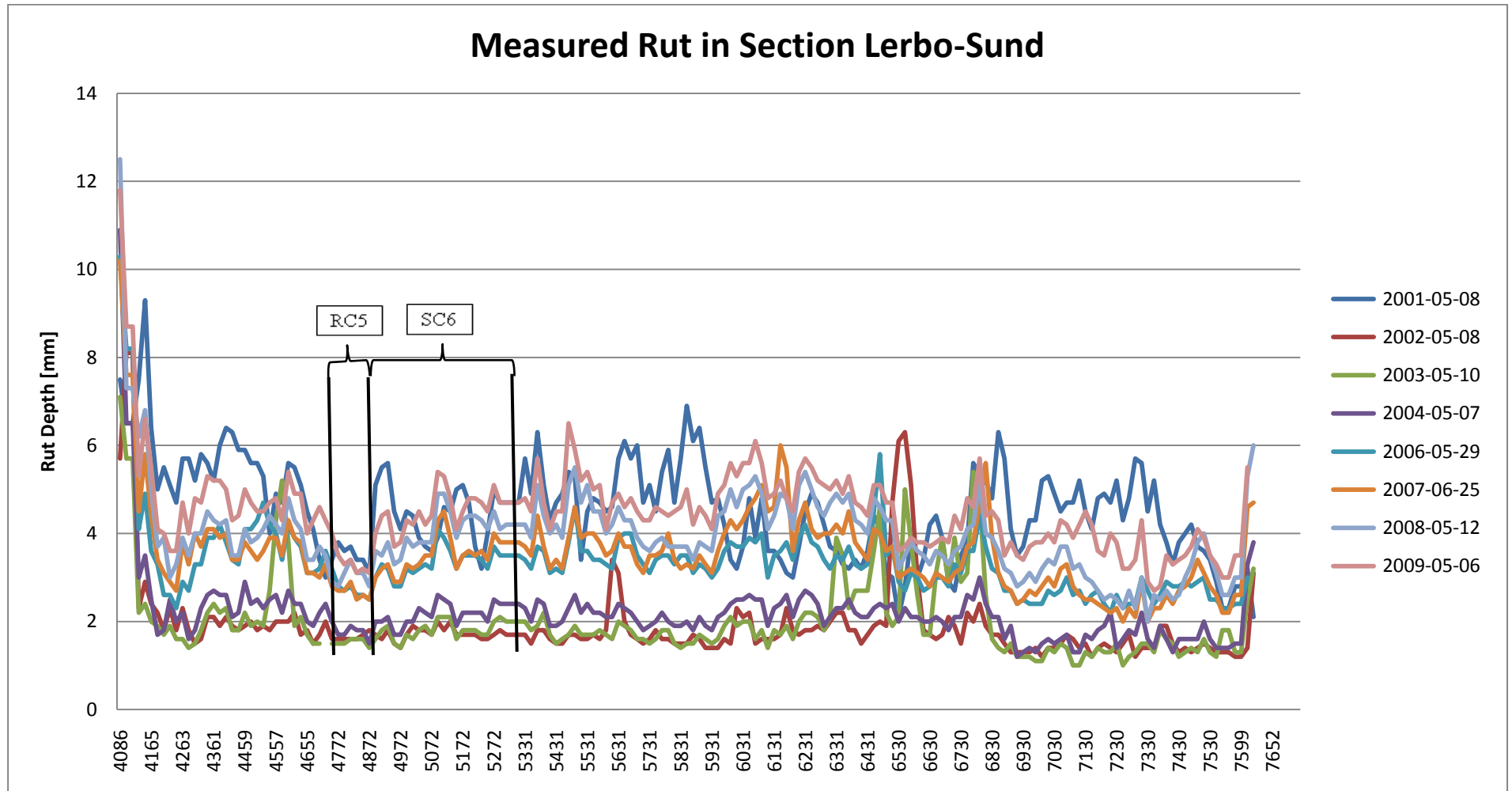
## 9.1 Appendix 1A



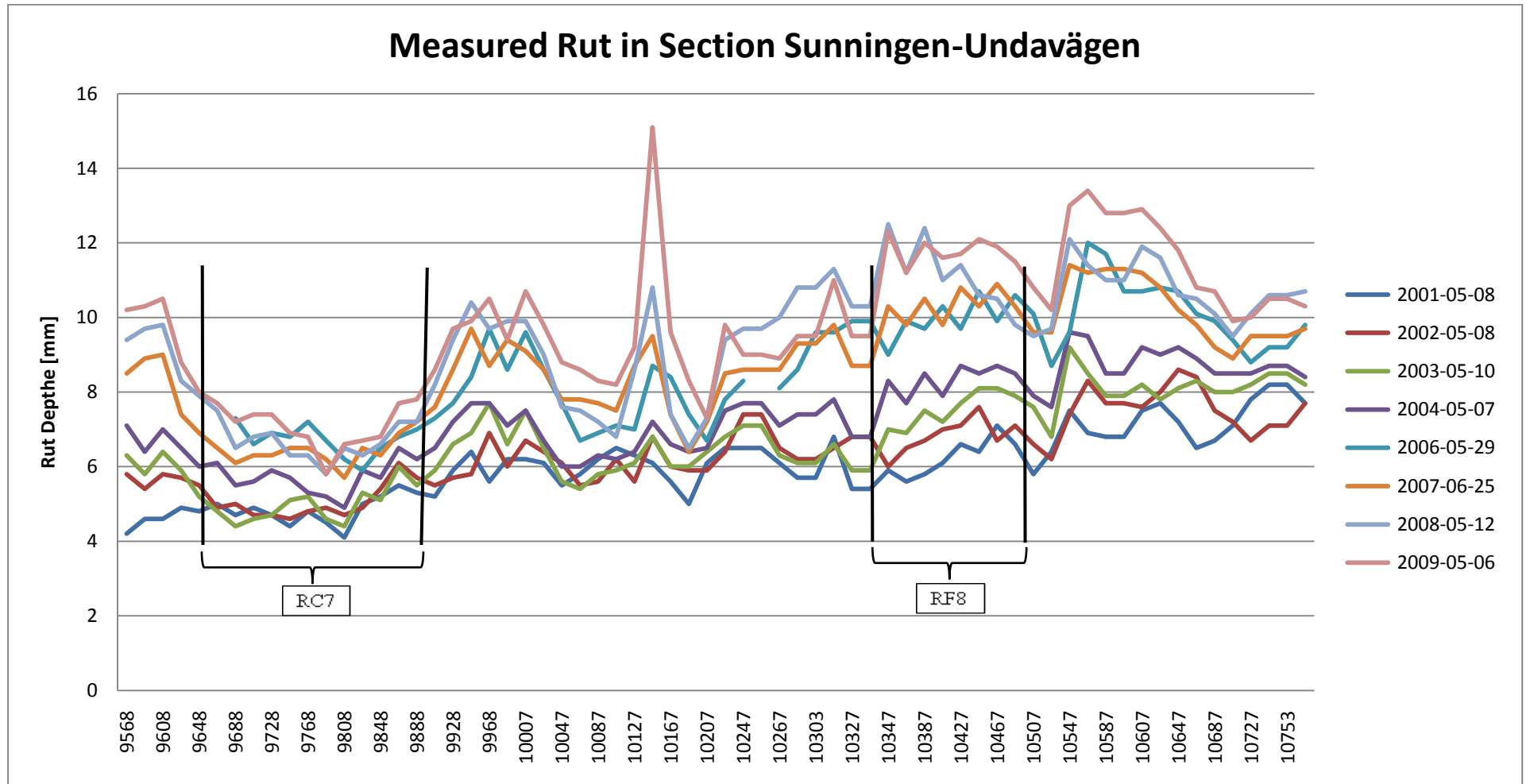
## 9.2 Appendix 1B



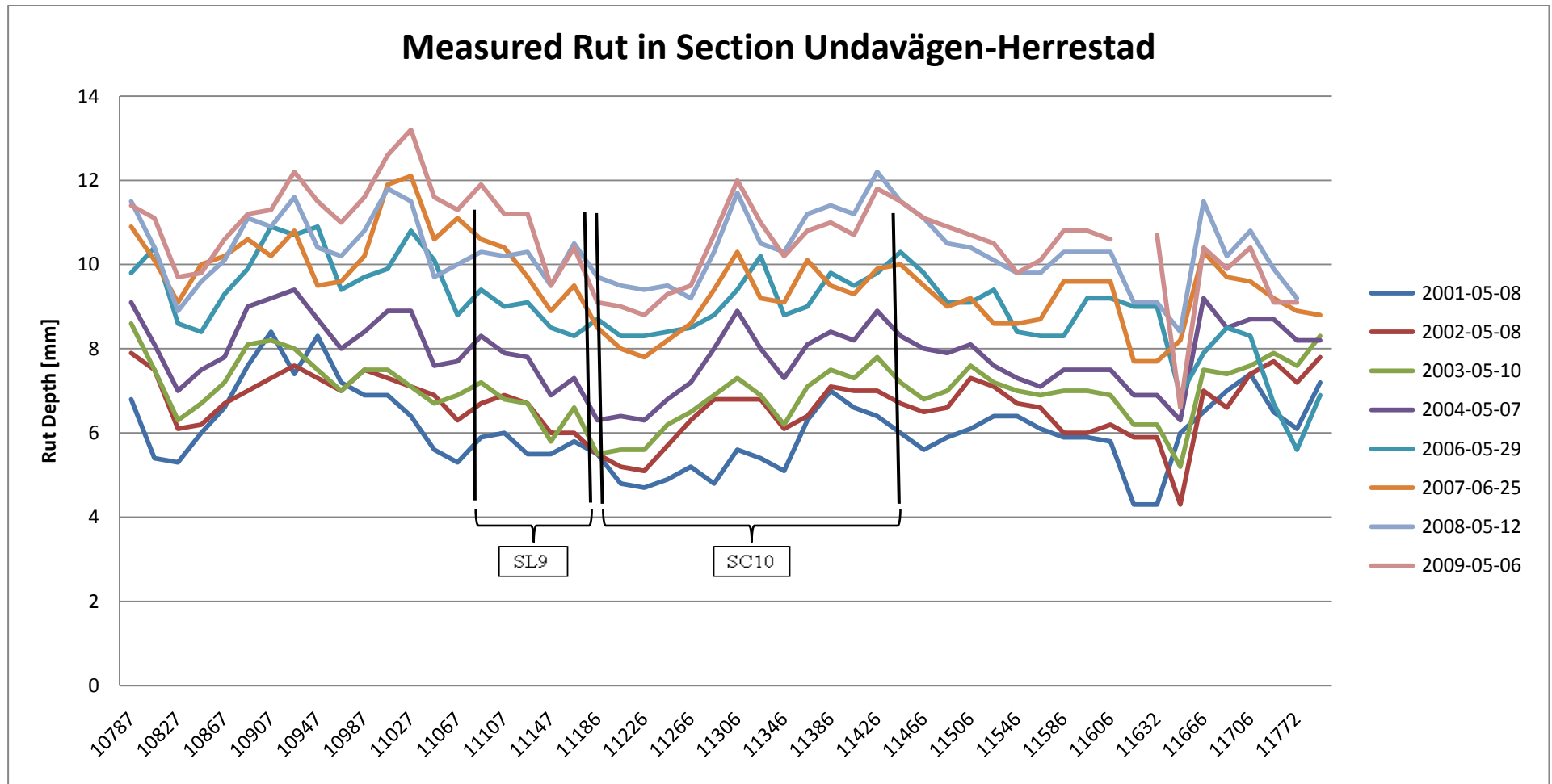
### 9.3 Appendix 1C



## 9.4 Appendix 1D



## 9.5 Appendix 1E



## 9.6 Appendix 2

Table 9.1: Measured rut depth in mm for section Ljungskile-Stinneröd.

Ljungskile-Stinneröd		RC1	SC2
Measurement Year	Time After Construction	56/800-56/900	57/155-57/275
1996	1	6,3	10,4
1997	2	8,6	13,7
1998	3	10,1	17
1999	4	10,6	20,5

Table 9.2: Measured rut depth in mm for section Stinneröd –Lerbo.

Stinneröd-Lerbo		SL3	RC4
Measurment Year	Time After Construction	1/494-1/753	1/950-2/040
1999	1	5,9	4,76
2000	2	7,5	5,5
2001	3	9	6,16
2002	4	9,2	6,42
2003	5	10,1	7
2004	6	11,7	7,56
2005	7	12,6*	8,42*
2006	8	13,4	9,28
2007	9	14	9,18
2008	10	14,4	10,12
2009	11	15,8	10,24

Table 9.3: Measured rut depth in mm for section Lerbo-Sund.

Lerbo-Sund		RC5	SC6
Measurment Year	Time After Construction	4/772-4/872	4/892-5/300
2002	1	1,7	1,72
2003	2	1,5	1,8
2004	3	1,7	2,2
2005	4	2,2*	2,8*
2006	5	2,7	3,34
2007	6	2,7	3,5
2008	7	3,1	4,04
2009	8	3,3	4,5

No RST measurements are done in 2005.

\* Linear interpolations between values from 2004 and 2006.

Appendix 2 Cont.

Table 9.4: Measured rut depth in mm for section Sunningen-Undavägen.

Sunningen-Undavägen		RC7	RF8
Measurment Year	Time After Construction	9/600-9/900	10/360-10/500
2001	1	4,8	6,3
2002	2	5,2	6,9
2003	3	5,1	7,6
2004	4	5,9	8,3
2005	5	6,3*	9,2*
2006	6	6,7	10,1
2007	7	6,7	10,3
2008	8	7,1	10,8
2009	9	7,5	11,6

Table 9.5: Measured rut depth in mm for section Undavägen-Herrestad.

Undavägen-Herrestad		SL9	SC10
Measurment Year	Time After Construction	11/100-11/200	11/220-11/460
2001	1	5,5	5,7
2002	2	6,1	6,5
2003	3	6,2	6,9
2004	4	7,1	7,9
2005	5	7,9*	8,6*
2006	6	8,7	9,2
2007	7	9,2	9,3
2008	8	10	10,7
2009	9	10,1	10,6

\*No RST measurements are done in 2005.

\*Linear interpolations between values from 2004 and 2006.

## 9.7 Appendix 3

### Ljungskile-Lerbo

Table 9.6: Traffic volumes and ESALs for section Ljungskile-Lerbo.

Heavy Traffic Growth	8,2	%	k		
Axles/Heavy Vehicle	4,3		C		
ESAL factor	0,3		D		
Distribution factor	0,8		E		
Year	# Years	AADT <sub>Heavy</sub>	AADT <sub>Heavy,K1</sub>	Accumulated ESALs	ESAL for Specific year
1996	1	660*	594	242070	242070
1997	2	714	643	503963	261893
1998	3	773	695	787302	283339
1999	4	836	752	1093843	306541
2000	5	904	814	1425486	331643
2001	6	978	880	1784287	358801
2002	7	1058	953	2172469	388182
2003	8	1145	1031	2592439	419970
2004	9	1239	1115	3046800	454361
2005	10	1340	1206	3538367	491567
2006	11	1450*	1305	4070188	531821
2007	12	1569	1412	4645559	575371
2008	13	1697	1527	5268046	622487
2009	14	1836	1653	5941507	673461

### Lerbo-Herrestad

Table 9.7: Traffic volumes and ESALs for section Lerbo-Herrestad.

Heavy Traffic Growth	9,2	k			
Axles/Heavy Vehicle	4,3	C			
ESAL factor	0,3	D			
Distribution factor	0,8	E			
Year	# Years	AADT <sub>Heavy</sub>	AADT <sub>Heavy,K1</sub>	Accumulated ESALs	ESAL for specific year
2000	1	680*	612	249406	249406
2001	2	714	643	519235	269829
2002	3	773	695	811160	291925
2003	4	836	752	1126990	315830
2004	5	904	814	1468683	341693
2005	6	978	880	1838356	369674
2006	7	1150*	1035	2238302	399946
2007	8	1145	1031	2670998	432696
2008	9	1239	1115	3139127	468129
2009	10	1340	1206	3645591	506463

\*Traffic count taken from SRA database.

## 9.8 Appendix 4A

### Results of Wearing Model

Input data:



Version 3.2.03  
oktober 2006

Section:	Ljungskile-Lerbo	
Wearing course:	HABS	
Road Type (1/2/3/4/5/6/7/8):	5	(1=7 m; 2=9 m; 3=13 m; 4= Broad lane; 5=Highway; 6=tunnel & (2)+1 Roads); 7=2+(1) Roads; 8= small lane)
Allowable Speed:	110	(50, 70, 90 alt 110 km/h)
AADT <sub>Initial, Winter</sub> :	2350	vehicles/day
Winterperiod/Year:	150	Winter days/Year
% of AADT <sub>Winter</sub> :	70	% (Average during wearing period)
Salt(Y/N):	Y	
Allowable rut depth:	17	mm
Estimated rut beside wearing:	4	mm
Existing rut depth:	13	mm
Stone portion >4mm:	75	Weight-%
Biggest stone Size (MS):	20	mm
Kulkvarn Value (KV):	6	

Results:

Wearing per year (mm):	0,32	mm
Design Life:	20	Year
Annual cost:	2,15	SEK/m <sup>2</sup>

## 9.9 Appendix 4B



Input data:

Section:	Lerbo-Herrestad	
Wearing course:	ABS	
Road Type (1/2/3/4/5/6/7/8):	5	(1=7 m; 2=9 m; 3=13 m; 4= Broad lane; 5=Highway; 6=tunnel & (2)+1 Roads); 7=2+(1) Roads; 8= small lane)
Allowable Speed:	110	(50, 70, 90 alt 110 km/h)
AADT <sub>Initial, Winter</sub> :	1937	vehicles/day
Winterperiod/Year:	150	Winter days/Year
% of AADT <sub>Winter</sub> :	70	% (Average during wearing period)
Salt(Y/N):	Y	
Allowable rut depth:	17	mm
Estimated rut beside wearing:	4	mm
Existing rut depth:	13	mm
Stone portion >4mm:	75	Weight-%
Biggest stone Size (MS):	20	mm
Kulkvarn Value (KV):	6	

Version 3.2.03  
oktober 2006

Results:

Wearing per year (mm):	0,26	mm
Design Life:	20	Year
Annual cost:	2,15	SEK/m <sup>2</sup>

## 9.10 Appendix 5

Table 9.8: Definition of pavement layers and E-Modulus in MMOPP for Section RC1.

Layer	Pavement material	Thickness [mm]	E-Modulus [MPa]
Bound layer	Bituminous material	200	3650
Unbound layer	Crushed rock	80	300
Subgrade	Bedrock	***	1000

Table 9.9: Definition of pavement layers and E-Modulus in MMOPP for Section SC2.

Layer	Pavement material	Thickness [mm]	E-Modulus [MPa]
Bound layer	Bituminous material	200	3650
Unbound layer	Crushed rock	700	300
Subgrade	Soft clay	***	5

Table 9.10: Definition of pavement layers and E-Modulus in MMOPP for Section SL3.

Layer	Pavement material	Thickness [mm]	E-Modulus [MPa]
Bound layer	Bituminous material	200	3650
Unbound layer	Crushed rock	700	300
Subgrade	Dry crust, clay	***	15

Table 9.11: Definition of pavement layers and E-Modulus in MMOPP for Section RC4.

Layer	Pavement material	Thickness [mm]	E-Modulus [MPa]
Bound layer	Bituminous material	200	3650
Unbound layer	Crushed rock	80	300
Subgrade	Bedrock	***	1000

Table 9.12: Definition of pavement layers and E-Modulus in MMOPP for Section RC5.

Layer	Pavement material	Thickness [mm]	E-Modulus [MPa]
Bound layer	Bituminous material	190	3650
Unbound layer	Crushed rock	80	300
Subgrade	Bedrock	***	1000

Table 9.13: Definition of pavement layers and E-Modulus in MMOPP for Section SC6.

Layer	Pavement material	Thickness [mm]	E-Modulus [MPa]
Bound layer	Bituminous material	190	3650
Unbound layer	Crushed rock	1300	300
Subgrade	Sand/clay	***	60

## Appendix 5 Cont.

Table 9.14: Definition of pavement layers and E-Modulus in MMOPP for Section RC7.

Layer	Pavement material	Thickness [mm]	E-Modulus [MPa]
Bound layer	Bituminous material	190	3650
Unbound layer	Crushed rock	80	300
Subgrade	Bedrock	***	1000

Table 9.15: Definition of pavement layers and E-Modulus in MMOPP for Section RF8.

Layer	Pavement material	Thickness [mm]	E-Modulus [MPa]
Bound layer	Bituminous material	190	3650
Unbound layer	Crushed rock	6000	300
Subgrade	Dry crust, clay	***	50

Table 9.16: Definition of pavement layers and E-Modulus in MMOPP for Section SL9.

Layer	Pavement material	Thickness [mm]	E-Modulus [MPa]
Bound layer	Bituminous material	190	3650
Unbound layer	Crushed rock	1080	300
Subgrade	Dry crust, clay	***	80

Table 9.17: Definition of pavement layers and E-Modulus in MMOPP for Section SC10.

Layer	Pavement material	Thickness [mm]	E-Modulus [MPa]
Bound layer	Bituminous material	190	3650
Unbound layer	Crushed rock	1080	300
Subgrade	Clay	***	15

## 9.11 Appendix 6

Table 9.18: Definition of pavement layers and E-Modulus in M-E PDG for Section RC1 and RC4.

Sub layers	Thickness [mm]	Bitumen penetration	E-modulus [MPa]
Asphalt concrete	40	85-100	***
Asphalt concrete	40	85-100	***
Asphalt base	120	120-150	***
Crushed stone	80	***	300
Bedrock	***	***	1000

Table 9.19: Definition of pavement layers and E-Modulus in M-E PDG for Section SL3.

Sub layers	Thickness [mm]	Bitumen penetration	E-modulus [MPa]
Asphalt concrete	40	85-100	***
Asphalt concrete	40	85-100	***
Asphalt base	120	120-150	***
Crushed stone	80	***	300
Crushed stone	620	***	300
Dry crust, clay	***	***	15

Table 9.20: Definition of pavement layers and E-Modulus in M-E PDG for Section SC6.

Sub layers	Thickness [mm]	Bitumen penetration	E-modulus [MPa]
Asphalt concrete	40	85-100	***
Asphalt concrete	60	85-100	***
Asphalt base	90	120-150	***
Crushed stone	1000	***	300
Clay	***	***	60

Table 9.21: Definition of pavement layers and E-Modulus in M-E PDG for Section RC7.

Sub layers	Thickness [mm]	Bitumen penetration	E-modulus [MPa]
Asphalt concrete	40	85-100	***
Asphalt concrete	60	85-100	***
Asphalt base	90	120-150	***
Crushed stone	80	***	300
Bedrock	***	***	1000

Table 9.22: Definition of pavement layers and E-Modulus in M-E PDG for Section RF8.

Sub layers	Thickness [mm]	Bitumen penetration	E-modulus [MPa]
Asphalt concrete	40	85-100	***
Asphalt concrete	60	85-100	***
Asphalt base	90	120-150	***
Crushed stone	80	***	300
Embankment*	***	***	300

\* The embankment in this section is defined as subgrade due to limitations in M-E PDG.

Appendix 6 Cont.

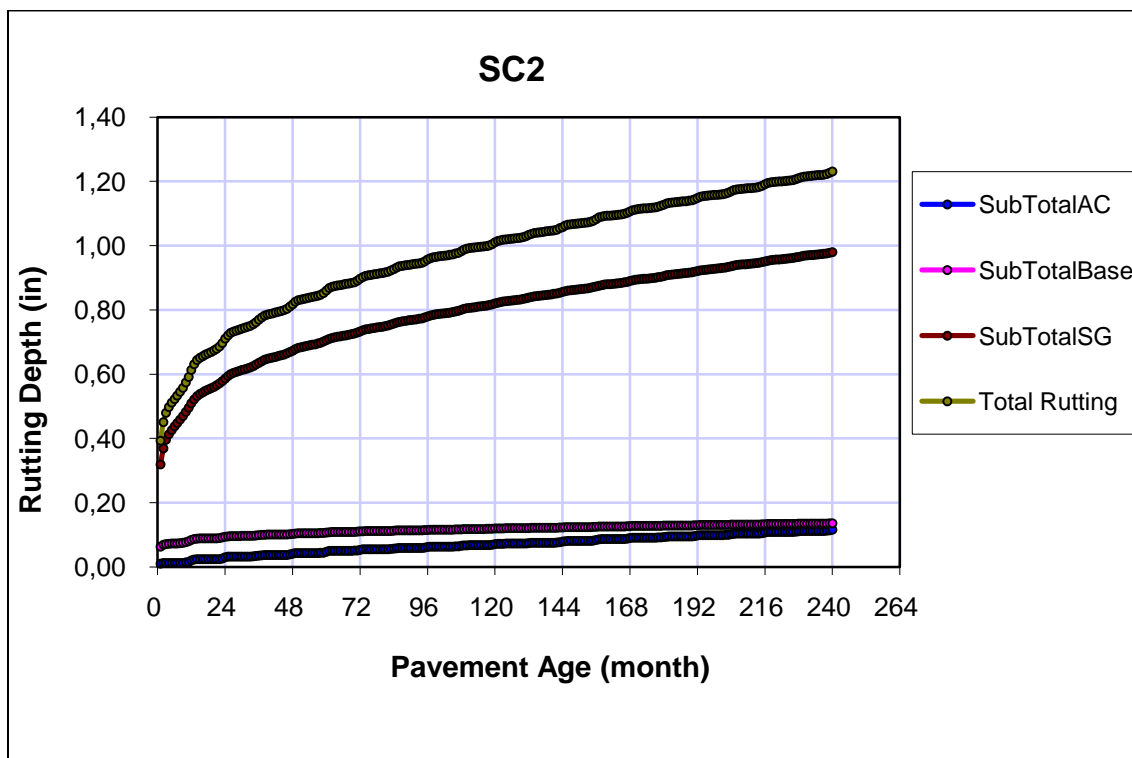
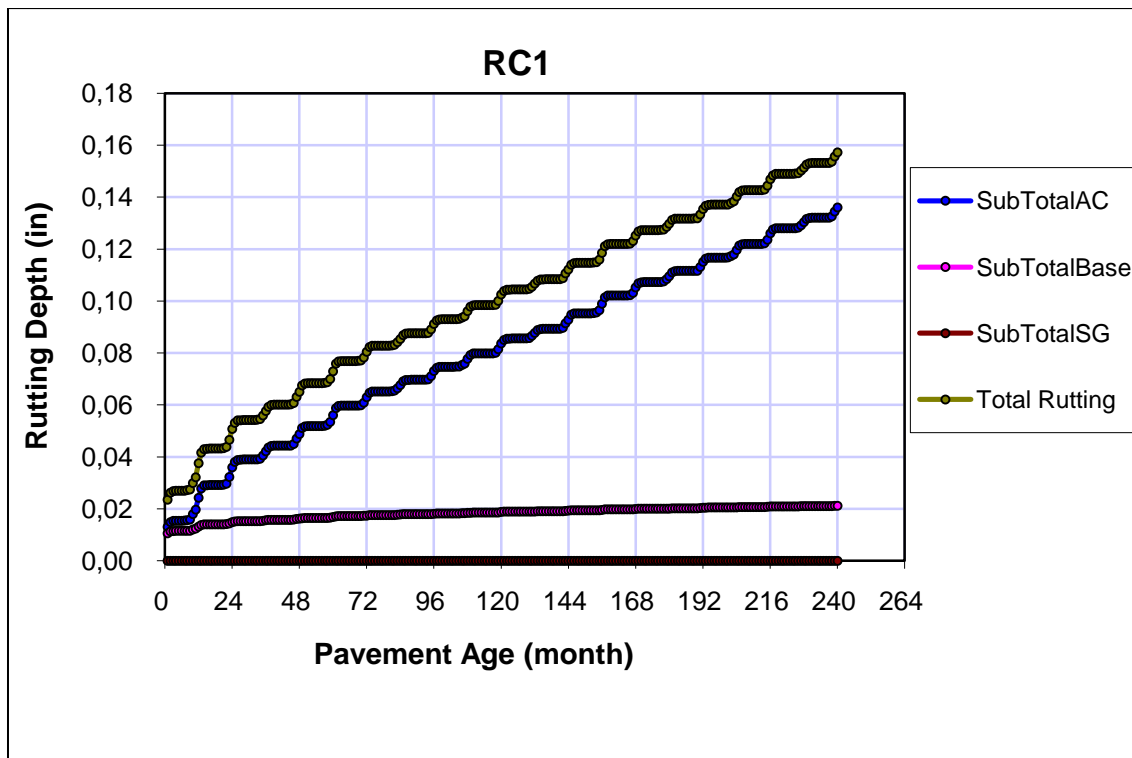
Table 9.23 Definition of pavement layers and E-Modulus in M-E PDG for Section SL9.

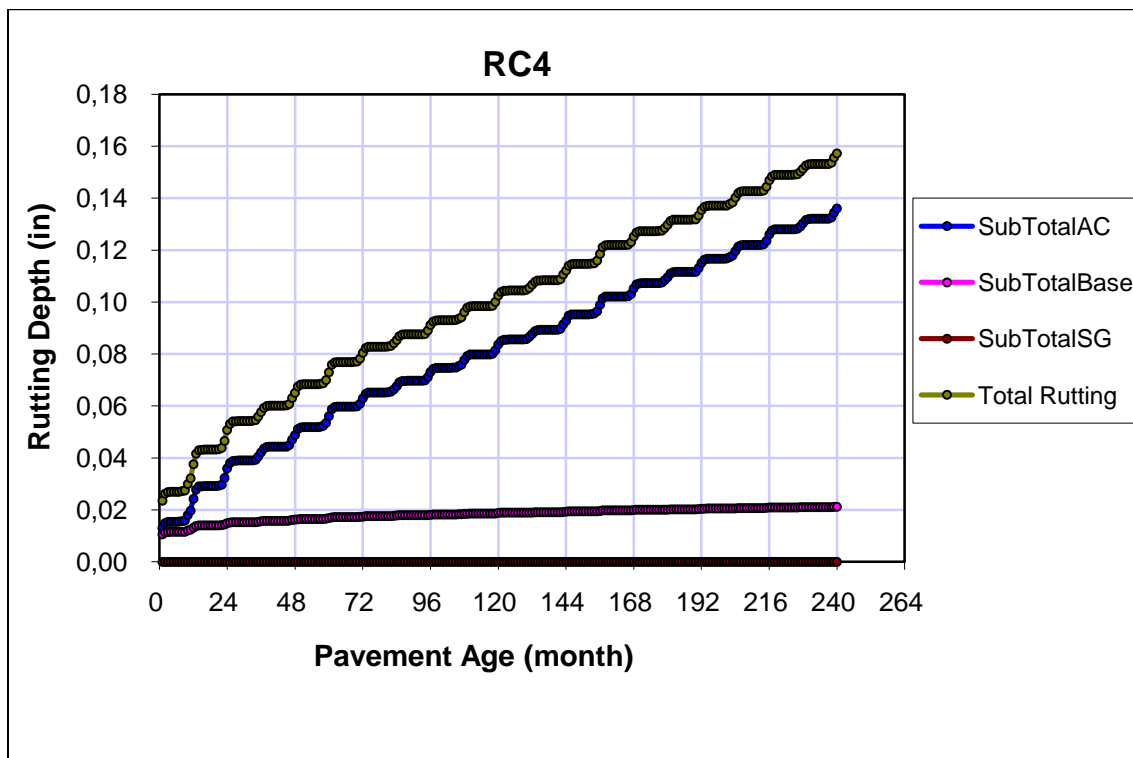
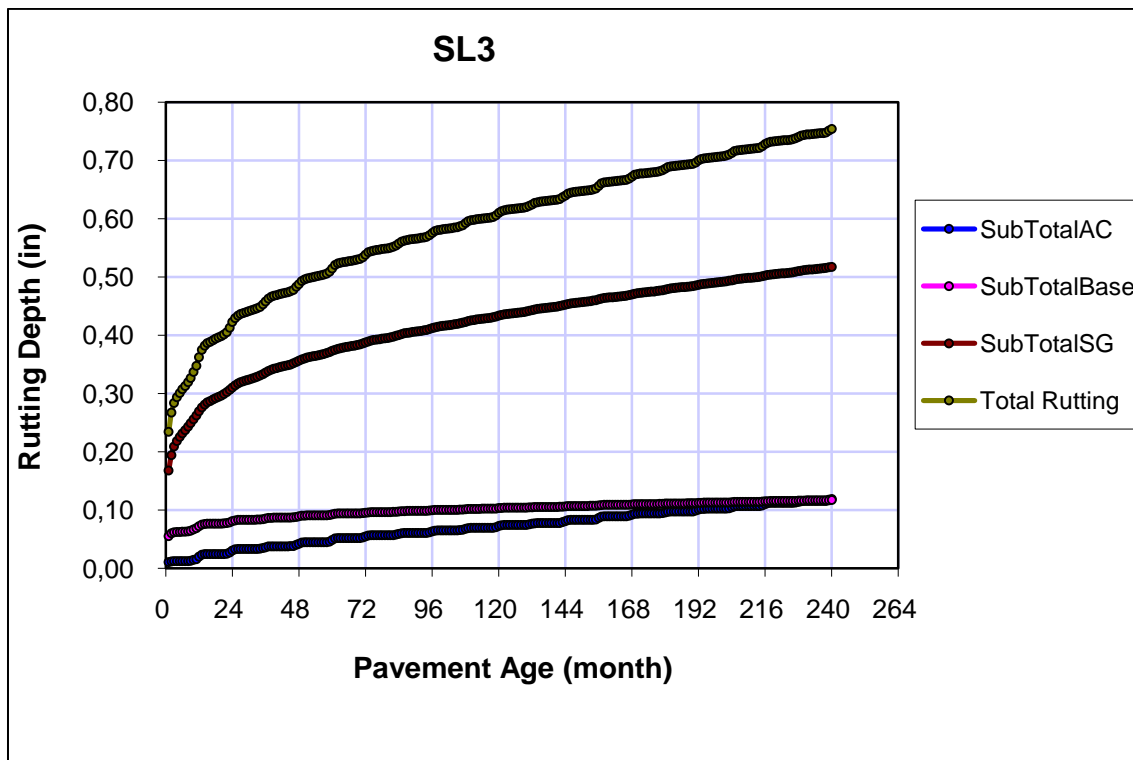
Sub layers	Thickness [mm]	Bitumen penetration	E-modulus [MPa]
Asphalt concrete	40	85-100	***
Asphalt concrete	60	85-100	***
Asphalt base	90	120-150	***
Crushed stone	80	***	300
Crushed stone	1000	***	200
Dry crust, clay	***	***	80

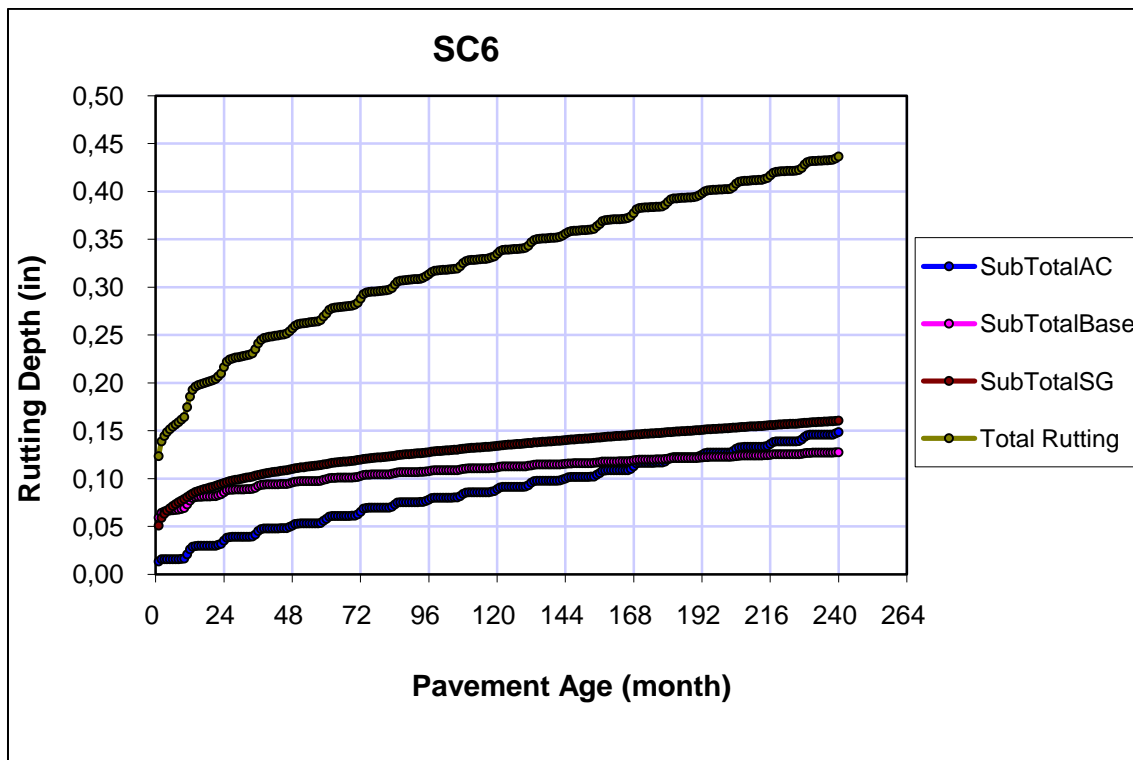
Table 9.24: Definition of pavement layers and E-Modulus in M-E PDG for Section SC10.

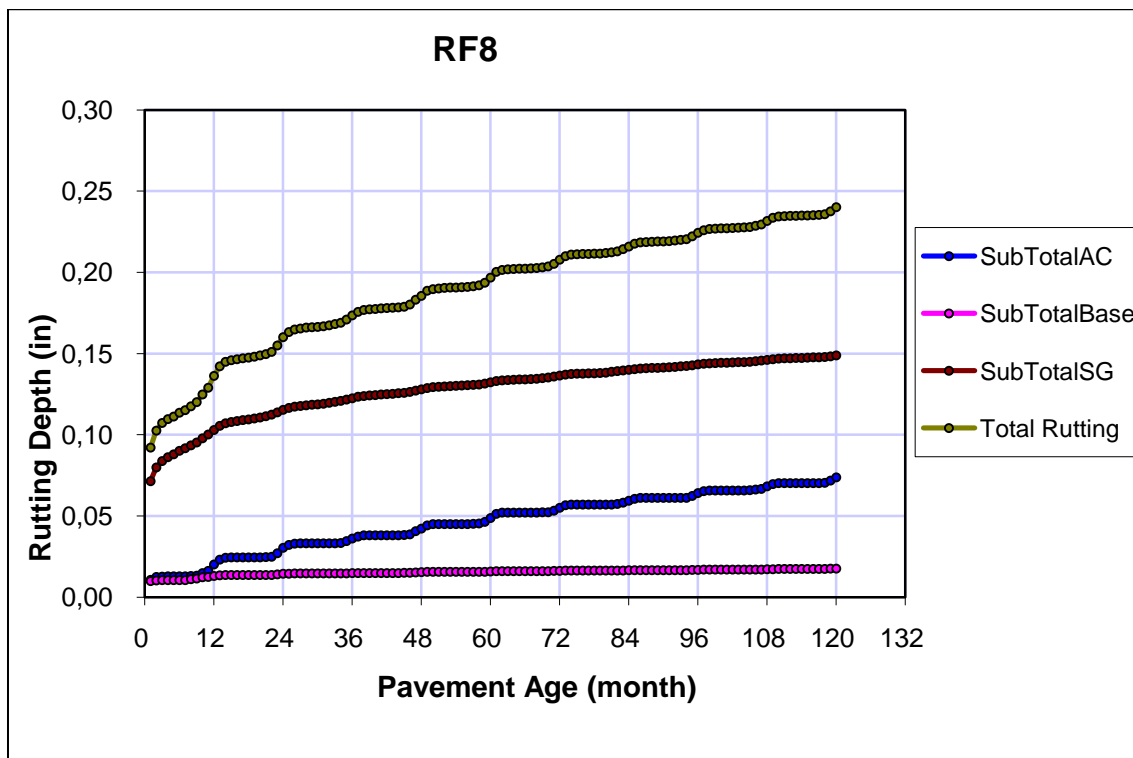
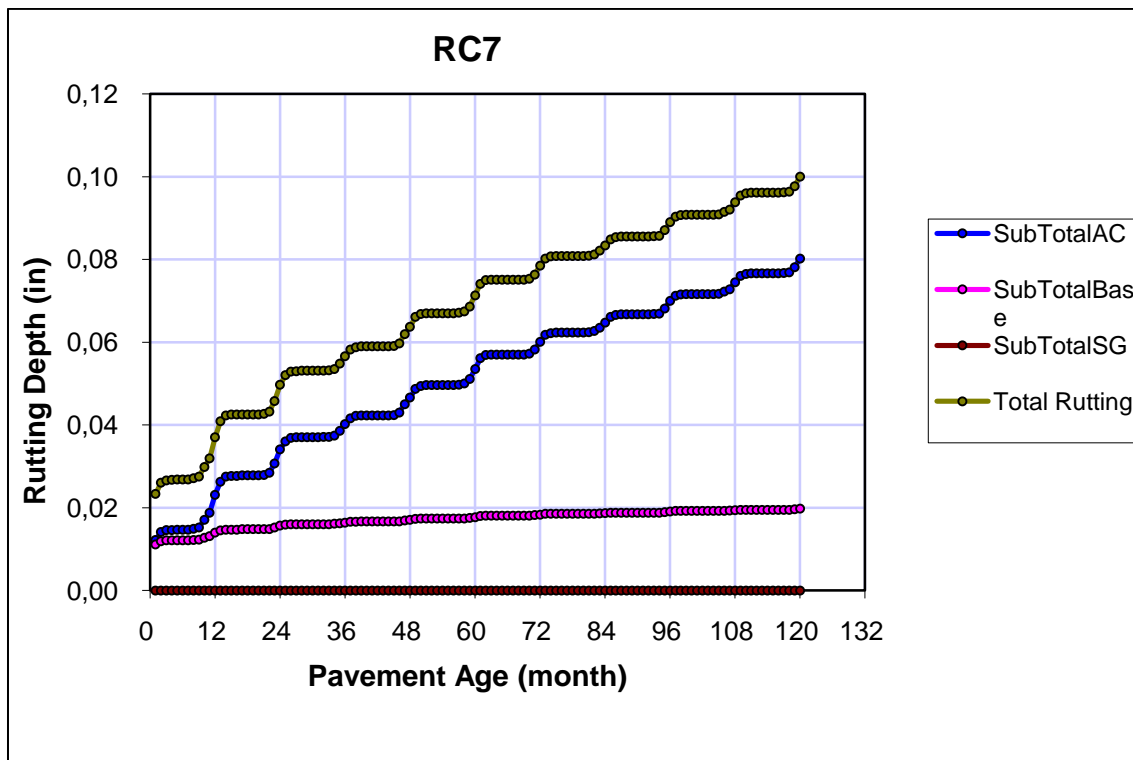
Sub layers	Thickness [mm]	Bitumen penetration	E-modulus [MPa]
Asphalt concrete	40	85-100	***
Asphalt concrete	60	85-100	***
Asphalt base	90	120-150	***
Crushed stone	80	***	300
Crushed stone	1000	***	200
Clay	***	***	15

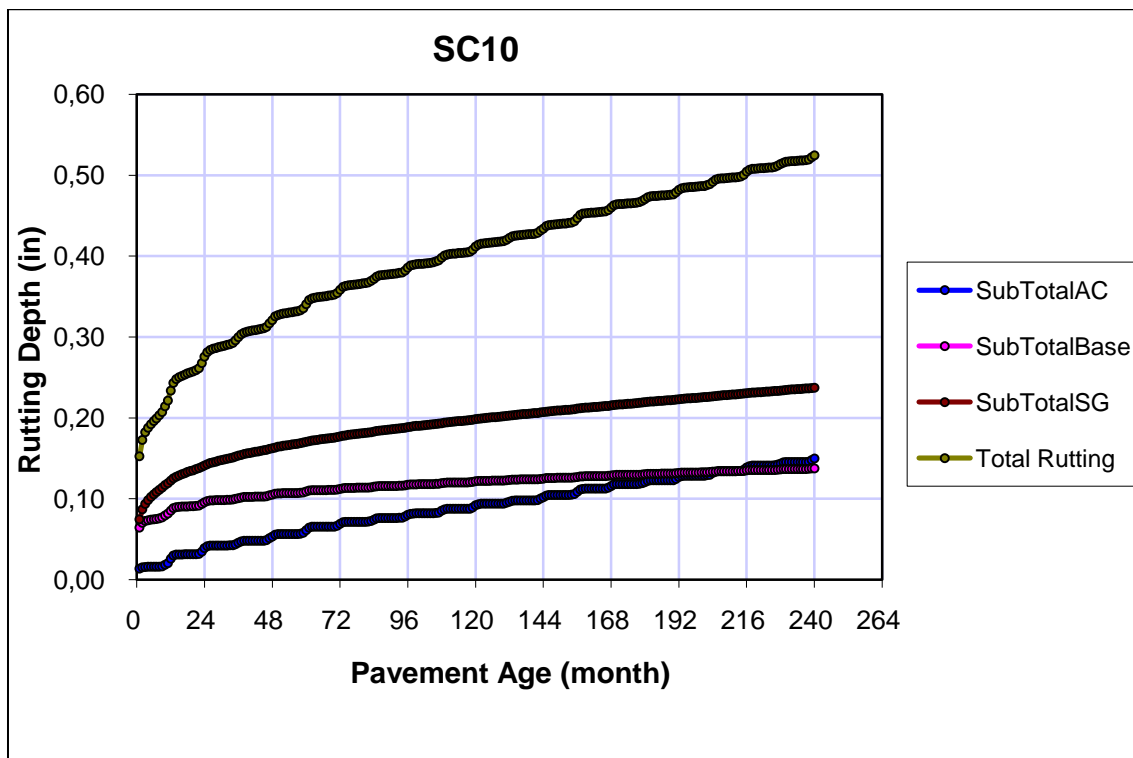
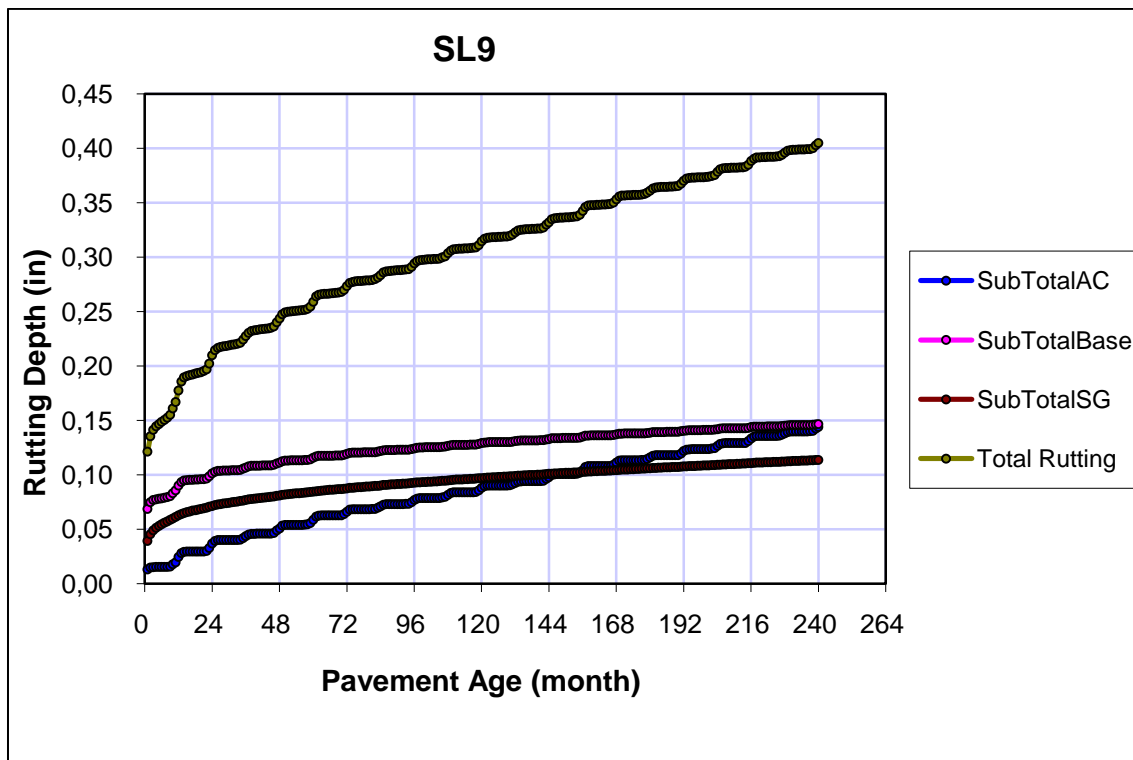
## 9.12 Appendix 7



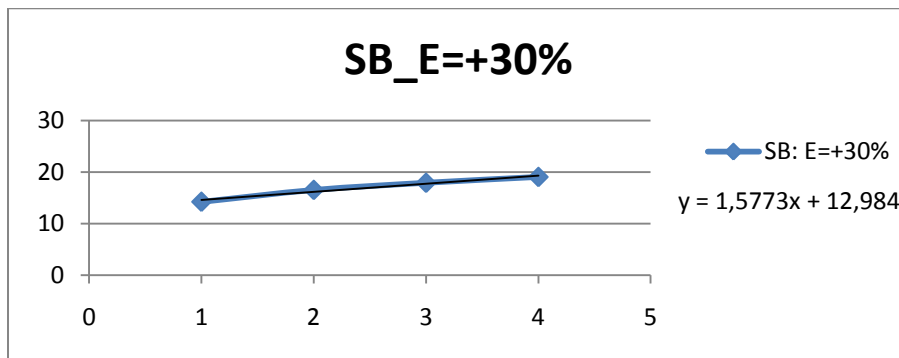
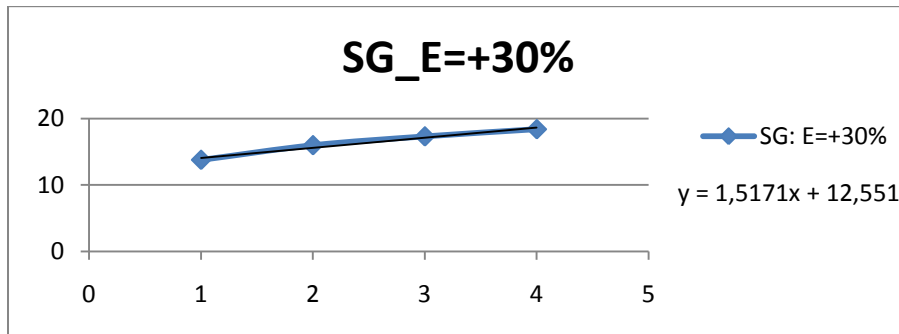
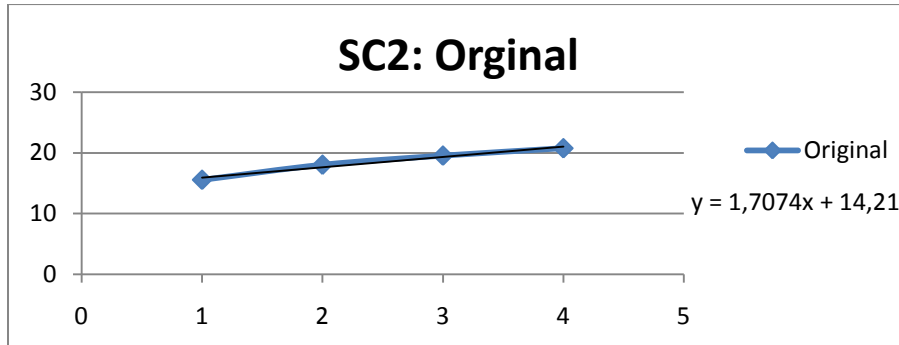








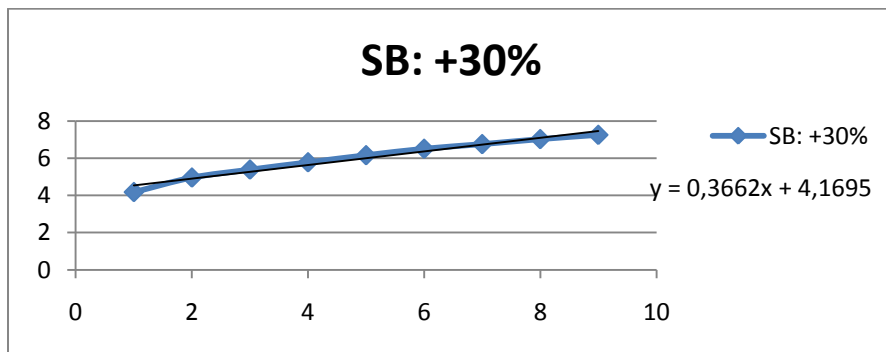
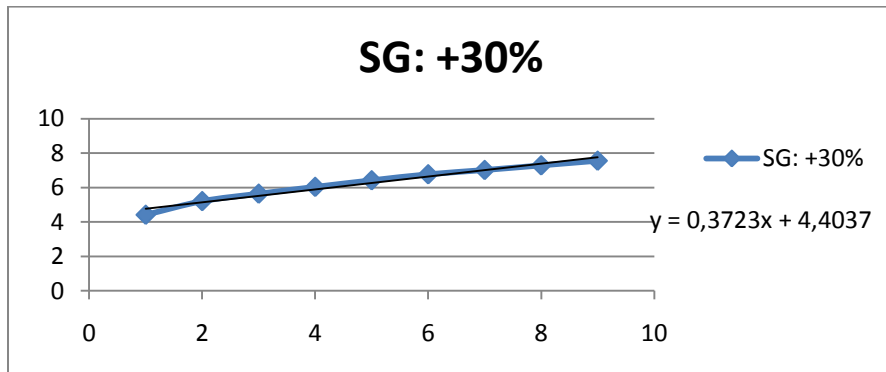
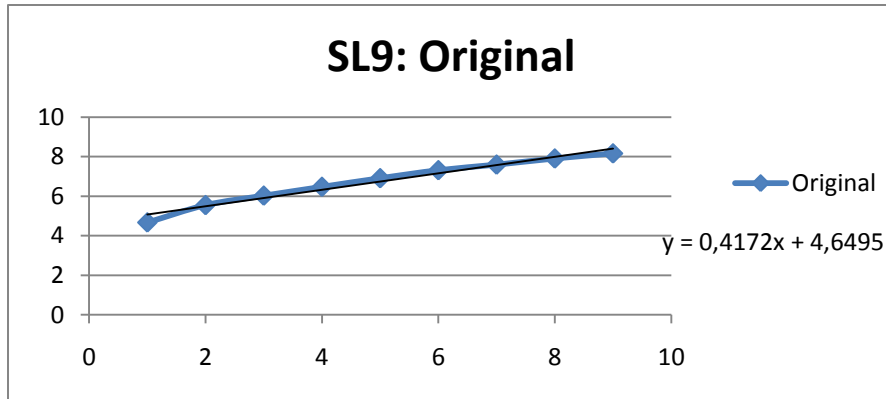
### 9.13 Appendix 8



$$S_P = \frac{\frac{\Delta V}{V}}{\frac{\Delta P}{P}}$$

$$S_{SG} = \frac{\frac{\Delta V}{V}}{\frac{\Delta SG}{SG}} = \frac{\frac{1.7074 - 1.5171}{1.7074}}{0.3} = 0.372$$

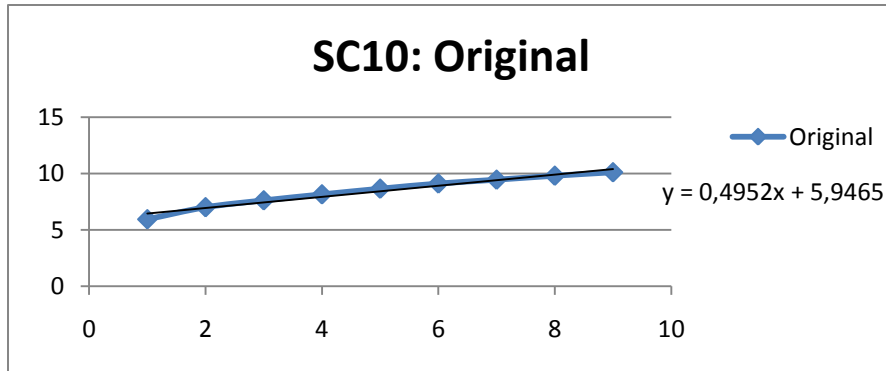
$$S_{SB} = \frac{\frac{\Delta V}{V}}{\frac{\Delta SB}{SB}} = \frac{\frac{1.7074 - 1.5773}{1.7074}}{0.3} = 0.254$$



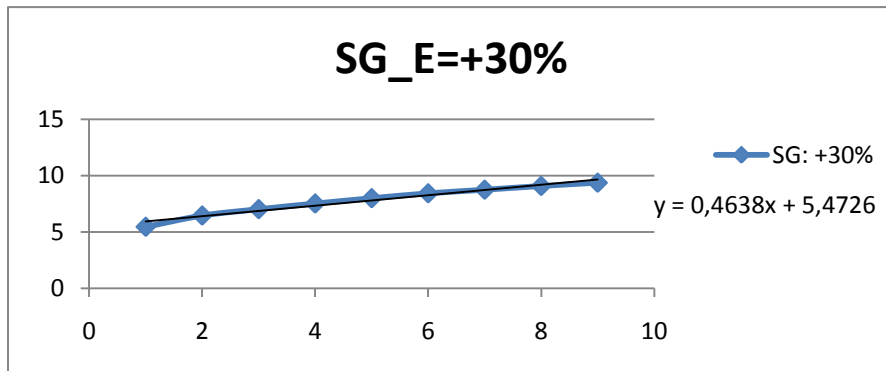
$$S_P = \frac{\frac{\Delta V}{V}}{\frac{\Delta P}{P}}$$

$$S_{SG} = \frac{\frac{\Delta V}{V}}{\frac{\Delta SG}{SG}} = \frac{\frac{0.4172 - 0.3723}{0.4172}}{0.3} = 0.359$$

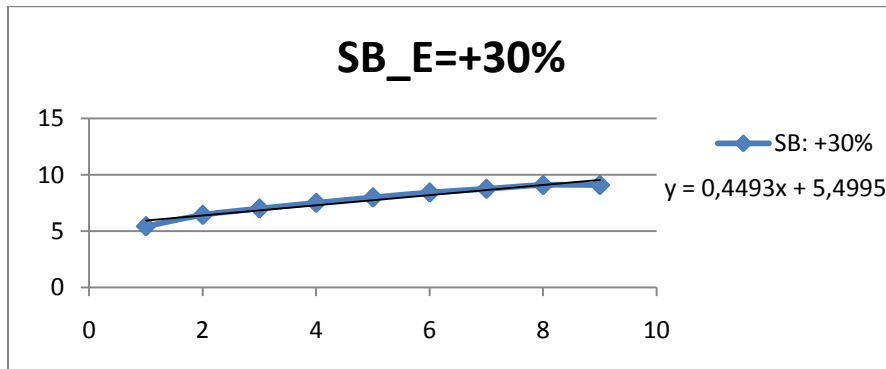
$$S_{SB} = \frac{\frac{\Delta V}{V}}{\frac{\Delta SB}{SB}} = \frac{\frac{0.4172 - 0.3662}{0.4172}}{0.3} = 0.407$$



$$S_P = \frac{\frac{\Delta V}{V}}{\frac{\Delta P}{P}}$$



$$S_{SG} = \frac{\frac{\Delta V}{V}}{\frac{\Delta SG}{SG}} = \frac{\frac{0.4476 - 0.4638}{0.4476}}{0.3} = 0.211$$



$$S_{SG} = \frac{\frac{\Delta V}{V}}{\frac{\Delta SG}{SG}} = \frac{\frac{0.4476 - 0.4493}{0.4476}}{0.3} = 0.309$$